Two-dimensional macroscopic models for large scale traffic networks

Stéphane Mollier

UNIVERSITÉ GRENOBLE ALPES

THÈSE

pour obtenir le grade de

DOCTEUR DE L'UNIVERSITÉ DE GRENOBLE ALPES

Spécialité : **Automatique-Productique**

Arrêté ministériel : 7 août 2006

Présentée par
Stéphane MOLLIER

Thèse dirigée par **Carlos Canudas-de-Wit** et
codirigée par **Maria Laura Delle Monache** et **Benjamin Seibold**

préparée au sein du laboratoire
Gipsa-Lab
dans l'école doctorale **EEATS**

Two-dimensional models for large-scale traffic networks

Thèse soutenue publiquement le **13 Février 2020**,
devant le jury composé de:

Didier Georges
Professeur des universités, Gipsa-Lab, Président du jury
Ludovic Leclercq
Directeur de Recherche, Université Gustave Eiffel, Rapporteur
Nikolas Geroliminis
Professeur associé, EPFL, Suisse, Rapporteur
Paola Goatin
Directrice de Recherche, Inria Sophia-Antipolis, Examinateur
Jordi Casas
Docteur en science, Aimsun-Barcelone, Examinateur
Maria Laura Delle Monache
Chargé de recherche, Inria Rhône-Alpes, Co-directice de thèse
Benjamin Seibold (Invité)
Professeur associé, Temple University, Co-encadrant de thèse

UNIVERSITÉ DE GRENOBLE ALPES

ÉCOLE DOCTORALE EEATS

Eléctronique, Eléctrotechnique, Automatique, Traitement du Signal

T H È S E

pour obtenir le titre de

docteur en sciences

de l'Université de Grenoble

Mention : AUTOMATIQUE

Présentée et soutenue par

Stéphane Mollier

Two-dimensional models for large-scale traffic networks

Thèse dirigée par Carlos Canudas-de-Wit

préparée au laboratoire Grenoble Images Parole Signal Automatique (GIPSA-lab)

soutenue le 13/02/2020

Jury :

Rapporteurs :	Ludovic LECLERCQ	-	IFSTTAR
	Nikolas GEROLIMINIS	-	EPFL
Examinateur :	Paola GOATIN	-	INRIA Sophia Antipolis
	Jordi CASAS	-	Aimsun
Président :	Didier GEORGES	-	GIPSA-lab
Encadrant :	Maria Laura DELLE MONACHE	-	Inria Grenoble

Invité :

Encadrant : Benjamin Seibold - Temple University

Remerciements

Si j'ai pu mener à bien ce projet de thèse, c'est grâce au soutien de nombreuses personnes que je souhaite remercier.
Tout d'abord, j'aimerais remercier mon directeur de thèse, Carlos Canudas-de-Wit, pour m'avoir fait confiance et accompagné dans la réalisation cette thèse. En revêtant aussi la casquette de chef de projet, il a su regrouper, au sein d'une équipe, des personnes qui ont fait de cette thèse une excellente expérience. Je tiens aussi à remercier ma codirectrice de thèse, Maria Laura Delle Monache, qui m'a soutenu avec beaucoup de bienveillance et de patience. Elle a su se rendre très disponible tout en me laissant travailler avec autonomie.
Then, I would like to write just a few words in English to thank my other co-advisor, Benjamin Seibold. Because of the distance, we did not exchange as much as we did with my other supervisors, but it was always interesting and very relevant discussions. Also, I wanted to thank you for welcoming me one week in Philadelphia.
Ensuite, je tiens à remercier Nikolas Geroliminis et Ludovic Leclercq d'avoir accepté d'être rapporteurs de ma thèse et d'avoir libérés de leur temps pour relire ma thèse, rédiger un rapport et assister à ma soutenance malgré un emploi du temps chargé. J'ai trouvé leur retours très pertinents et les discussions lors de la soutenance intérressantes.
De la même façon, je souhaite remercier les autres membres de mon jury, Paola Goatin, Didier Georges et Jordi Casas, d'avoir accepté de faire partie de mon jury et de s'être intéressés à mon travail.
Je voudrais remercier tous les membres actuels ou passés de l'équipe NECS qui m'ont tant apportés tout au long de ma thèse tant intellectuellement qu'humainement. Tout d'abord, je voudrais remercier Vadim Bertrand, ingénieur de recherche, pour toute l'aide informatique qu'il m'a apporté. Cela a été un plaisir de faire équipe avec toi tant professionnellement que sportivement. Ensuite, j'aimerais remercier tous les permanents de l'équipe pour leur accueil et le cadre de travail agréable. Enfin, je tiens à remercier tous les autres doctorants, assistantes, stagiaires et postdoctorants de l'équipe : Andres, Pietro, Remy, Hannah, Giacomo, Baptiste, Sebin, Thibaud, Aleksandra, Thibault, Lydie, Martin, Umar, Diego, Julie, Bassel, Tianyi, Liudmila, Denis, Ujjwal qui ont rendu ces 3 années inoubliables. Merci à vous. Je vous souhaite à tous le meilleur pour la suite.
Pour finir, je souhaiterais remercier tout particulièrement Nicolas Martin, qui a partagé mon bureau pendant ces 3 années. Des questions Matlab, aux longues discussions existentielles, j'ai énormément appris à tes côtés notamment sur la façon de mieux débattre.
Et aux amis, à la famille, et à tous ceux que je n'aurais pas cités, merci encore !

Résumé — Les fréquentes congestions que connaissent les réseaux routiers des grandes métropoles mondiales ont de lourdes conséquences économiques et environnementales. La compréhension et la modélisation dynamique des mécanismes à l'origine de ces congestions permettent d'en prédire l'évolution et donc d'améliorer l'efficacité des politiques de régulations utilisées par les opérateurs du réseau. La modélisation des réseaux routiers a commencé par le cas d'une route isolée puis a été étendue à des réseaux urbains. Ce changement d'échelle présente de nombreuses difficultés en matière de temps de calcul, de calibrage et de scénarisation, ce qui a incité la communauté scientifique à s'intéresser à des modèles agrégés, décrivant une représentation simplifiée de la réalité. Un de ces modèles vise à représenter de denses réseaux urbains par une équation aux dérivées partielles continue dans le plan. Ainsi, les véhicules sont représentés par une densité bi-dimensionnelle et leurs trajectoires sont décrites comme des directions de flux. L'objectif de la thèse est de développer cette approche et de proposer des méthodes pour son calibrage et sa validation. Les contributions correspondent à trois extensions successives du modèle. Tout d'abord, un simple modèle bi-dimensionnel est proposé pour le cas de réseaux homogènes –avec des limitations de vitesse et des concentrations de routes similaires en tout point– et dans lesquels une direction de propagation privilégiée existe. Une méthode de comparaison avec un microsimulateur est présentée. Ensuite, le modèle est étendu au cas de réseaux hétérogènes –avec des limitations de vitesse et des concentrations de routes variables– mais toujours avec une direction privilégiée. Ces dépendances spatiales permettent de décrire les phénomènes d'engorgement existant dans les réseaux routiers. Enfin, un modèle constitué de plusieurs couches, chacune représentant une direction de flux différente, est étudié. La complexité de la modélisation réside dans la formulation des interactions entre les différentes directions. Ce type de modèle n'est pas toujours hyperbolique ce qui impacte sa stabilité.
Mots clés : Modélisation du trafic routier, Simulation numérique, Equation aux dérivées partielles

Abstract — Congestion in traffic networks is a common issue in big cities and has considerable economic and environmental impacts. Traffic policies and real-time network management can reduce congestion using prediction of dynamical modeling. Initially, researchers studied traffic flow on a single road and then, they extended it to a network of roads. However, large-scale networks present challenges in terms of computation time and parameters' calibration. This led the researchers to focus on aggregated models and to look for a good balance between accuracy and practicality. One of the approaches describes traffic evolution with a continuous partial differential equation on a 2D-plane. Vehicles are represented by a two-dimensional density and their propagation is described by the flow direction. The thesis aims to develop these models and devises methods for their calibration and their validation. The contributions follow three extensions of the model. First, a simple model in two-dimensional space to describe a homogeneous network with a preferred direction of flow propagation is considered. A homogeneous network has the same speed limits and a similar concentration of roads everywhere. A method for validation using GPS probes from microsimulation is provided. Then, a space-dependent extension to describe a heterogeneous network with a preferred direction of flow propagation is presented. A heterogeneous network has different speed limits and a variable concentration of roads. Such networks are of interest because they can show how bottleneck affects traffic dynamics. Finally, the case of multiple directions of flow is considered using multiple layers of density, each layer representing a different flow direction. Due to the interaction between layers, these models are not always hyperbolic which can impact their stability.
Keywords: Traffic flow modeling, Numerical simulation, Partial differential equation

GIPSA-lab, 11 Rue des Mathématiques
Saint-Martin-d'Hères

Contents

List of Figures

List of Tables

List of Symbols

Main notations for the models description:

- $\rho(t,x,y)$: Two dimensional density function
- $\vec{v}(t,x,y)$: Velocity function (vector)
- $\vec{\Phi}(t,x,y)$: Flux function (vector)
- $\vec{d_\theta}(t,x,y)$: Two dimensional direction field
- $\rho_0(x,y)$: Initial two dimensional density function
- $\rho_{\max}$: Maximum density (Constant)
- $v_{\max}$: Maximum velocity (Constant)
- ρ_{crit}: Critical density (Constant)
- $\rho_{\text{m}}(x,y)$: Space dependent maximum density
- $v_{\text{m}}(x,y)$: Space dependent maximum velocity
- $\rho_{\text{c}}(x,y)$: Space dependent critical density
- $\tilde{\rho}_{\max}$: Maximum of the space dependent maximum density
- $\rho^{\ell_1}(t,x,y)$: Two dimensional density function of the layer 1
- $\vec{v}^{\ell_1}(t,x,y)$: Velocity function (vector) of the layer 1
- $\vec{\Phi}^{\ell_1}(t,x,y)$: Flux function (vector) of the layer 1
- $\vec{d_\theta}^{\,\ell_1}(t,x,y)$: Two dimensional direction field of the layer 1
- Ψ^{ℓ_1}: Interaction term describing the impacts of the layers density to the layer 1

Main notations for the numerical methods

- $\Delta x, \Delta y$: Space discretization with respect to the x-axis and the y-axis, respectively
- Δt: Time step
- $(C_{\text{i,j}})_{i,j\in[0,\cdot,I]\times[0,\cdot,J]}$: Rectangular cells ($\Delta x \times \Delta y$ representing the space discretization.
- $\rho^n_{\text{i,j}}$: Discrete density in cell $C_{\text{i,j}}$ at time $t^n = t^0 + n \cdot \Delta t$
- $\theta_{\text{i,j}}$: Discrete flow direction in cell $C_{\text{i,j}}$

- $F_{i,j+\frac{1}{2}}$: Numerical flux at the interface between cells $C_{\mathrm{i,j}}$ and $C_{\mathrm{i,j+1}}$.
- Ω: Domain considered for simulation
- L_x, L_y: Spatial limits of the network
- $\rho^*_{i,j}, \rho^{**}_{i,j}, \rho^{inter}_{i,j}$: Intermediate computation of density used for the dimensional splitting
- $\rho^{\mathrm{TVD}_1}_{i,j}, \rho^{\mathrm{TVD}_2}_{i,j}$: Intermediate computation of density used for the TVD limiter
- $\rho^+_{i,j}, \rho^-_{i,j}$: Respectively the upper and lower limits of the WENO interpolation of the density in cell $C_{\mathrm{i,j}}$
- $L(\rho)$: Operator corresponding to the dimensional splitting used to describe the TVD limiter

Main notations for other methods

- Δt_{Aim}: Time steps of the Aimsun microsimulator. It equals 0.8s.
- (x^n_k, y^n_k): Position of the vehicles k of the microsimulation at time t^n
- $K(n)$: Total number of vehicles in the microsimulation at time t^n
- $G_{2d}(x, y)$: Gaussian kernel used for the reconstruction of a two-dimensional density.
- d_0: Range of the Gaussian kernel used for the reconstruction of a two-dimensional density.
- w: Weight function for the estimation of the direction field from the network geometry
- β: Parameter for the estimation of the direction field from the network
- $W_p(\rho^0, \rho^1)$: Wasserstein distance with norm p between two densities ρ^0 and ρ^1 of equal mass.
- $\mu_{j,k}$: Transfer of mass between the cell j of a first density distribution and the cell k of a second density distribution computed to approximate the Wasserstein distance
- $d_{j,k}$: Euclidean distance between the cell j and the cell k

List of acronyms

1D	One dimension
2D	Two dimensions
CBD	Central Business District
CFL	Courant-Friedrichs-Lewy
CTM	Cell Transmission model
FD	Fundamental Diagram
GPS	Global Positioning System
GTL	Grenoble Traffic Lab
KDE	Kernel Density Estimation
LWR	Lighthill Whitham Richards
MFD	Macroscopic Fundamental Diagram
OD	Origin-Destination
ODE	Ordinary Differential Equation
PDE	Partial Differential Equation
TTT	Total Traveling Time
TVD	Total Variation Diminishing
WENO	Weighted Essentially Non-Oscillatory

Summary

Objective

Traffic congestion is a common issue in most of the large cities in the world. The management of traffic networks is a complicated problem that is generally considered at the local level. To be able to take the right decision, the operator of traffic networks need to predict how traffic conditions are going to evolve in the next hours. The aim of this research is to design a suitable model to describe the evolution of the traffic conditions in a large scale network. One difficulty relies on finding a good balance between precision, reliability, aggregation and low numerical cost. This thesis focus on a particular family of models which describes traffic evolution through conservation laws with a two-dimensional density:

$$\begin{cases} \dfrac{\partial \rho}{\partial t}(t,x,y) + \nabla \cdot \vec{\Phi}(x,y,\rho(t,x,y)) = 0, & \forall t \in \mathbb{R}^+, \forall (x,y) \in \Omega \subset \mathbb{R}^2 \\ \rho(0,x,y) = \rho_0(x,y). & \forall (x,y) \in \Omega \end{cases} \tag{1}$$

This is an aggregated representation of traffic. The density ρ of cars is represented on a 2D-plane instead of on the road network. The flux $\vec{\Phi}$ is a vector that describes the magnitude and the direction in which traffic flow propagates.

Contribution

The main contribution is the development and the study of two-dimensional macroscopic traffic flow models. In practice, this contribution can be split as follows:

1. Modeling: We gradually extend the two-dimensional model first from a simple model for homogeneous networks with a dominant traffic direction, then to a model with space-dependent flux adapted for heterogeneous networks but still with a dominant traffic direction and finally to a multidirectional model based on several layers of densities. These successive extensions enable us to approach progressively a more realistic scenario.

2. Methodology for parameters estimation: We develop methods to estimate the direction field by using first the network topology and then using data of vehicles trajectories, and the parameters of the fundamental diagram.

3. Simulation and validation: We suggest numerical methods, we design scenarios for simulation and we present comparison and validation using microsimulation.

Research dissemination: Conferences and publications

Journal Papers:

- Stéphane Mollier, Maria Laura Delle Monache, Carlos Canudas de Wit. A simple example of two dimensional model for traffic: discussion about assumptions and numerical methods. Transportation Research Record (TRR), Journal of the Transportation Research Board, 2018, pp.1-20. `https://hal.archives-ouvertes.fr/hal-01665285/document`.
- Stéphane Mollier, Maria Laura Delle Monache, Carlos Canudas de Wit, Benjamin Seibold. Two-dimensional macroscopic model for large scale traffic networks. Transportation Research Part B: Methodological, Elsevier, 2019, 122, pp.309-326. `https://hal.archives-ouvertes.fr/hal-01819013/document`.

Conference Papers:

- Stéphane Mollier, Maria Laura Delle Monache, Carlos Canudas-de-Wit. 2D-LWR in large-scale network with space dependent fundemental digram. ITSC 2018 - 21st IEEE International Conference on Intelligent Transportation Systems, Nov 2018, Maui, United States. pp. 1-8 (hal-01866959) `https://hal.archives-ouvertes.fr/hal-01866959/document`.
- Stéphane Mollier, Maria Laura Delle Monache, Carlos Canudas de Wit. A step towards a multidirectional 2D model for large scale traffic networks. TRB 2019 - 98th Annual Meeting Transportation Research Board, Jan 2019, Washington D.C., United States. pp.1-7. `https://hal.archives-ouvertes.fr/hal-01948466/document`.
- Stéphane Mollier, Maria Laura Delle Monache, Carlos Canudas de Wit. A decision support and planning mobility method for large scale traffic network. ECC 2019 - European Control Conference, June 2019, Naples, Italy. `https://hal.archives-ouvertes.fr/hal-02157899/document`.

Workshops, conferences and presentations:

- Transport Modeling and Management: Vehicles and Crowds VIII Workshop on the Mathematical Foundations of Traffic Rome, March 6-10, 2017 (Attendee)
- Modeling Reduction Tools for Large Scale Complex Networks ERC Scale-FreeBack, Workshop, September 21-22, 2017, Grenoble France (Talk)
- TRB 2018. Transportation Research Board - 97th Annual Meeting. January 7-11, 2018, Washington, D.C., USA (Poster presentation)
- CTS 2018, 15th IFAC Symposium on Control in Transportation Systems, June 6-8, 2018, Savona, Italy (Attendee)

- PhD Days DAUTO 2019, Midterm presentation for PhD of Gipsa-lab DAUTO department, June 21st, Grenoble, France (Talk)
- Analysis and Control of Large Scale Complex Networks ERC Scale-FreeBack, Workshop, September 10-11, 2018, Grenoble France (Poster Presentation)
- MATTS 2018, Mathematics Applied in Transport and Traffic Systems, October 17-19, 2018, Delft Netherlands (Talk)
- TRB 2019. Transportation Research Board - 98th Annual Meeting. January 13-17, 2019, Washington, D.C., USA (Poster presentation)
- Applied Mathematics and Scientific Computing Seminar, January 23, 2019, Temple University, Philadelphia, USA (Talk)
- GTATT 2019, Groupe de Travail Automatique et Transport Terrestre, January 29-30, Grenoble, France (Poster presentation).

Introduction

Contents

0.1 Traffic modeling on a road

0.1.1 History of traffic flow

The modeling of traffic flow started in the 30s. One of the first study [24] was led by B. D. Greenshields who was interested in analyzing traffic behavior. He sat along the road and started to collect data on traffic behavior, see an example in Figure 1. The observation of traffic conditions can be done through different variables -speed v, flow Φ, density ρ- that are all derived from the vehicles' position. The speed or acceleration are obtained from successive vehicles position over time. The flow is the number of vehicles passing by a position during a given interval of time. The density, or concentration, of vehicles is the measure of the inverse of the distance between vehicles (called headway for two vehicles). When Greenshield put his data together and computed the main variables of traffic, he noticed that there is a linear relation between the density of vehicles and their speed. The flow, product of the speed and the density, has a concave shape as it can be seen in Figure 2. This relation between flow and density is called fundamental diagram (FD). One can notice, that the flow is maximal for an intermediate level of density. For control applications, it is interesting to maintain the traffic density at this level to maximize the production of the network.
Later, a lot of different shapes of fundamental diagrams have been investigated, see [51], [18]. A review of the main ones is presented in [6]. These fundamental diagrams are based on the assumption that the speed can be expressed only as a function of the density. In practice, most of the fundamental diagrams have the following properties on the flow function Φ:

Figure 1: Observation of traffic and data collection done by Greenshield in 1933. Source [24]

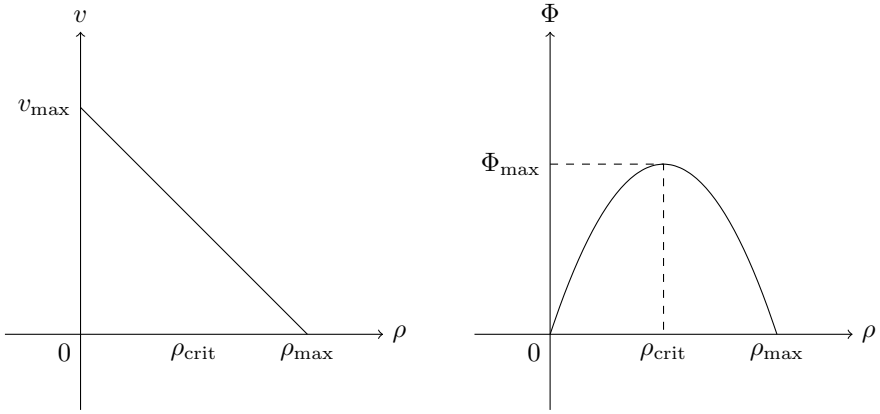

(a) Relation velocity-density (b) Relation flux-density (FD)

Figure 2: Speed and flow vs. density

- Φ is a continuous function defined on $[0, \rho_{\max}]$ where $\rho_{\max}$ correspond to the maximum density, the density of a fully congested road.
- Φ is a concave function
- $\Phi(0) = \Phi(\rho_{\max}) = 0$: the flux of vehicles goes to zero when the density goes to $\rho_{\max}$

The Fundamental Diagram can not be used directly to predict traffic flow evolution but it is useful for many models. After this first study, numerous modeling approaches have been developed. The main ones are described below.
First, a distinction can be made between static models and dynamic models. Static models aim to describe traffic flow in steady state conditions. These models can be useful to locate the position of bottlenecks and then improve the design of the network. Dynamic models aim to represent traffic evolving in real-time. They can be used to improve traffic condition using real-time control and to predict the evolution of traffic in case of an emergency.
Further, one can distinguish microscopic, mesoscopic and macroscopic models. Microscopic models describe traffic by modeling the dynamics of each vehicle by an ordinary differential

equation (ODE). One of the first models suggested, the car-following model, defines the acceleration of vehicles as a function of the distance of the vehicle in front [52]. Tools have been developed using this family of models as Aimsun or Vissim. However, these models can be too expensive for large scale traffic networks. Indeed, they require to tune a lot of parameters that are generally not known. Furthermore, there is generally random effect in the simulation such that a run of simulation can appear to be very specific.
Macroscopic models attempt to predict traffic evolution with macroscopic quantities, such as the density and the average speed of vehicles. The most known macroscopic model was proposed independently by Lighthill and Whithmam and by Richards and is called LWR model. This category of models is the one considered in this thesis and it will be described more in detail in the next section.
Mesoscopic models approach traffic modeling at an intermediate representation scale, between macroscopic and microscopic models. In mesoscopic modeling, a distribution function is considered, usually denoted f, which, for every position x and every velocity v gives the density of vehicles at position x with speed v. The usual macroscopic density ρ can be recovered by integration of f:

$$\rho(t,x) = \int_0^\infty f(t,x,v)dv. \tag{2}$$

Mesoscopic models contain more information than macroscopic ones but also lead to more complex problems.
A very general review of traffic modeling with the different family of models is done in [64].

0.1.2 The LWR model

Presentation LWR model:
In the fifties Lighthill, Whitham and independently Richards [41], [54] introduced a hydrodynamic model (LWR model) for traffic flow. This model is inspired from fluid dynamics. As mentioned previously, this model is based on the hypothesis that the velocity $v \in [0, v_{\max}]$ depends only on the main traffic density $\rho \in [0, \rho_{\max}]$. In the LWR model the flux function is given by $\Phi(\rho) : \rho(t,x) \in [0, \rho_{\max}] \to v(\rho(t,x))\rho(t,x) \in \mathbb{R}$.
The evolution in time of the main traffic density is given by the following scalar conservation law:

$$\begin{cases} \dfrac{\partial \rho(t,x)}{\partial t} + \dfrac{\partial \Phi(\rho(t,x))}{\partial x} = 0 & (t,x) \in \mathbb{R}^+ \times \mathbb{R} \\ \rho(0,x) = \rho_0(x). & x \in \mathbb{R} \end{cases} \tag{3}$$

Where the velocity and the flux are given by:

$$v(\rho) = \Big(1 - \frac{\rho}{\rho_{\max}}\Big) v_{\max} \tag{4}$$

$$\Phi(\rho) = \rho\Big(1 - \frac{\rho}{\rho_{\max}}\Big) v_{\max} \tag{5}$$

Generally, the density for which the flow is maximum is denoted critical density ρ_{crit}. A traffic state is considered in congestion if the density is higher than the critical density and is

considered in free flow if the density is lower than the critical density.
The number vehicles n_{veh}, also called mass, can be reconstructed by integrating the density over the roads:

$$n_{\text{veh}} = \int_{x_a}^{x_b} \rho(t,x)dx \tag{6}$$

Riemann problem and analysis of solutions:
The LWR model is a nonlinear conservation law due to the dependency between the velocity and the density. The first building block to construct a solution is to consider the Riemann problem i.e., to study the equation with the following initial condition:

$$\rho(0,x) = \begin{cases} \rho^- & \text{if } x < 0 \\ \rho^+ & \text{if } x \geq 0 \end{cases} \tag{7}$$

If $\rho^- \leq \rho^+$, then the solution is a shock wave as it is represented in Figure 3 and the speed of propagation λ of the wave is given by the Rankine-Hugoniot condition:

$$\lambda = \frac{\Phi(\rho^+) - \Phi(\rho^-)}{\rho^+ - \rho^-}. \tag{8}$$

If the state is globally congested, then λ is negative and the shock waves will move backward. If the traffic states is in free flow, the λ is positive and the shock wave will move forward. In

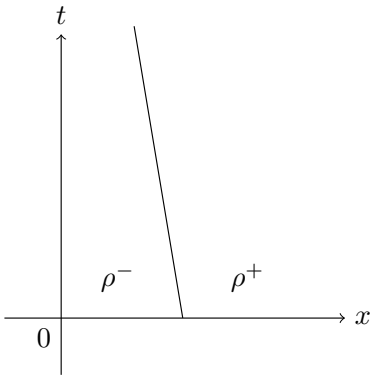

Figure 3: Representation of a shock wave

physical traffic systems, a shock is an upstream end of a traffic jam.
If $\rho^- \geq \rho^+$, then the solution is a rarefaction wave and we have a fan of waves of densities going progressively from the density on the left ρ^- to the density on the right ρ^+. A visual representation is given in Figure 4. A physical example of these rarefaction waves can be observed next to a traffic light. When the light turn green, a rarefaction wave is generated.
Numerical methods:
Many numerical methods available in the literature to approximate the solutions are based on finite volume methods. Let $(x_{\text{i}})_{i\in[1..I]}$ be a regular space discretization with step Δx. Let $(t^{\text{n}})_{n\in[1..N]}$ be the time discretization with step Δt.
Then, the discrete density $(\rho_{\text{i}})_{i\in[1..I]}$ can be defined as a step function such that for any discrete

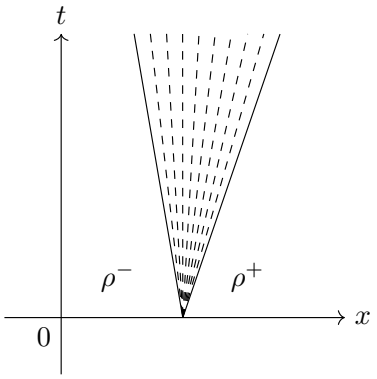

Figure 4: Representation of a rarefaction wave

time:

$$\rho_{\mathrm{i}}(t^{\mathrm{n}}) = \int_{x_{\mathrm{i}}}^{x_{\mathrm{i+1}}} \rho(t^{\mathrm{n}}, x)dx \tag{9}$$

To update this discrete density we need to introduce the notion of flux at the interface $(F_{\mathrm{i}+\frac{1}{2}})_{i\in[1,\cdots,I]}$. This flux represent the transfer of mass between the discrete density ρ_{i} and its neighbour $\rho_{\mathrm{i+1}}$. The notation can be visualized in Figure 5. Then, the density at time t^n

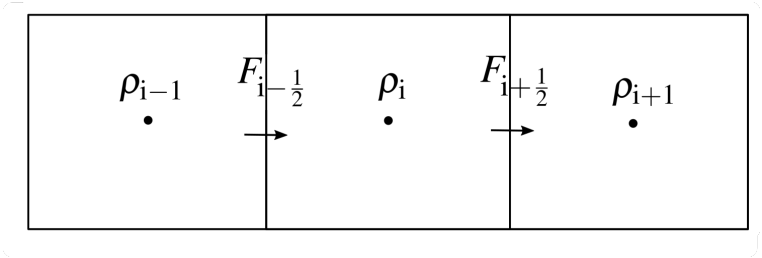

Figure 5: Notations for the space discretization

can be updated as follows $\forall i \in [1, \cdots, I]$:

$$\rho_i^{t^{n+1}} = \rho_i^{t^n} - \frac{\Delta t}{\Delta x}\left(F_{\mathrm{i}+\frac{1}{2}} - F_{\mathrm{i}-\frac{1}{2}}\right) \tag{10}$$

There exists different methods to compute the flux at the interface. The Godunov flux, introduced first in [22], is a classical one to solve the LWR equation and is described as follows:

$$F_{\mathrm{i}+\frac{1}{2}} = F(\rho_i, \rho_{i+1}) = \begin{cases} \min(\Phi(\rho_i), \Phi(\rho_{i+1})), & \text{if } \rho_i < \rho_{i+1} \\ \Phi(\rho_i), & \text{if } \rho_{i+1} \leq \rho_i \leq \rho_{\mathrm{crit}} \\ \Phi(\rho_{i+1}), & \text{if } \rho_{\mathrm{crit}} \leq \rho_{i+1} \leq \rho_i \\ \Phi_{\max}, & \text{if } \rho_{i+1} \leq \rho_{\mathrm{crit}} \leq \rho_i. \end{cases} \tag{11}$$

Later, an equivalent formulation based on traffic demand and traffic supply called Cell Transmission model (CTM) is suggested by [11]. The demand function $(D_i)_{i\in[1,\cdots,I]}$ corresponds to the flux of vehicles that are willing to leave the link i. Its shape, that we can see in Figure 6, is equal to the fundamental diagram for a density lower than the critical density ρ_{crit} and

equal to the maximum flux when the road is congested. The supply function $(S_i)_{i\in[1,\cdots,I]}$ corresponds to the flux that can enter the cell i. Its shape, displayed in Figure 6, contrary to the demand, is maximal if the density is lower than ρ_{crit} and given by the fundamental diagram otherwise. Then, the flux at the interface between two cells is given by the relation:

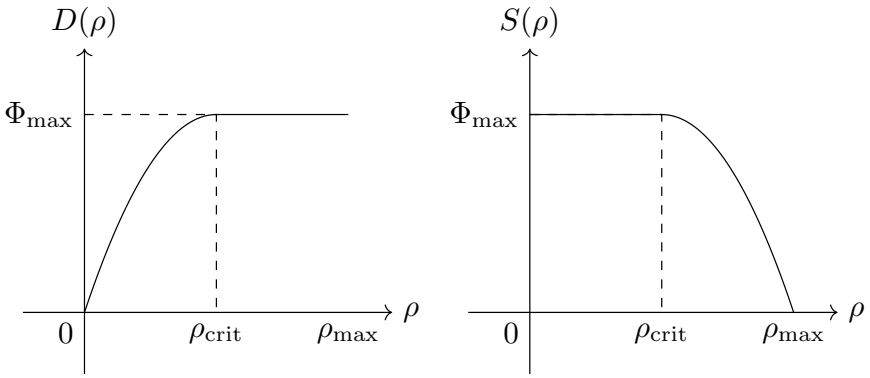

Figure 6: Example of demand (left) and supply (right) functions used by the CTM

$$F_{\mathrm{i}+\frac{1}{2}} = \min(D_{\mathrm{i}}, S_{\mathrm{i}+1}). \tag{12}$$

The Godunov scheme and the Cell Transmission model are different notation for the same method.

0.2 Traffic modeling on a network

Traffic congestion exists in many cities around the world and not only at the local level of an individual road but also at the city network. Therefore, the modeling of the traffic in an individual road presented previously need to be extended to the modeling of a network.

0.2.1 Network modeling: models of junctions

Traffic networks are described by graphs where the nodes are the junctions (intersections) and the links the roads. Each link can be partitioned into cells and the propagation can be based on the Cell Transmission model.
Network models aim to combine modeling on different links as previously described using models of junctions. These models aim to maximize the flow through the intersection and have been proposed first in [10], [37] and a full description is available in [19]. To exemplify, let us consider the problem of a 2×2 intersection. We denote by a and b the entering links and by c and d the exiting ones as represented in Figure 7. To describe the directions chosen by the vehicles, the notion of split ratio is introduced. A split ratio is the percentage of vehicles coming from an entering link that goes to an exiting link. Let F_a, F_a be the flows of vehicles that go through the junction distributing respectively with the following split ratios:

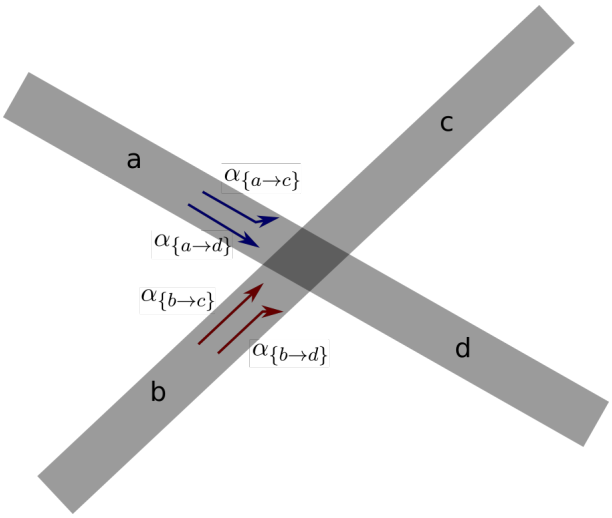

Figure 7: Representation of a 2×2 intersection. The links a and b correspond to entering roads and the links c and d correspond to exiting roads.

- $\alpha_{\{a\to c\}}$ from node a to c
- $\alpha_{\{a\to d\}}$ from node b to c
- $\alpha_{\{b\to c\}}$ from node a to d
- $\alpha_{\{b\to d\}}$ from node b to d

with $\alpha_{\{a\to c\}} + \alpha_{\{a\to d\}} = 1$ and $\alpha_{\{b\to c\}} + \alpha_{\{b\to d\}} = 1$ that ensure that no vehicles are lost or created in the junction.
We denote by D_a, D_b and S_c, S_d respectively the demand of the entering link and the supply of the exiting links. Then, the model try to maximize the flux through the junction:

$$\max\left(F_a + F_b\right) \tag{13}$$

with the following constraints:

- $F_a \leq D_a$
- $F_b \leq D_b$
- $\alpha_{\{\mathrm{a}\to\mathrm{c}\}} F_{\mathrm{a}} + \alpha_{\{\mathrm{b}\to\mathrm{c}\}} F_{\mathrm{b}} \leq S_{\mathrm{c}}$
- $\alpha_{\{a\to d\}} F_d + \alpha_{\{b\to d\}} F_b \leq S_d$

The maximization problem with constraints can be understood with Figure 8. Visually, the solution is the point that maximizes the sum of the x and y coordinates and remains below the four straight lines. In Figure 8, the two pictures represent two example of this maximum problem.

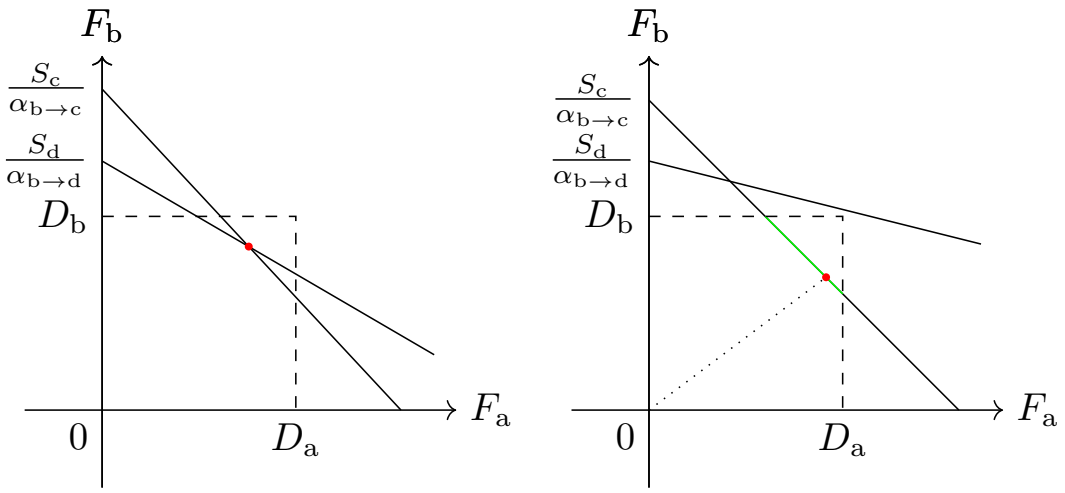

Figure 8: Visualisation of the solution of two examples for the 2×2 junction problem.

In the left picture, the dashed lines correspond to the demand constraint and the full lines correspond to the supply constraint. The solution is the point that maximizes the flux in the intersection. It corresponds in this example to the intersection point between the two full lines, represented in red. Thus, the active constraints in this intersection are the supply constraints of the two outgoing roads c and d.
In the right picture, the dashed lines and the full lines correspond respectively to the demand and supply constraints. Contrary to the previous example, only the supply of the outgoing c is active which mean that the road c is already partially occupied. However, there is an infinite number of solution, represented by the line in green, satisfying the constraint and maximizing the flux through the intersection. In this situation, we need to introduce the notion of priority $P_{\frac{a}{b}} \in \mathbb{R}^+$. The priority $P_{\frac{a}{b}}$ gives the ratio of vehicles from the ingoing road a over vehicles from the outgoing road b that can go through the intersection. If $P_{\frac{a}{b}}$ is close to zero, it means that the priority is given to vehicles from the road b. If $P_{\frac{a}{b}} = 1$, then the same number of vehicle from a and b can cross the interaction. In Figure 8, an example of priority in favor of the flux F_a is represented by a dotted line. The solution is at the intersection of the constraint with the dotted line of coeficient $P_{\frac{a}{b}}$ and is represented in red. This is an example of priority slightly advantageous for the flow coming from the link a.
This model can be extended to any number of entering or exiting roads. Furthermore, some specific model can be developed to describe different types of junction. For instance, the case of the roundabout is investigated in [53]. However, when the scale of the network is too large, the numerical cost of this kind of model can be very high. Then, it is beneficial to consider aggregated models in these situations. Aggregated models aim to represent complex physical systems with a high level of abstraction. They contain fewer details than the classical models but they give a simple representation useful in practice.

0.2.2 Static continuous models

In the early development of traffic modeling in urban areas, some aggregated models, continuous and two-dimensional have been investigated [4]. However, these studies only consider the case of static models and can not describe the evolution of traffic in real-time. Authors represent the traffic states in the 2D-plane using densities of vehicles per area. An overview of static models in two dimensions is available in [27].
These models aim to find the equilibrium of traffic networks in order to identify possible bottlenecks or weaknesses of the network. This is interesting in order to design a new network and make it more resilient to future congestion.
In [66], a two-dimensional static model is presented in order to describe the traffic flow distribution in the peak hour in an urban area. This urban area contains two Central Business Districts (CBD). Then, the drivers are split into two layers depending of which CBD they are trying to join. The conservation equation in steady states in a domain Ω is defined as follows:

$$\nabla f_l(x, y) + q_l(x, y) = 0, \quad \forall (x, y) \in \Omega \tag{14}$$

where l represent the layer considered, f the flow of vehicles and q their demand generation. The direction taken by the flux function is computed using a cost function such that drivers try to avoid congested area. This enables to compute the flux of vehicles at equilibrium for any position. Thus, the part of the network tense in term of traffic congestion could be reinforced in network construction to avoid creating a bottleneck. An example of results is given in Figure 9. In this case, the traffic flow is higher around the two CBDs.

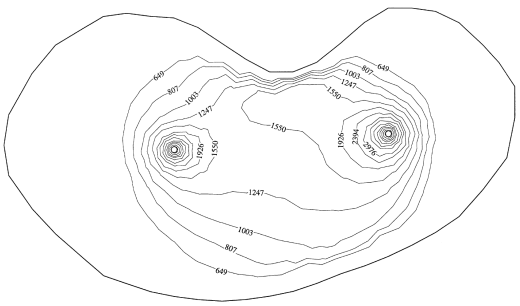

Figure 9: Example of 2D static simulation to estimate traffic flow at the equilibrium. Image from [66].

Two-dimensional static modeling is an interesting option to study the equilibrium state even for a very large network. However, these model can not be apply in real time situation and thus are not able to react to a unusual event -accident, big crowd.

0.2.3 Macroscopic Fundamental Diagram: Multi-reservoir models

Among the large-scale models, another important field of research concentrates on the notion of Macroscopic (or Network) Fundamental Diagram (MFD). Starting with some empirical observation of traffic in a city, [12] and [20] show that it is possible to exhibit a relation

between the average density and the average flow over a whole network. In practice, the shape of the link between these average quantities is quite similar to the classical FD and thus leads to the name of MFD. A figure of the first MFD reconstructed from real data is displayed in Figure 10.

This result enables the introduction of accumulation models — also called reservoir models —

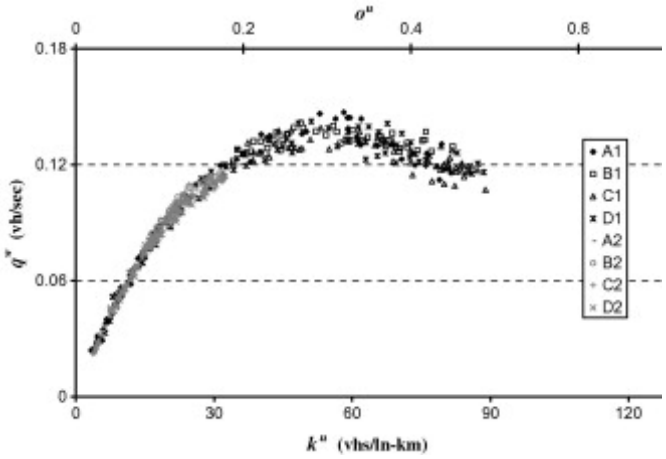

Figure 10: Estimation of the MFD from real sensor loop data that represent average flux vs average occupancy. Image taken from [20].

which consist of representing the traffic state of a network by the total number or accumulation, $n(t)$, of vehicles within the network. The reservoir could represent a road network of different size: a town, a district or even a large city. These models can be formulated as follows:

$$\frac{dn}{dt}(t) = \Phi_{in}(t) - \Phi_{out}(n(t)), \qquad \forall t \in \mathbb{R}^+ \tag{15}$$

where n represent the cumulative number of cars in the considered area, Φ_{in} and Φ_{out} are the

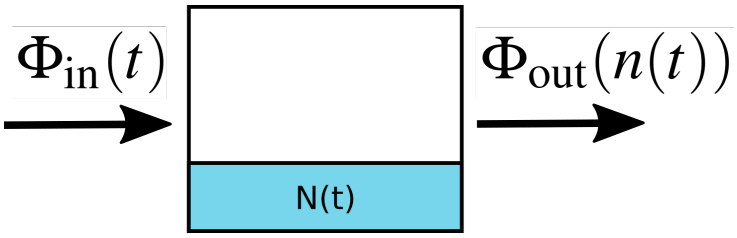

Figure 11: Representation of a reservoir of the MFD-based model

area inflow and outflow, respectively. In this set-up, the inputs are the initial accumulation of vehicles, $n(0)$, and the inflow at all time, $\Phi_{in}(t)$. The outflow $\Phi_{out}(t)$ is computed using the concept of MFD and the trip length L of vehicles across the reservoir and assumed to be known:

$$\Phi_{out}(t) = \frac{n(t)\bar{V}(n(t))}{L}, \qquad \forall t \in \mathbb{R}^+ \tag{16}$$

where $\bar{V}$ is the mean speed of vehicles over the network and is given by the MFD. The product $n(t) \times \bar{V}(n(t))$ represents the production of the network i.e. the distance traveled by all the

vehicles within the network. Then, in this framework, it means that a vehicle completes his destination each time a distance L is produced by the network. It is interesting to notice that it can describe both a vehicle exiting the network or parking within the network. However, some limitation of this first approach were identified:

- The assumption that all the users of the network have the same trip length may not be always realistic.
- The model is sensitive to fast variations of the inflows see [45]. Indeed, vehicles entering the network contribute directly to increase the outflow. Then, vehicles entering an empty network have an infinite speed of propagation.
- A reservoir can only contain roads with similar traffic condition which is generally not for very large urban network.

A new computational method has been suggested in [38] and [36] in order to face some of these issues. The concept is to synchronize the update of the model with the vehicles leaving or entering the network instead of using a constant time step.
Then, the speed of vehicles is a function of the accumulation of vehicles and the accumulation changes only when a vehicle enter or leave the network. Thus, for a known trip length of vehicles (not necessarily constant among vehicle anymore), it is possible to compute when and which vehicle will exit the network. Each time a vehicle enters or leaves the network the accumulation $n(t)$ changes and a new mean speed for vehicles $V(n(t))$ is computed. We can remark that, when a vehicle enters or exits the network, the updates of the accumulation and the mean speed change the time for which vehicles are staying in the network. If the flow production decreases, the exit of vehicles is delayed whereas if the flow production increases, it is shortened. However, the order in which the vehicles are leaving is preserved. Using this approach the vehicles exit the network after completing their individual distance trip. Then, it canceled the issue of the infinite speed of vehicles entering an empty network.
An additional point to take into consideration, is that vehicles are not homogeneously distributed over traffic networks for every time of the days especially when a very large area is considered. Thus, a half congested MFD based model can describe different situations. It could be that all the roads are half congested or that half of the network is fully congested and the rest is totally empty. To reduce this effect, researchers investigated the division of a very large network into several reservoirs [39], and [25]. With this division, it is easier to obtain similar traffic condition within each reservoir. A method to build the clustering based on data can be found in [57]. Moreover, a multi-reservoir model required a methodology to do the merging between the reservoirs. This kind of interaction can create spillbacks as it is developed in [44]. To conclude, MFD-based models are practical because they are understandable, with few parameters to tune and a low computational cost. However, they contain little spatial information about the traffic states. and they are not able to describe precisely where vehicles are located over the reservoirs. Thus, in some situations, the formulation of the exchanges between different reservoirs may be tedious.

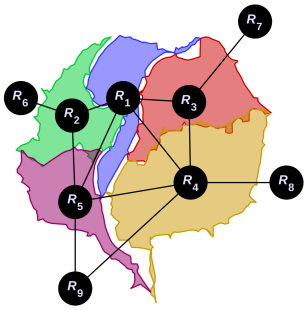

Figure 12: Example of multi-reservoirs MFD simulation in the city of Lyon. Image from [43]

0.3 State of the art of 2D models

0.3.1 Two-dimensional models for traffic networks

Traffic in urban areas can be modeled by two-dimensional continuous and dynamic models. These models aim to be aggregated models but one level under the MFD-based model such that more information about the spatial distribution of vehicle and congestion could be known. A review of some of these models has been done by [2]. These models represent the traffic density ρ as a variable over a 2D-plane $(x, y) \in \Omega$. Such models are based on a two-dimensional conservation law and take the following general structure:

$$\begin{cases} \frac{\partial \rho(t,x,y)}{\partial t} + \nabla \cdot \vec{\Phi}(\rho(t,x,y)) = 0 \\ \rho(0,x,y) = \rho_0(x,y) \end{cases}, \qquad \forall t \in \mathbb{R}^+, \forall (x,y) \in \Omega \tag{17}$$

where ρ is the aggregated density and $\vec{\Phi}$ the flow vector defined as the product of the density ρ and velocity field vector $\vec{v}$.
A first assumption for the application of this kind of equations to traffic is to consider that the urban network is dense enough to be approximated as a continuum. Generally, 2D models are not expected to describe very precisely the density evolution at space coordinates, but focus more on capturing the main traffic features and the global evolution of the density. The literature concerning this type of models is scarce, but there are several studies which start considering the problem. First, in [55], an advection diffusion equation is introduced with a function of flux $\vec{\Phi}$ that depends on the space coordinates instead of depending on the density. Thus, the velocity is predetermined and the equation becomes linear. Another study ([13]) considers a model including a diffusion term and a drift term dependent on the density. The direction of the drift vector is fixed in some area and is determined by the shape of the network. The diffusion term is used to describe the tendency of drivers to avoid highly congested areas. However, it also enables some nonphysical trajectories as vehicles moving backward in front of important congestion independently of their destination. In [32] and [14], the authors take inspiration from pedestrian modeling in order to model vehicular traffic. They define the flux $\vec{\Phi}$ by solving an Eikonal equation such that the flow follows the path of the lowest cost — usually in terms of travel time, but other criteria could be used as well. Another extension of this model is done in [31]. Their extension considers a second order equation such that

it improves the description of the vehicle acceleration in the aim of pollutant estimation. In [58] and [60], the authors investigate the representation of intersections and how it could be interpreted in a 2D model. Following this idea, they take inspiration of junction models in one dimension like [37] and build extensions to 2D models. Lastly, in [26], [9], [62], the authors consider two-dimensional models for the case of multilane roads instead of a road network. Thus, the methodology and the model have several similarities but the objectives and the results are different.
However, in all the 2D models introduced previously, the direction of the flow at a given space and time position is unique. Thus, these models are not able to describe the multiple origin destination that can exist in a real traffic scenario. A possible solution is to consider multiple layers of density such that each layer can represent a main direction of flow. A first and interesting study in this direction of research is done in [42]. Nevertheless, the model suggested, inspired from pedestrian models, is not based on the road network and thus, for instance, does not assume that traffic flow density has a maximal value. Lastly, another paper [1] proposes a two-dimensional model considering multiple origins and destinations and aims to create a link between the two-dimensional approach and the MFD based model.

0.3.2 Another application of the 2D representation: Pedestrian modeling

In this thesis, the model we develop does not aim to be applicable for pedestrians. However, the existing models for pedestrians have a similar mathematical formulation and thus, are interesting to study.
Pedestrian modeling is used to predict and improve potential evacuations of a crowd in case of emergencies. The same way, it has been developed for traffic, there is a microscopic approach that describes the trajectories of each pedestrian and a macroscopic approach that is interested in aggregated quantities.
One of the well know microscopic approach is called agent based model [34]. In this model, each pedestrian, called agent, define his trajectories to achieve their final target and to avoid collision with other pedestrian. This method can be very useful in particular to describe the behavior of a pedestrian group. However, these methods require a lot computation which could make them inappropriate to simulate a very large crown evacuation.
The macroscopic approach for pedestrian is, contrary to traffic flow modeling, naturally 2D. Thus, 2D traffic model has many similarities with pedestrians modeling: both are 2D conservation laws, with the notion of a flux vector and a two-dimensional density. The main difference is that pedestrian evolves in a 2D environment whereas traffic flow is constraint by the network. Furthermore, pedestrians dynamic creates phenomenons that are not observed in traffic flow such as the lane formation. This phenomena appears in the case of two highly congested crowds walking in opposite direction. Pedestrians react by taking a structure in lane to reduce the probability collision. An example can be seen in Figure 13. This phenomena and other as flow crossing can also be reproduced by finite volume method [29].
In a traffic network, the circulation of car is constrained by the network rather by the avoidance of collision as in pedestrians modeling. Then, phenomena like lane formation probably does not exists in traffic model on network. For this reason, the structure of the two-dimensional

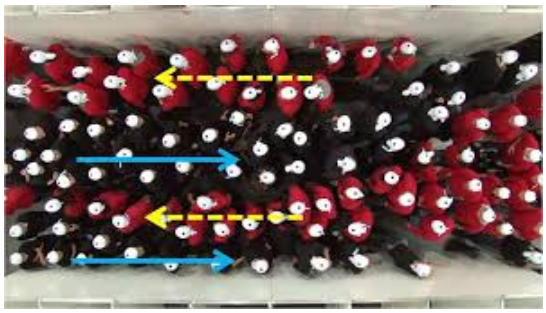

Figure 13: Observation of lane formation in a real experiment done by [67]

model we consider should be different to the two-dimensional pedestrian model and thus we do not investigate direction of flow based Eikonal equation in this manuscript.

Outline of the thesis

This thesis aims to develop new extensions for 2D models and devise methods for their calibration and their validation.
The manuscript is organized as follows:

- In Chapter 1, we aim to give a general background of the methods considered in this thesis. First, we discuss the physical meaning of the two-dimensional conservation law. Then, we present the dimensional splitting and finite volume methods which are the main numerical methods used for the simulations. Finally, we develop a method to compare the two-dimensional model with trajectories obtained by microsimulation and using the software Aimsun.

- In Chapter 2, we consider a simple model in two-dimensional space to describe a homogeneous network with a preferred direction of flow propagation. A homogeneous network has the same speed limits and a similar concentration of roads everywhere. The density evolves according to a direction field estimated from the network geometry. First, the simulation results of the model are compared with network modeling which corresponds to the CTM combined with models of junctions. Then, another method of validation using GPS probes from microsimulation is provided.

- In Chapter 3, we consider a space-dependent extension of the model to describe a heterogeneous network with a preferred direction of flow propagation. A heterogeneous network has different speed limits and a variable concentration of roads. Such networks are of interest because they can show how bottleneck affects traffic dynamics. The results of simulations and the comparison with microsimulation are presented.

- In Chapter 4, for the case of multiple directions of flow, we consider a system of equations with multiple layers of density. We show that these models are not always hyperbolic. Thus, we develop certain numerical methods to solve them. On the other hand, the estimation of the direction field using network geometry may not be suitable for modeling several flow directions. Thus, we present an estimation method based on optimal transport and density data.

- In Chapter 5, we present a study case applied to the city center of Grenoble. The scenario of the simulation considers a portion of the real Grenoble network and uses the data from some existing sensors loops. The thesis is part of a European Project, ERC Scale-FreeBack, that aims to develop modeling, control and estimation methods for traffic flow on large scale network and Grenoble will be considered as the city of validation.

Chapter 1

Methodology: Theory, numerical method and microsimulation

Contents

In this chapter, we first present some discussions about multidimensional conservation laws. Then, we introduce the numerical method used for simulations. A method of comparison and validation of the model using microsimulation is presented.

1.1 Background and physical representation of two-dimensional conservation laws

1.1.1 Origin and derivation of the equation

First, one could be interested in knowing where the two-dimensional conservation that we consider in this work come from. It is possible to derive a two-dimensional balance equation in a domain $\Omega \subset \mathbb{R}^2$ using the conservation of the mass. Let $A \subset \Omega$ be an arbitrary subdomain,

$n_{\mathrm{A}}(t)$ the number the vehicle within A at time t and $n_{\mathrm{in}}^{\Delta \mathrm{t}}$, $n_{\mathrm{out}}^{\Delta \mathrm{t}}$ the number of vehicles which respectively enter and exit A between t and $t + \Delta t$. Then:

$$n_{\mathrm{A}}(t + \Delta t) - n_{\mathrm{A}}(t) = n_{\mathrm{in}}^{\Delta \mathrm{t}} - n_{\mathrm{out}}^{\Delta \mathrm{t}}, \qquad \forall t \in \mathbb{R}^+ \tag{1.1}$$

dividing by Δt and passing at the limit when $\Delta t \to 0$, we obtain:

$$\frac{\partial \Big(n_{\mathrm{A}}(t) \Big)}{\partial t} = \Phi_{\mathrm{in}}(t) - \Phi_{\mathrm{out}}(t), \qquad \forall t \in \mathbb{R}^+ \tag{1.2}$$

where Φ_{in} the inflow and Φ_{out} the outflow of the subdomain A.
We define the density of vehicle $\rho(t, x, y) : \mathbb{R}_+ \times \Omega \to [0, \rho_{\max}]$ and the flux of vehicle $\vec{\Phi}(t, x, y, \rho) : \mathbb{R}_+ \times \Omega \times [0, \rho_{\max}] \to \mathbb{R}^2$. By definition of the density and the flux, we have:

$$\frac{\partial}{\partial t}(\iint\limits_A \rho(t, x, y)\, dx\, dy) = - \oint\limits_{\partial A} \vec{\Phi}(t, x, y, \rho) \cdot \vec{n}(x, y)\, dl, \qquad \forall t \in \mathbb{R}^+ \tag{1.3}$$

where $\vec{n}$ is the vector normal to the boundary and l the variable which follows the boundary of the subdomain.
Thanks to the divergence theorem, we have:

$$\iint\limits_A \frac{\partial \rho(t, x, y)}{\partial t}\, dx\, dy = - \iint\limits_A \nabla \cdot \vec{\Phi}(t, x, y, \rho)\, dx\, dy, \qquad \forall t \in \mathbb{R}^+. \tag{1.4}$$

The equality (1.4) hold for all $A \subset \Omega$, therefore we get:

$$\frac{\partial \rho}{\partial t}(t, x, y) + \nabla \cdot \vec{\Phi}(t, x, y, \rho) = 0, \qquad \forall t \in \mathbb{R}^+, \forall (x, y) \in \Omega \tag{1.5}$$

This equation is completed with the following initial condition:

$$\rho(0, x, y) = \rho_0(x, y). \qquad \forall (x, y) \in \Omega \tag{1.6}$$

As it is always the case in physics, the flow can be rewritten as the product of density of speed:

$$\vec{\Phi} = \rho \dot{\vec{v}} \vec{d}_\theta \tag{1.7}$$

where ρ is the density, v the magnitude of the speed and $\vec{d_\theta}$ his direction.

1.1.2 Existence of solution and Riemann problem in 2D:

The existence and uniqueness of solution have been studied in [35] for equation (1.5) and more generally for conservation laws that can be expressed as:

$$\frac{\partial \rho}{\partial t}(t, x) + \sum_{i=1}^{n} \frac{\partial \Phi(t, x, \rho)}{\partial x_i} = S(t, x, \rho) \tag{1.8}$$

where $\rho \in \mathbb{R}$, $x \in \mathbb{R}^n$ and Φ, $S : \mathbb{R}^+ \times \mathbb{R}^n \times \mathbb{R} \to \mathbb{R}$ can be seen respectively as the flux and the source function. A notion of generalized solution is introduced and the existence

and uniqueness is proven for this equation and this definition of solution under conditions of smoothness and bounded of the function Φ and S. Existence and uniqueness of solution have been studied more recently in [33] and [56].

The two-dimensional Riemann problem:

Later, the Riemann problem in two dimension has been investigated in [65]. Similarly to the one dimensional case, the Riemann problem in 2D aims to solve equation (1.5) with the following initial value problem:

$$\rho(0,x,y) = \begin{cases} \rho_1 & \text{if } x \geq 0 \text{ and } y \geq 0 \\ \rho_2 & \text{if } x \leq 0 \text{ and } y \geq 0 \\ \rho_3 & \text{if } x \leq 0 \text{ and } y \leq 0 \\ \rho_4 & \text{if } x \geq 0 \text{ and } y \leq 0 \end{cases} \tag{1.9}$$

The Riemann problem in 2D contains potentially four different initial values. The solution between two axis are similar than the one dimensional case. However, the solution that appear at the intersection of the four initial values can lead to new specific solution. All combination are studied in [65] and later in [7].

1.1.3 Meaning of the equation for traffic flow:

The model described by the equation (1.5) is a direct extension in two dimensions of the LWR model. Units and model structure between 1D and 2D are compared in the table 4.1: However, several differences remain in the expression of the flux which make the modeling

	1D model	2D model
density	$[\rho] = veh/m$ (scalar)	$[\rho] = veh/m^2$ (scalar)
velocity	$[v] = m/s$ (scalar)	$[\vec{v}] = m/s$ (vector)
flux	$[\Phi = v\rho] = veh/s$ (scalar)	$[\vec{\Phi} = \vec{v}\rho] = veh/s/m$ (vector)
equation	$\partial_t \rho + \partial_x \Phi(\rho) = 0$	$\partial_t \rho + \nabla \cdot \vec{\Phi}(t,x,y,\rho) = 0$

Table 1.1: Comparison of model structure (unit are veh for vehicle, m for space and s for time.)

problem more complex. To be valid, a first assumption is that 2D models have to describe a road network dense enough such that the flux, the velocity and the density can be defined at any point of the plane as an extension of the road nearby. The flux in 2D models is a vector and without loss of generality, we can split it into a flux magnitude m and a normalized vector of direction $\vec{d_\theta}$ such that $\vec{\Phi}(t,x,y,\rho) = m(t,x,y,\rho)\vec{d_\theta}(t,x,y,\rho)$. We can notice that the notion of direction does not exist in one dimension, and a specific attention should be paid to introduce the direction in the 2D model. The flux is defined as the product of the density and the velocity $\vec{\Phi}(t,x,y,\rho) = \vec{v}(t,x,y,\rho)\rho(t,x,y)$. Thus in two dimensions, the velocity and the flux direction coincide.

1.2 Numerical methods

1.2.1 Splitting methods coupled with Godunov numerical flux

Numerical methods for conservation laws have been broadly studied in one dimension, multidimension and variable coefficient [63]. In [40], the authors consider space-dependence for quasilinear equations and show that it is possible to use dimensional splitting if the flux function is bounded and Lipschitz continuous. As the space and density dependencies of the flux can be split, one can rewrite equation (3.1) to have an equation with a quasilinear term and a source term: $\forall t \in \mathbb{R}^+, \forall (x,y) \in \Omega$,

$$\frac{\partial \rho}{\partial t} + \underbrace{\cos\Big(\theta\Big)\frac{\partial\ \rho v(\rho)}{\partial x} + \sin\Big(\theta\Big)\frac{\partial\ \rho v(\rho)}{\partial y}}_{Quasilinear} = \underbrace{-\rho v(\rho)\Big(\frac{\partial\ \cos(\theta)}{\partial x} + \frac{\partial\ \sin(\theta)}{\partial y}\Big)}_{Source}. \tag{1.10}$$

The splitting method, or method of fractional steps, was considered first by [22] and then properly introduced by [61]. The principle of dimensional splitting is to compute separately the different term of the equation for each discrete interval of time. Thus, the equation of our model can be split in three parts:

$$\frac{\partial \rho}{\partial t} + \underbrace{\cos(\theta(x,y))\frac{\partial\ \rho v(\rho)}{\partial x}}_{1} + \underbrace{\sin(\theta(x,y))\frac{\partial\ \rho v(\rho)}{\partial y}}_{2} = \underbrace{-\rho v(\rho)\Big(\frac{\partial\ \cos(\theta)}{\partial x} + \frac{\partial\ \sin(\theta)}{\partial y}\Big)}_{3}.$$

Then, the dimensional and operator splitting consist of dividing for each time step, the computation of the solution by 3 steps. In the first step, the propagation of the density along the x-coordinates is computed. Then in the second step, the propagation of density along the y-coordinates is updated. Finally, using the operator splitting method ([63], [23]) the source term is taken into account.
For each dimension, the flux is computed using the Godunov scheme ([22]). Note that the splitting approach presented here is only one, simple, way to discretize the model equations. Other, potentially more efficient computationally, discretizations are possible. In the numerical results, the numerical approximation is conducted with a fine spatio-temporal resolution, so that the errors due to the discretization are negligible compared to the model and upscaling errors.
Let $(C_{i,j})_{(i,j)\in[1..I]\times[1..J]}$ be the cell space discretization and $(x_{C_{i,j}}, y_{C_{i,j}})$ be the coordinates of each cell center. Let $\vec{d_\theta}(x_i, y_j)$ be flux direction introduced in Equation (1.7) discretized in each cell. Let us define the density in the cells with $(\rho_{i,j})_{(i,j)\in[1..I]\times[1..J]}$, then the numerical flux is defined at cell interfaces with the notation $F_{i+\frac{1}{2},j} = F(\rho_{i,j}, \rho_{i+1,j})$ and the function F is defined as follows:

$$F(\rho_{i,j}, \rho_{i+1,j}) = \begin{cases} \min(\Phi(\rho_{i,j}), \Phi(\rho_{i+1,j})), & \text{if } \rho_{i,j} < \rho_{i+1,j} \\ \Phi(\rho_{i,j}), & \text{if } \rho_{i+1,j} \leq \rho_{i,j} \leq \rho_{\text{crit}} \\ \Phi(\rho_{i+1,j}), & \text{if } \rho_{\text{crit}} \leq \rho_{i+1,j} \leq \rho_{i,j} \\ \Phi_{\max}, & \text{if } \rho_{i+1,j} \leq \rho_{\text{crit}} \leq \rho_{i,j}. \end{cases} \tag{1.11}$$

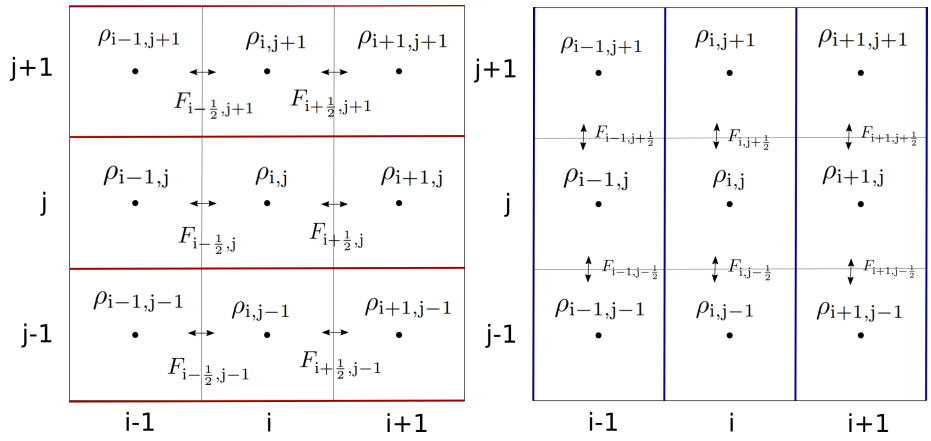

Figure 1.1: Application of the dimensional splitting with the representation of the cell interfaces.

The vertical flux $F_{i,j+\frac{1}{2}}$ is defined analogously.
Let Δt be the time step, and Δx and Δy the space discretization with respect to the x-axis and the y-axis, respectively. The time step Δt is chosen in practice to respect the Courant–Friedrichs–Lewy (CFL) condition in order to guarantee the stability of the numerical scheme. In two dimensions, this condition can be described as follows:

$$\Delta t \leq \frac{\Delta x \Delta y}{(\Delta x + \Delta y) v_{\max}}. \tag{1.12}$$

Then the global scheme for the computation of the model can be defined as follows:

$$\rho^{*}_{\mathrm{i,j}} = \rho^{\mathrm{n}}_{\mathrm{i,j}} - \cos(\theta_{\mathrm{i,j}}) \frac{\Delta t}{\Delta x} (F^{n}_{\mathrm{i}+\frac{1}{2},\mathrm{j}} - F^{n}_{\mathrm{i}-\frac{1}{2},\mathrm{j}}), \tag{1.13}$$

$$\rho^{**}_{\mathrm{i,j}} = \rho^{*}_{\mathrm{i,j}} - \sin(\theta_{\mathrm{i,j}}) \frac{\Delta t}{\Delta y} (F^{*}_{\mathrm{i,j}+\frac{1}{2}} - F^{*}_{\mathrm{i,j}-\frac{1}{2}}), \tag{1.14}$$

$$\rho^{\mathrm{n+1}}_{\mathrm{i,j}} = \rho^{**}_{\mathrm{i,j}} - \rho^{**}_{\mathrm{i,j}} v(\rho^{**}_{\mathrm{i,j}}) \left(\frac{\Delta t}{\Delta x} (\cos(\theta_{\mathrm{i}+\frac{1}{2},\mathrm{j}}) - \cos(\theta_{\mathrm{i}-\frac{1}{2},\mathrm{j}})) + \frac{\Delta t}{\Delta y} (\sin(\theta_{\mathrm{i,j}+\frac{1}{2}}) - \sin(\theta_{\mathrm{i,j}-\frac{1}{2}})) \right). \tag{1.15}$$

Here $\theta_{\mathrm{i,j}}$ is the angle of the unit vector direction of the flux $\vec{d_\theta}(x_\mathrm{i}, y_\mathrm{j})$ introduced in Equation (1.7) and that will be defined later on at cell $C_{i,j}$, and $cos(\theta_{\mathrm{i}+\frac{1}{2},\mathrm{j}})$ is equal to $\frac{cos(\theta_{\mathrm{i}+1,\mathrm{j}})+cos(\theta_{\mathrm{i,j}})}{2}$ the average between cosinus of the angles in cell $C_{i,j}$ and $C_{i+1,j}$. Figure 4.3 shows a graphical representation of the dimensional splitting, on the left the propagation of the density and the flow interface in the x-axis, and on the right the y-axis propagation. In summary, the splitting separates the computation of every time iteration into three steps: propagation along the horizontal axis, propagation along the vertical axes, and source term.

1.2.2 Boundary conditions

The boundary conditions are defined by using Ghost Cells. The concept of this method is to compute the flux crossing the boundary $F_{\mathrm{I_x}+\frac{1}{2},\mathrm{j}}$ by considering fictitious cells $\rho_{\mathrm{I_x}+\frac{1}{2},\mathrm{j}}$ outside

of the domain. The method have been introduced first by [17]. The representation of this situation are displayed in Figure 1.2.

The flux across the boundary $F_{\mathrm{I_x}+\frac{1}{2},\mathrm{j}} = F(\rho_{I_x,j}, \rho_{I_x+1,j})$ is defined in the same way as the

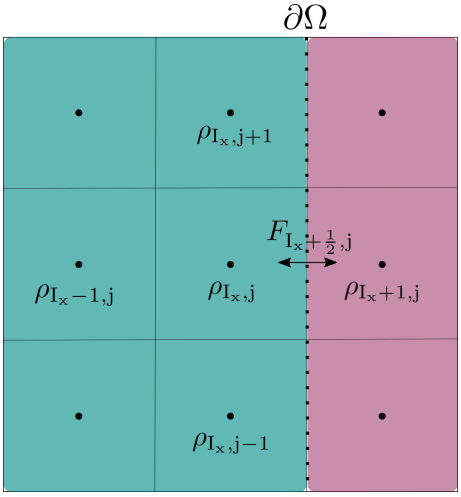

Figure 1.2: Representation of the boundary conditions using Ghost Cell: the domain Ω is represented in green and the area outside the domain is represented in purple.

internal numerical flux using the internal density at the boundary and the fictitious ghost cell outside the domain.

1.3 A method of validation using microsimulation

1.3.1 Aimsun microsimulator

Aimsun is a commercial software specialized in traffic microsimulation. This software can be used to run different scales of traffic simulation from a single highway corridor to an entire road network of a big city. These simulations can be used for real-time decisions, management of the road network or dynamic forecasting based on the network states.

In this thesis, I have used Aimsun simulator to reproduce and then validate the two-dimensional macroscopic model. However, the microsimulation given by Aimsun can not be seen as the reality and thus can also be a source of error. Thus, the objective of the comparison is not to look exactly for the results given of the microsimulation but more to guarantee the consistency of the solution obtained by the 2D model if it is similar to the microsimulation results.

In this section, we develop the methodology of the comparison between Aimsun microsimulation and the two-dimensional macroscopic model.

1.3.2 Reconstruction of the two-dimensional density from individual GPS traces

In the following part, the Kernel Density Estimation (KDE) method is presented.The idea of this method is that each observation has a spatial contribution to the estimated density, defined by the function chosen as kernel. The final estimated density then corresponds to the superposition of all those contributions. Note that, in contrast to the estimation of probability densities that are normalized to integrate to 1, the resulting vehicle density is scaled to integrate to the total number of vehicles. During the simulations, the vehicles' positions in the network are collected at each time step, yielding the data points x_k^n, y_k^n for vehicle indices $k \in [1, \dots, K(n)]$ and at times $t^n = n\Delta t_{Aim}$, $n \in [0, \dots, N]$. We start with the one-dimensional case to establish the concepts and notations.

Reconstruction of density with kernel estimation in 1D:

Let x_k^n be the position of vehicle k at time t^n. Then, the density at that time can be estimated as follows:

$$\tilde{\rho}^n(x) = \sum_{k=1}^{K(n)} G_{1d}(x - x_k^n) \tag{1.16}$$

where G_{1d} is the kernel function used to describe the contribution of each vehicle. We choose the kernel to be a Gaussian function:

$$G_{1d}(x) = \frac{e^{-\frac{x^2}{2d_0^2}}}{\sqrt{2\pi} d_0} \quad \text{which satisfies} \quad \int_{\mathbb{R}} G_{1d}(x)\, dx = 1$$

Here the parameter d_0 is a length scale determining the width of the Gaussian. The integral of the estimated density over space is equal to the number of vehicles:

$$\int_{\mathbb{R}} \tilde{\rho}^n(x)\, dx = \text{Number of vehicles on the road at time } t^n. \tag{1.17}$$

Reconstruction of density with kernel estimation in 2D:

Let $(x_k^n, y_k^n)_{k\in[1,\dots,K(n)],n\in[0,\dots,N]}$ be the position of the vehicles at time t^n. Then the density over the 2D-plane can be estimated as follows:

$$\tilde{\rho}^n(x, y) = \sum_{k=1}^{K(n)} G_{2d}\left(\begin{pmatrix} x \\ y \end{pmatrix} - \begin{pmatrix} x_k^n \\ y_k^n \end{pmatrix}\right) \tag{1.18}$$

with

$$G_{2d}(x, y) = \frac{e^{-\frac{x^2+y^2}{2d_0^2}}}{2\pi d_0^2} \quad \text{which satisfies} \quad \iint_{\mathbb{R}^2} G_{2d}(x, y)\, dx\, dy = 1.$$

The density $\tilde{\rho}_{i,j}^n$ in the cell $C_{i,j}$ is estimated with the value at the center of the cell. An example of the reconstruction of the density is given in Figure 1.3.

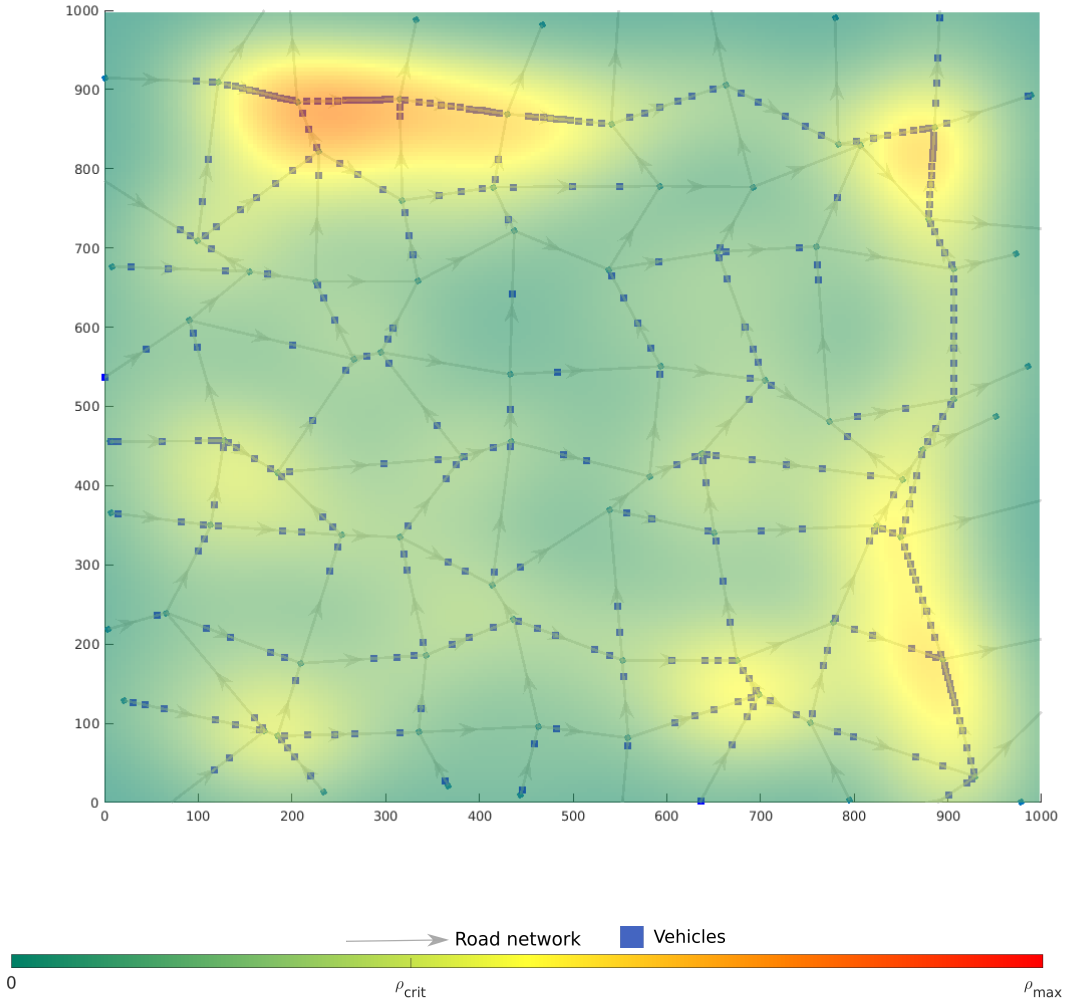

Figure 1.3: Example of 2d density reconstruction from data by kernel density estimation method: the density is represented by the colormap, the blue squares represent the positions of vehicles and the considered network can be seen in the background.

1.3.3 Estimation of the range of the Gaussian kernel used for reconstruction of the two-dimensional density

In practice, the parameter d_0, which determines how the range impacts of the Gaussian kernel, has to be properly chosen. There are several works regarding the optimal choice of this parameter including some applications on traffic modeling, see for example [16], [15]. In these articles, the authors study the choice of this parameter for an application of the kernel density approximation for a 1D model of traffic. They based their choice of the parameter d_0 on the idea that if the headway between vehicles is constant then the reconstructed density should be constant as well. However, there must be an exception to this principle when the

density of vehicles is very low. An example is given in Figure 1.4. We can observe that a

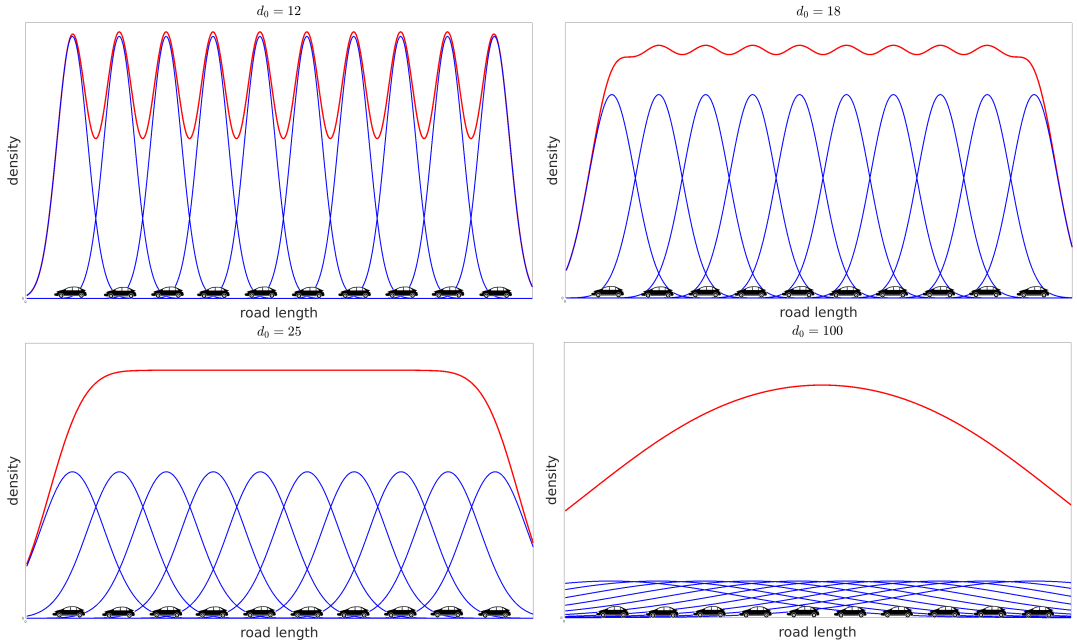

Figure 1.4: Reconstruction of density in 1D for vehicles with a constant headway of 37m and for a d_0 of respectively 12m, 18m, 25m, and 100m.

choice of a small d_0 (smaller than the vehicle spacing) leads to the creation of peaks in the reconstructed density. Conversely, a d_0 chosen too high invalidates the reconstructed density due to boundary effects and leads to a bell-shaped reconstruction. For an intermediate value of d_0, the reconstructed density is almost constant, with only small layers of reduced density near the boundaries.

Next we try to extend this idea for density reconstructions in two dimensions. First, let us consider equidistant vehicles in the 2D-plane without taking into account the network (e.g., vehicles on a parking lot). The density reconstructed in this case can be seen in Figure 1.5. The same qualitative effects as in one dimension can be observed in the 2D case. When the d_0 is chosen too large or too small, the reconstructed density tends to a bell or to have multiple peaks, respectively. If d_0 takes an intermediate value, then the reconstructed density is almost constant in space and has the shape of a plateau.

Next we consider the test network and place vehicles equidistantly along the roads. This means that on the whole network, we consider that vehicles are distributed with a constant spacing. Figure 1.6 shows the result of the reconstructed density for this scenario.

In the cases that d_0 is too high or too low, we face the same problem than encountered previously. In practice, it seems difficult to obtain a totally flat estimation of the density in this case even when d_0 is chosen with an intermediate value. Thus, the parameter d_0 is chosen by an optimization process. Consider vehicles placed at a minimal distance — one vehicle every 6m — over the network and let $\tilde{\rho}$ be the corresponding estimated density. The parameter d_0 is chosen such that it reduces as much as possible the distance between maximum of the density evaluated over Ω and the rest of the estimated density.

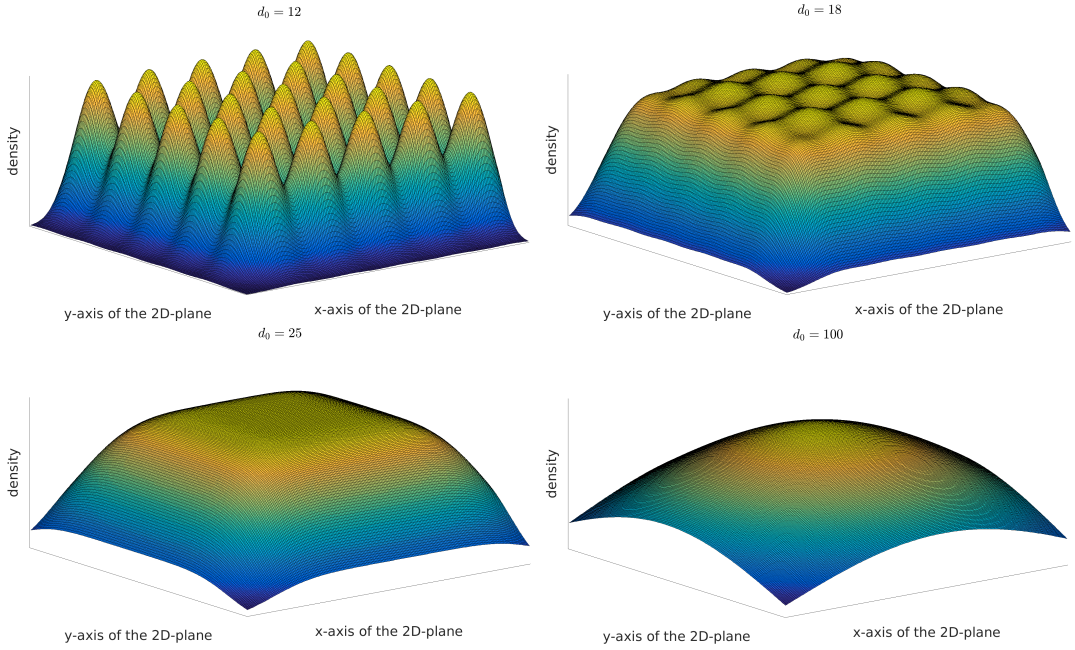

Figure 1.5: Reconstruction of 2D density for vehicles uniformly distributed every 37m in the 2D-plane and for d_0 of respectively 12m, 18m, 25m, and 100m.

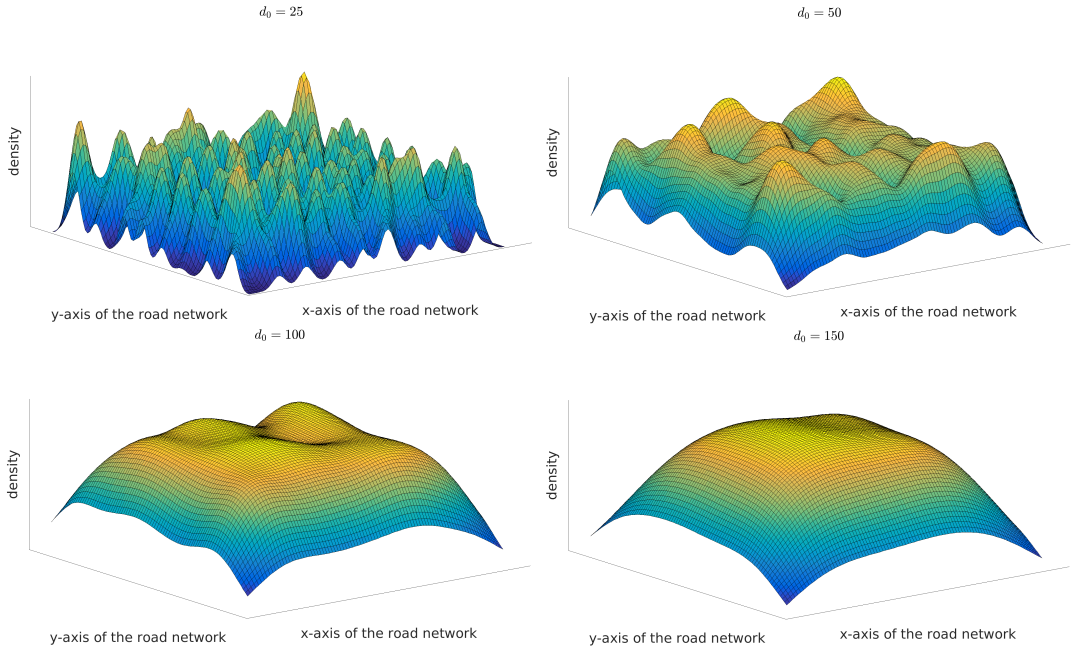

Figure 1.6: Reconstruction of 2D density for vehicles with a constant spacing of 37m on the network and for d_0 of respectively 25m, 50m, 100m, and 150m.

$$d_0 = \underset{d_0 \in \mathbb{R}_+^*}{\operatorname{argmin}} \|\tilde{\rho}(.,.) - \max_{(x,y)\in\Omega} \tilde{\rho}(x,y)\|_2 \tag{1.19}$$

The density $\tilde{\rho}$ depend on the parameter d_0 in a non linear way given by the Equation (3.10).

1.3.4 Data collection with Aimsun, microsimulation of a traffic network,

In this subsection, this subsection contains a description of the different steps for the comparison between the Aimsun microsimulation and the two-dimensional model simulations. We also discuss some possibilities and limitations of the microsimulator.

Methodology for the data collected from Aimsun:
The main step of the use of Aimsun simulator to collect the simulated data:

1. Creation of a network using Matlab. A network is defined by a vector that contains the position of the nodes (junctions) and an adjacency matrix that describes the existing connections between these nodes (roads).
2. Conversion of the network in ".shp" and importation in Aimsun.
3. Importation of the traffic states in Aimsun: Split ratio with inflow or OD matrices.
4. Definition of the traffic scenario in Aimsun: duration, traffic light planning, vehicles behaviors (speed, headways ...)
5. Simulation in Aimsun collecting the position of every vehicle within the network at each time step in a csv-files.
6. Read these data in Matlab and reconstruct a two-dimensional density using Kernel density estimation.

In Aimsun, it is interesting to notice that each simulation is unique due to the randomness added in the simulator. The random comes from: the vehicles inflows that are distributed around an average, the path of vehicles determined by splitting ratio or by OD matrices, and the speed of vehicles that is also varying. Thus, results of a microsimulation can be not relevant, and thus, it is interesting to smooth the results by considering many runs of the same scenario and averaging them.
Discussion about possibilities of Aimsun:
The Aimsun software already offers a lot of possibilities to design scenarios: traffic demand, split ratio, OD matrices, vehicles classes, traffic light. However, most of these parameters are defined at the local level and can not be changed easily in the main interface at a network level. Examples of the functionality that could be added are:

- Set the initial density data in all the network (in % of occupancy)

- Change the signalization of the intersection at the network level.
- Generate vehicles within any roads, for example to represent cars in a city center that can park or start a trip from anywhere.
- Define dynamic traffic assignment in the possibility of OD matrices choice of routes path. It is difficult to define a realistic scenario otherwise because users usually learn from their experience and create an equilibrium.
- Allow to constraint traffic outflows as it is possible to set the traffic inflows.

Data set of academics scenarios
In addition to the simulation used as materials in the following chapters of this manuscript, data sets of five scenarios using Aimsun microsimulator have been collected and will be available online. Some of these simulations are used for future discussion about split ratio in microsimulation. These scenarios can be summarized as follows:

1. Regular square Manhattan grid, 50×50 intersections with a distance of 100m between them. The possible directions for traffic are the North and the West.
2. Irregular square Manhattan grid, 50×50 intersections with an average distance of 100m between them. The possible directions for traffic are the North and the West.
3. Regular rectangular Manhattan grid, 50×50 intersections with a distance between them respectively equal to 50m vertically and 200m horizontally. The possible directions for traffic are the North, and the West.
4. Regular square Manhattan grid, 50×50 intersections with a distance of 100m between them. The possible directions for traffic are the North, the East, and the West.
5. Regular square Manhattan grid, 50×50 intersections with a distance of 100m between them. The possible directions for traffic are all the North, the East, the West, and the South.

For each of these situations, 3 scenarios with different split ratios have been tested with respectively 50%, 10% and 0% chance to turn at the intersections. For all the scenarios, the maximum desired speed of vehicle is set equal to an average of $50km/h$ with a 10 km deviation.

Vehicles trajectories in a network: Split ratio vs OD matrices
To construct a traffic scenario using a microsimulator, a path or a trajectory for vehicles need to be defined. There are two classical ways to do it. The first method is to consider split ratios and inflows. The split ratios are defined as the percentage of vehicles distributing in each direction at the intersection. The inflows represent the number of vehicles entering the network from its boundary. The second method is called Origin-Destination matrices. Origin-Destination matrices are defined by the number of vehicles going from an origin to a

destination. The path of the vehicles are based on the shortest distance or can be estimated using a more complex method.
If the split ratio method works very well at the intersection level, it can reveal issues when considered in a large-scale network. In particular, the split ratio may not be appropriate to simulate networks with many circles. Indeed, in this situation, the vehicles may go round in circles. However, split ratios can still be used in many cases if the network considered is oriented towards a direction.
We consider the results of the data set as an example. The network considered the four directions of traffic propagation (North, East, South, West) and Figures 1.7 and 1.8 show the results of simulation over time with two different split ratios which respectively give a probability to turn of 0% and 50%. We can see that the vehicles in the second scenario diffuse really slowly towards the center because many vehicles go round in circles. This effect is a limitation of the split ratio modeling, which is a local concept, when it is applied at large scale.

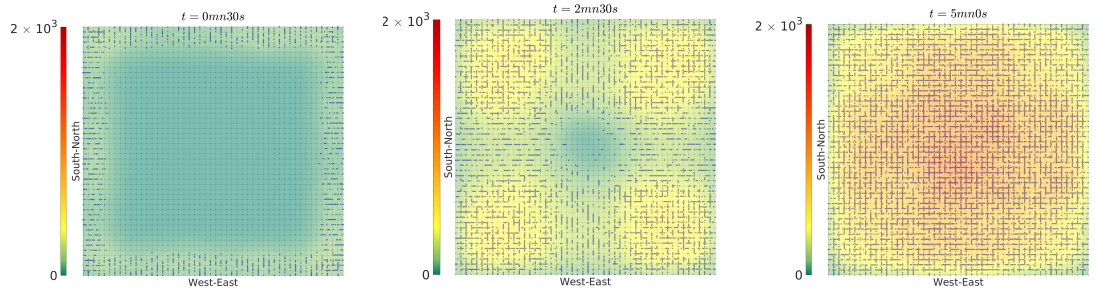

Figure 1.7: Simulation results of traffic with all direction and a splitting ratio corresponding to a probability of 0% to turn at junctions

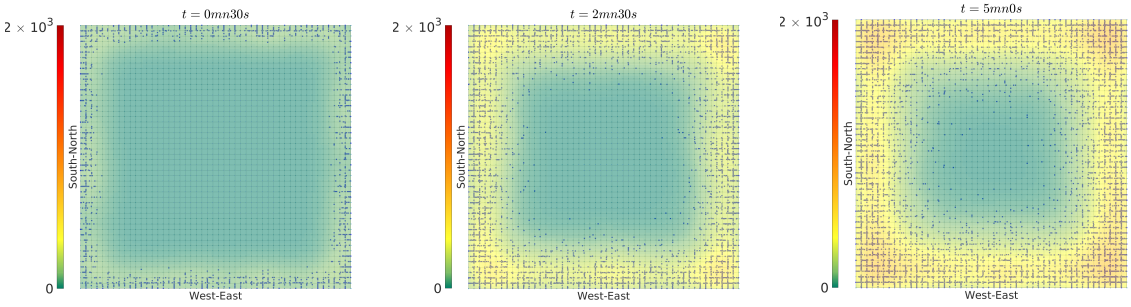

Figure 1.8: Simulation results of traffic with all direction and a splitting ratio corresponding to a probability of 50% to turn at junctions

In conclusion, to define the trajectories of vehicles in a network using a microsimulator, the OD matrices method can be used in most of the scenarios whereas the split ratio method should be used only for oriented networks.

Chapter conclusion: Summary, limitations and possible extensions

In this chapter, the derivation of the two-dimensional partial differential equation from the mass conservation has been presented. There exists in the literature studies about the existence of solution or the two-dimensional Riemann problems but it is not as largely studied as the 1D case. The two-dimensional representation is consistent to describe traffic flow only if the network is large and dense enough to be considered as a continuum. A key difference with 1D modeling is that the flow is represented through a vector for which a direction needs to be specified.
The simulation of this equation required the implementation of numerical methods. In this thesis, we apply finite volume methods with dimensional splitting to handle the two-dimensional aspect. These methods are interesting because they are relatively simple to implement and quite efficient for the numerical cost. To increase the precision around a specific topological structure, one could consider finite element methods.
A methodology to compare of the model against microsimulation is presented. The idea is to reconstruct a two-dimensional density from vehicles' trajectories to be able to compare microsimulation and models easily. However, we can emphasis on two limitations of the reconstruction. First, the Gaussian kernel that we used is symmetric, thus it can be difficult to reconstruct the density around the boundaries. Second, the Gaussian kernel can only produce smooth function, so a sharp discontinuity in the simulator can not be captured by the reconstruction.
Finally, we explain thet steps for the collection of vehicles' trajectories from Aimsun and we show results of microsimulation to show the limitation of "split ratio" contrary to OD matrices to represent vehicle propagation in a very large scale network. This issue concerns mainly network with roads in every direction. Indeed, vehicles trajectories based on splitting ratio applied to a network with many loops can have difficulty propagating in the network and tend to go round in circles.

Chapter 2

Homogeneous network with one direction of flow

Contents

2.1 Model construction

In this section, we introduce a first simple version of 2D model for traffic applicable to homogeneous network with a preferred direction of flow.

2.1.1 Description of the model

In this section, we introduce a 2D model for traffic flow based on a two-dimensional conservation law. We consider a model in the two-dimensional plane where the density represents the number of vehicles per square area. An example can be seen in Figure 2.1, giving a comparison between the same traffic situation described with a 1D density (left) and a 2D density (right). Based on the different variables that could influence the flux function, several models could be designed. In this chapter, we make the following assumptions :

1. The velocity magnitude is decreasing with respect to density.
2. The drivers do not adapt their paths with respect to density, i.e., there is no re-routing.

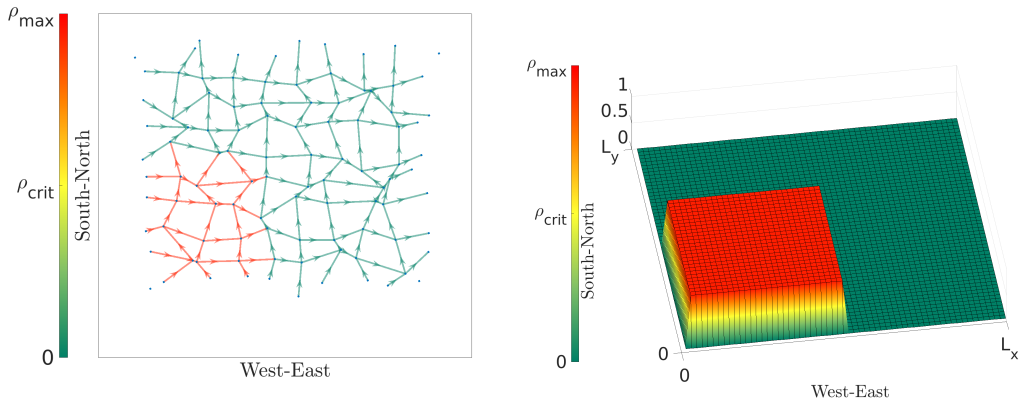

Figure 2.1: Representation of an urban area as a road network (left) and as a continuum (right).

3. The maximal speed and the capacity is constant with respect to space.
4. The direction of the flow is given by the geometry of the network.

As most relevant roads are commonly bi-directional, this last assumption requires some justification. Large-scale urban traffic modeling is of particular relevance during (morning and afternoon) rush hour times of peak congestion. During those times, most urban areas exhibit a dominant direction of traffic flow (e.g., from the suburbs to downtown in the morning), and it is generally known (from historic data and/or travel demand modeling) which roads in the network carry this peak flow. In that spirit, we consider the following model.

$$\begin{cases} \dfrac{\partial \rho}{\partial t}(t,x,y) + \nabla \cdot \vec{\Phi}(x,y,\rho(t,x,y)) = 0, & \forall t \in \mathbb{R}^+, \forall (x,y) \in \Omega \subset \mathbb{R}^2 \\ \rho(0,x,y) = \rho_0(x,y). & \forall (x,y) \in \Omega \end{cases} \tag{2.1}$$

The density ρ is a two-dimensional quantity (number of vehicles per square meter) and it is a function of time t and space (x,y) defined in an area $\Omega \subset \mathbb{R}^2$. The flux function $\vec{\Phi}(x,y,\rho) : [0,\rho_{\max}] \times \Omega \to [0,\Phi_{\max}]$ is given by

$$\vec{\Phi}(x,y,\rho) = \rho \vec{v}(\rho) \tag{2.2}$$

where the velocity field $\vec{v}(x,y,\rho) : [0,\rho_{\max}] \times \Omega \to [0,v_{\max}]$ is given by

$$\vec{v}(x,y,\rho) = \underbrace{v(\rho)}_{\text{magnitude}} \cdot \underbrace{\vec{d_\theta}(x,y)}_{direction} \tag{2.3}$$

We denote by θ the angle between $\vec{d_\theta}$ and the x-axis. The magnitude of the velocity, $v(\rho)$, is determined by the Fundamental Diagram (FD).

2.1.2 Parameters estimation

In the model description (3.1), we have presented a velocity field that is the product of the a magnitude that depends on the density only, and a direction that depends on position only.

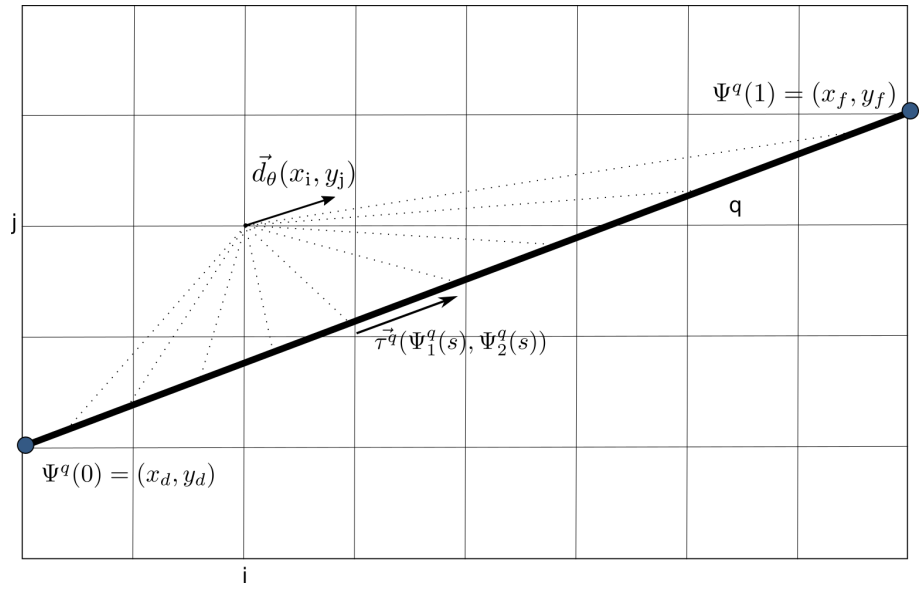

Figure 2.2: Variables considered for the estimation of the velocity direction field. ($s_{\max} = 1$)

In this section, we suggest one possible way to construct the direction function $\vec{d}_\theta$ from the geometry of the road network, see [47]. The motivation behind this is due to the fact that, contrary to what happens with crowds [30], vehicles are constrained to the physical road network.

Remark 1. *This method is valid only for a traffic network defined by an oriented graph, i.e. without two directional roads. We assume as well, that we do not have any detail on driver trajectories. The split ratio, the origin-destination matrices or any information on driver behavior are unknown. The method presented here aims to analyze which traffic features a simple two-dimensional model can capture in the situation where we just know that a preferred flow direction exists.*

Before describing in detail how the function $\vec{d}_\theta$ is constructed we need to introduce some notation. We describe a road as a path from one intersection to another. We denote by $q \in \{1, .., Q\}$ the different roads of the network. The spatial path of each road is described by a parametric curve $\Psi^q : \ s \in [0, s_{\max}] \to (\Psi_1^q(s), \Psi_2^q(s)) \in \mathbb{R}^2$. The variable $s \in [0, s_{\max}]$ allows to progress along the road curvature from an intersection to the next one. Let $\vec{\tau^q}(\Psi^q(s))$ be the tangent vector of the road q at position $(\Psi_1^q(s), \Psi_2^q(s))$. For example in a network with only straight roads, this tangent vector is constant along each road. An example is given in Figure 2.2. The estimation of the unit vector $\vec{d}_\theta$ at the discrete cell level is done by a spatial interpolation method called Inverse Distance Weighting:

$$\vec{d}_\theta(x,y) = \frac{\sum_{q=1}^{Q} \int_{s\in[0,1]} w(\|(x,y) - (\Psi_1^q(s), \Psi_2^q(s))\|) \quad \vec{\tau^q}(\Psi^q(s)) \quad ds}{\left|\left| \sum_{q=1}^{Q} \int_{s\in[0,1]} w(\|(x,y) - (\Psi_1^q(s), \Psi_2^q(s))\|) \ \vec{\tau^q}(\Psi^q(s)) \quad ds \right|\right|} \tag{2.4}$$

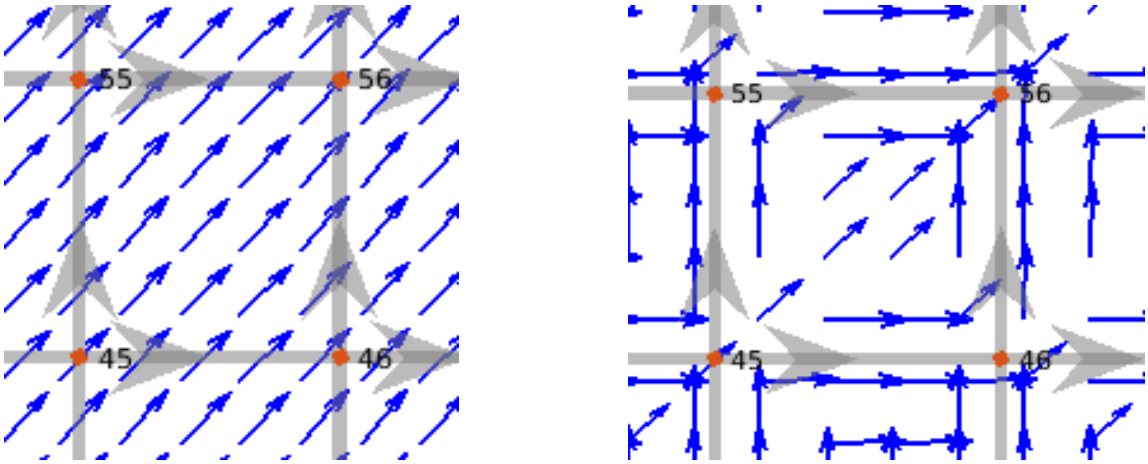

Figure 2.3: Comparison between the estimation of the velocity direction for a small β (left) and large β (right).

Equation (2.4) constructs a direction at any point in the domain as a (normalized) weighted average of the road direction $\vec{\tau^q}$ of all points in the network, where the weight of a contributing point on a road depends on its distance to the evaluation point. The weight function $w : \mathbf{R}^+ \to \mathbf{R}^+$ should be a decreasing function of the distance. Here we use an exponential function:

$$w : X \to e^{-\beta X} \qquad \text{with} \qquad \beta > 0.$$

However, other weight functions, particularly compactly supported ones, are also possible. The parameter β represents the localization of the weighted average: for small β, the velocity direction field provides only the global trend of the direction, while with a large β, the velocity field follows the detailed features of the roads. Figure 2.3 demonstrates these two extreme cases in an example. As we are interested in a model that captures the large-scale two-dimensional vehicle transport, but without over-resolving the details of the network, we need to choose a value of β that lies between these two extremes. Figure 2.4 shows the velocity direction field on the network considered for simulation: as the β chosen is not large, the direction field is smooth and quite close to the global direction of the network which is towards the North-East direction. It is important to stress that for a general network, the weighted average (2.4) could potentially generate an undefined direction (due to the numerator and denominator vanishing). However, for dominant direction flow networks considered here, this scenario cannot happen.

2.1.3 Discussion about the direction field and the choice of a preferred direction for traffic

It is interesting to notice that the roads of the considered network are oriented toward the one main direction (here the North-East direction). The model introduced in Section 2.1.1 can not be applied in any real scenario. In particular, the double way roads can not be included. However, this does not mean that every road have to be oriented in one preferred direction. In fact, the exact limitation of this model is that it can only describe one direction of flow for

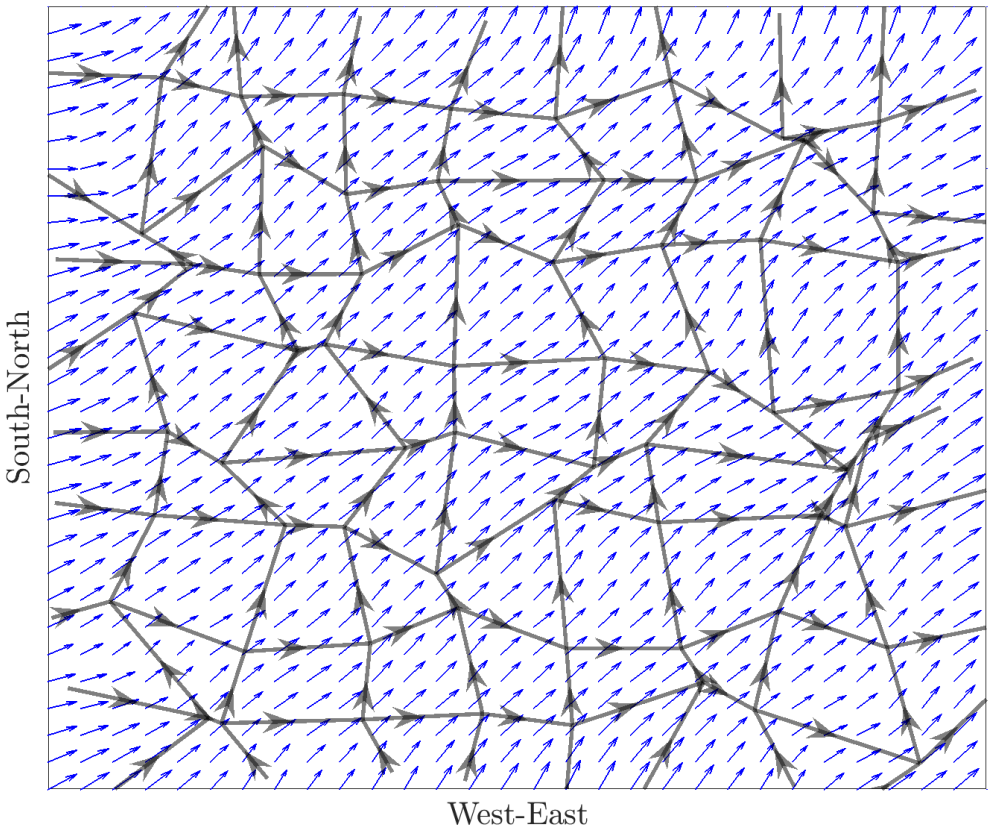

Figure 2.4: Example of a velocity direction field in a modified Manhattan grid network.

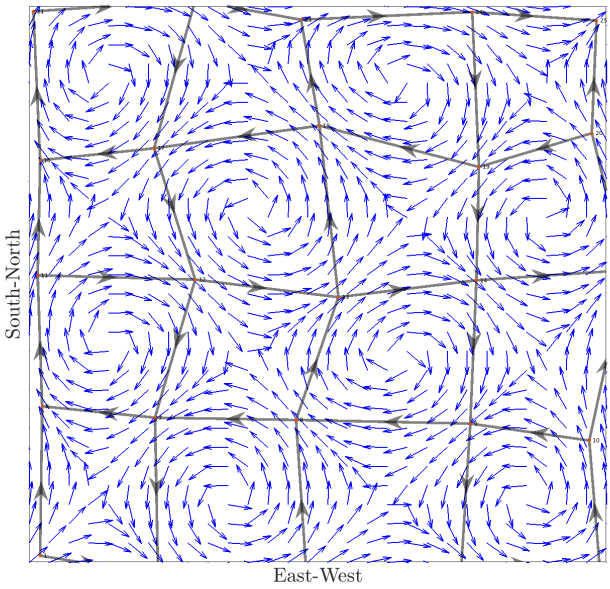

Figure 2.5: Direction field estimated for an oriented graph with single way road in every direction and for a medium value of the parameters β.

each space coordinate. Thus, in practice, we could model theoretically every traffic network defined by an oriented graph, which means every network without two-directional roads. An example of the velocity field reconstruction in a network without a preferred direction of flow is displayed in Figure 2.5. However, the precision of the discretization required to solve the traffic flow propagation depends on his regularity in term of road direction. If there is many "counter-flow" i.e. roads oriented in different direction in the network, the discretization have to be fine in order to describe the details of these roads which may cancel the advantages of these 2D model in term of aggregation possibility, whereas if the roads of the network follow a global flow direction, it becomes possible to go for a rougher discretization.
To conclude, it is in theory possible to define the velocity field for a network without a preferred direction of traffic propagation. However, the lack of consistency in the flow direction may degrade the numerical effectiveness of the model. When several directions of traffic flow propagation exists, the best option seems to consider a multilayer model as it is described in Chapter 4.

2.2 Results of simulation

In this section, we present the simulation results of two study case with two main differences. First the fundamental diagram considered is different and has different strategies for the estimation of the parameters. Also, the comparison is respectively with Network modeling and model of junction at the intersection and with a microsimulator.

2.2.1 Recall numerical method and scenario considered

In this subsection, we recall briefly the numerical method presented in the Section 1.2.1 with the Algorithm 1. This numerical method is used for each of the two study case.

Algorithm 1 2D model simulation

1. Define the parameters: $v_{\max}$ the maximum velocity, $\rho_{\max}$ the maximum density, $T_{\max}$ the time horizon, the constant coefficient CFL, dx and dy the spatial discretisation and I and J the number of discrete interval of the spatial discretisation.
2. Define the time step $dt = cfl * min(dx, dy)/V_{\max}$
3. Import or create the road network of the study case
4. Compute the velocity field d_θ ▷ Using the estimation method
5. Initialize the density ρ to a given value, the current time t to zero.
6. **while** $t < T_{\max}$ **do**
7. Evalue the density at the next time step using the function Propagation_2D
8. **function** PROPAGATION_2D($\rho^{\mathrm{n}}, dt, dx, dy, I, J, v_{\max}, \rho_{\max}, d_\theta$)
9. Define the intermediate densities ρ^* and ρ^{**}
10. **for** $i = 1$ to I and $j = 1$ to J **do**
11. Update of ρ^* with flux along the x dimension computed with ρ^{n}
12. **end for**
13. **for** $i = 1$ to I and $j = 1$ to J **do**
14. Update of ρ^{**} with flux along the y dimension computed with ρ^*
15. **end for**
16. **for** $i = 1$ to I and $j = 1$ to J **do**
17. Update of the density value $\rho^{\mathrm{n}+1}$ due to the source term computed with ρ^{**}
18. **end for**
19. **end function**
20. t=t+dt
21. **end while**

This algorithm introduces the numerical method that are used in both of the two study cases presented in this chapter.

Scenario and network considered:
For the two following set of simulations, we use a test network, shown in Figure 2.6, of a deformed 10×10 Manhattan grid, laid out on a 1km $\times$ 1km domain. To cut the regularity and therefore have a more generic network, we start from a regular Manhattan grid and add a normally distributed perturbation (of standard deviation 30m) to the position of each node. Horizontal edges go East-bound, and vertical edges go North-bound. In line with this, all roads in the West and South are entrance roads ("I" number 1 to 16), whereas the roads in the East and North are exit roads ("O" number 1 to 16). Each network edge is a single-lane road.

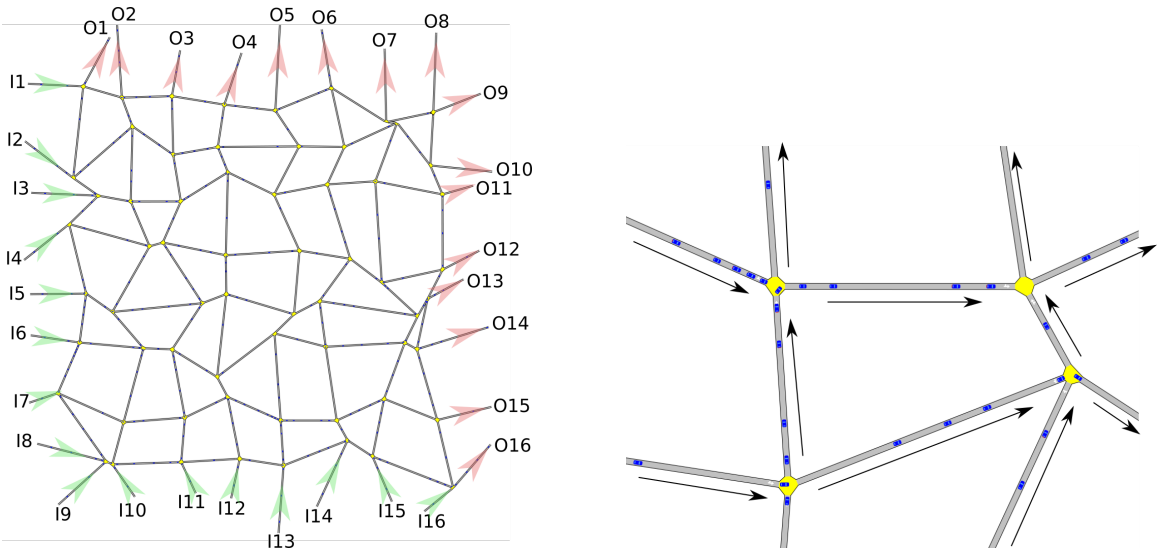

Figure 2.6: Manhattan grid oriented towards the North-East direction (left) and a zoom of the road network (in Aimsun) (right).

2.2.2 Simulations results and comparisons with Network modeling

Fundamental Diagram considered: Greenshields:
In this subsection, the simulations are based on the Greenshields Fundamental Diagram that can be defined as follow:

$$v(\rho) = \Big(1 - \frac{\rho}{\rho_{\max}}\Big) v_{\max} \tag{2.5}$$

$$\Phi(\rho) = \rho\Big(1 - \frac{\rho}{\rho_{\max}}\Big) v_{\max} \tag{2.6}$$

This Fundamental Diagram is known to be one of first proposed and also it is a simple one. However, it could be difficult to match perfectly traffic data with it.

Forward propagation on an artificial Manhattan grid
First, we present the results of the simulations for an initial condition given by equation (2.7):

$$\rho_0(x,y) = \begin{cases} \frac{1}{2}\rho_{\max} & \text{if} \quad \frac{1}{8}L_{\mathrm{x}} \le x \le \frac{4}{8}L_{\mathrm{x}} \quad \text{and} \quad \frac{1}{8}L_{\mathrm{y}} \le y \le \frac{4}{8}L_{\mathrm{y}} \\ 0 & \text{otherwise} \end{cases} \tag{2.7}$$

where L_{x} and L_{y} are respectively the length of the domain along the x-axis and the y-axis. In Figure 2.7, we show the results for different times.

First, we can remark that at the initial time, the initial conditions generate two main discontinuities. On the North-East, the discontinuity corresponds to a rarefaction wave whereas in the South-West it is a shock wave. The shape of the shock wave is globally preserved.

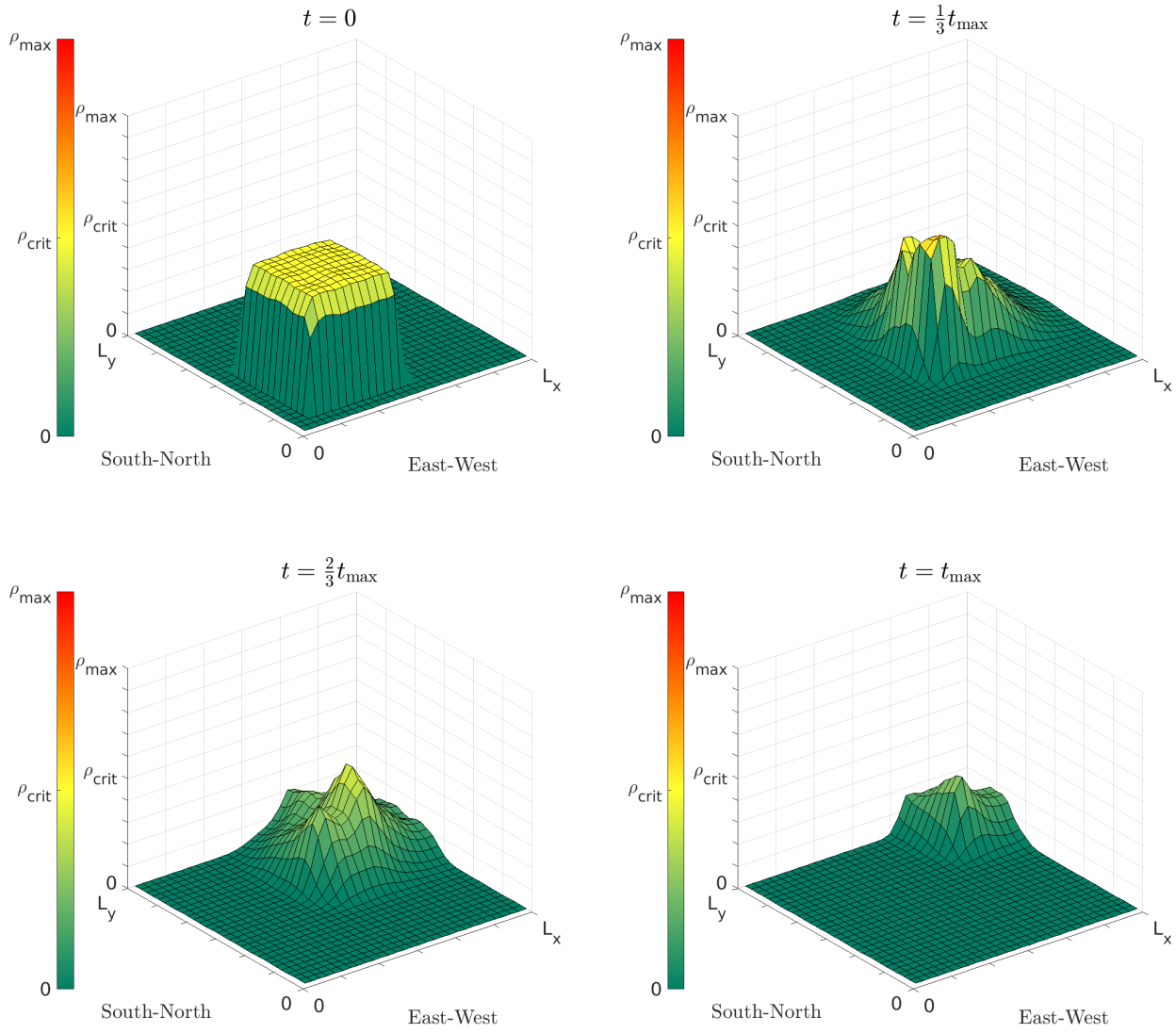

Figure 2.7: Simulation results at different times of 2D model with initial traffic state given by equation (2.7)

.

Backward propagation and comparison with the CTM model

Then, we present the results of the simulations for an initial condition given by equation (2.8):

$$\rho_0(x,y) = \begin{cases} \rho_{\max} & \text{if} \quad \frac{2}{3}L_x \leq x \quad \text{and} \quad \frac{2}{3}L_y \leq y \\ \frac{9}{16}\rho_{\max} & \text{otherwise} \end{cases} \tag{2.8}$$

The results at different times are given in Figure 2.8:

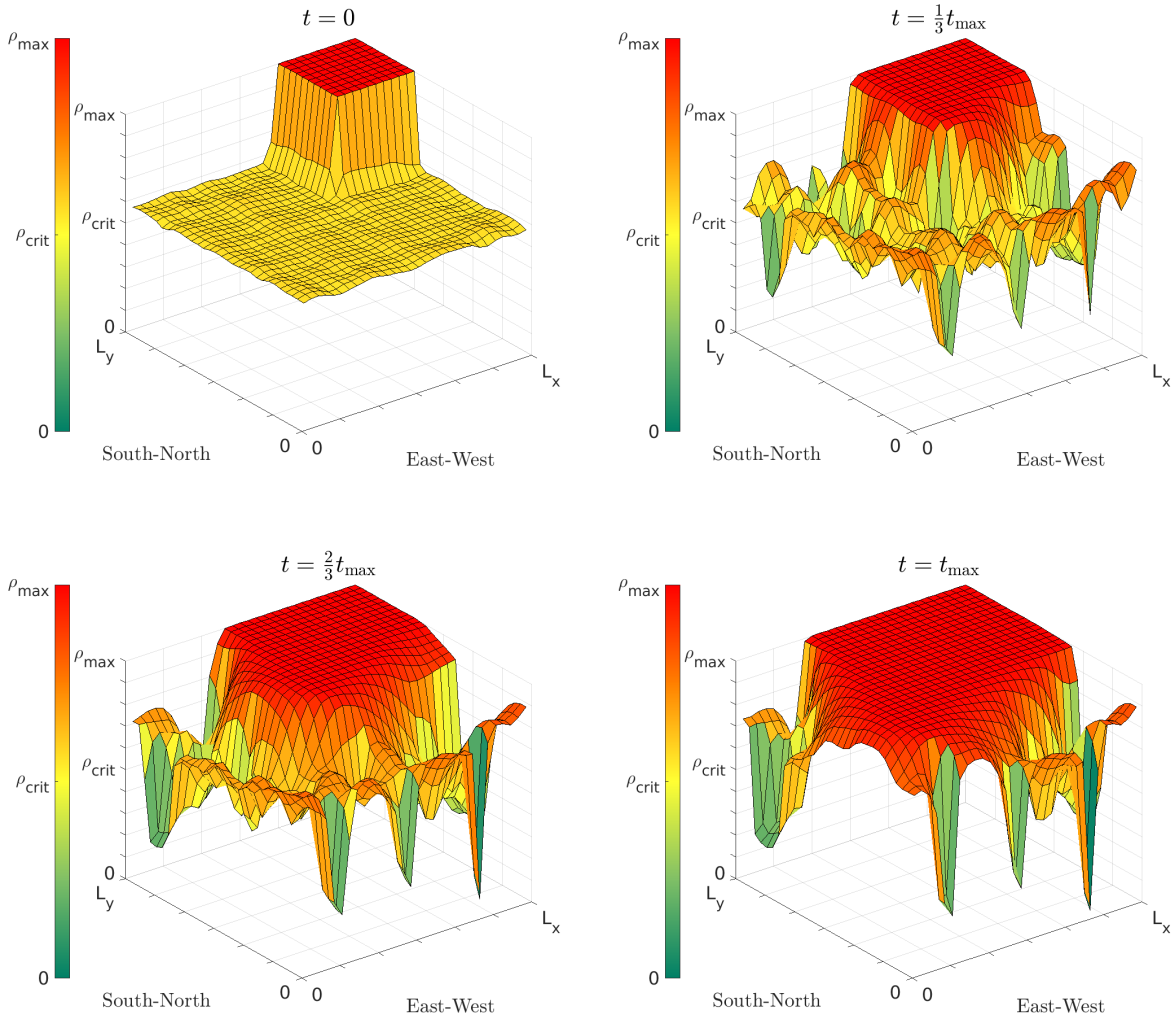

Figure 2.8: Simulation results at different times of 2D model with initial traffic state given by equation (2.8)

We can observe how the density over all the network raises and the network is quickly filled.

We have also simulated in parallel a Cell Transmission Model [11] [10] on the same network and with the same initial condition, for comparison. The results of simulation are presented

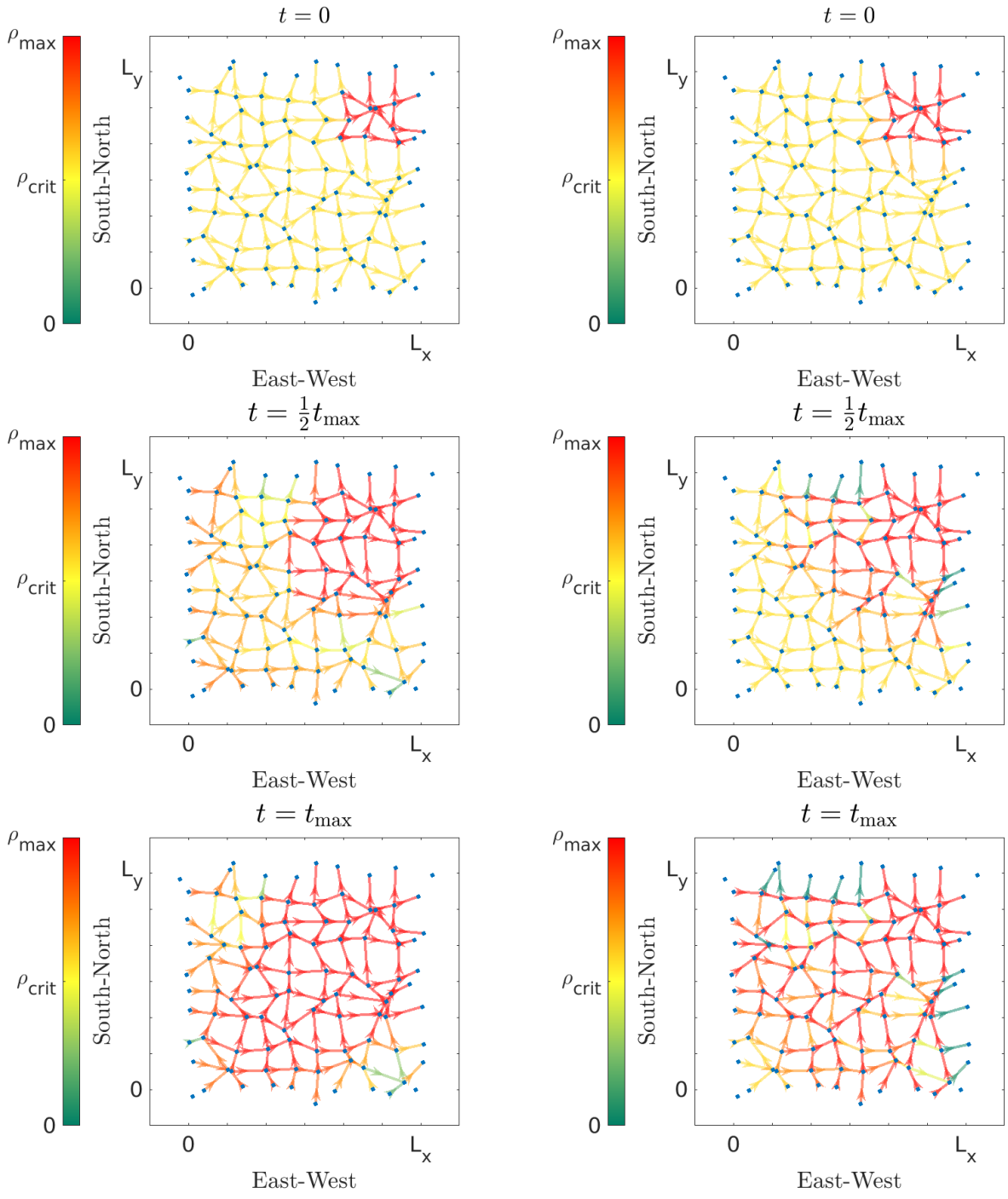

Figure 2.9: Comparison of simulation between 2D model (left) and CTM (right) for an initial traffic state given by equation (2.8)

in Figure 2.9: We represent both simulation at the graph level. For the two-dimensional model, the representation is only visual. Indeed, we have just done the projection of the two-dimensional grid coloring on the graph. Both in the 2D model and in the junction model, the wave propagate backward as expected with approximately the same speed of propagation.

2.2.3 Simulation results and comparisons with Aimsun microsimulation

In this subsection, we compare the results of several scenarios in the microsimulator Aimsun and the 2D model. This study was lead in [50].

Fundamental diagram considered: Newell Franklin

In this study case, the FD chosen is the one introduced by [51] and [18], whose velocity function is:

$$v(\rho) = v_{\max}\left(1 - \exp\left(\frac{c}{v_{\max}}\left(1 - \frac{\rho_{\max}}{\rho}\right)\right)\right) \tag{2.9}$$

This specific FD has been considered as the best one to fit the data among the concave FD. This function possesses three parameters: the maximum velocity $v_{\max}$, the maximum density $\rho_{\max}$, and a velocity c that determines how rapidly the velocity decreases with increasing density, and thus affects the value of the critical density. The resulting flux function is strictly concave down. An example of this FD is displayed in Figure 2.10.

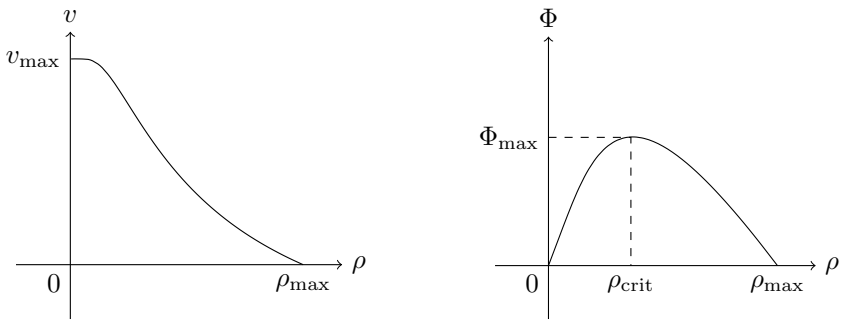

Figure 2.10: Speed and flow vs. density.

Estimation of the range of the Gaussian kernel for two-dimensional density reconstruction We apply the method described in Section 1.3.3 to choose the range d_0 of the Gaussian kernel to reconstruct two-dimensional density from individual trajectories. For the 10×10 Manhattan square grid of 1km length considered, the resulting value of d_0 is 85.1 meters. The method suggested for the estimation of d_0 enables to remain consistent with the assumption that the FD is defined as constant over the 2D-plane.

Parameters of the fundamental diagram estimated from simulated data:

Contrary to the first study case, the parameters of the fundamental diagram in this scenario

are estimated from the microsimulation in Aimsun. Since we consider densities as number of vehicles per meter square, we need to introduce a new way to estimate from synthetic data the fundamental diagram for the two-dimensional models. The definition of a fundamental diagram is closely linked to the definition of density. In Section 1.3.2, a way to reconstruct density from traffic data was presented. Thus, it is consistent that the fundamental diagram is also based on the kernel reconstruction method. For clarity purposes, one may emphasize that this FD aims to be applied for network modeling, but it is not related to the notion of Macroscopic Fundamental Diagram (MFD). Indeed, this FD links the two-dimensional density and the velocity of vehicles and it is applied locally.
The parameters of the microsimulator have to be set before collecting data of simulation. The main ones are the following:

- The minimum gap between two vehicles is 4m
- The length of vehicles is 2m
- The roads capacity is then equal to 166.67 vehicles per kilometer but this is not equal to the maximum two-dimensional density of the model.
- The time step in Aimsum $\Delta t_{\text{Aim}} = 0.8$s. This parameter is fixed and cannot be changed because it controls also the reaction time of drivers.

The data for the construction of the FD is collected from a simulation in Aimsun in which we recorded the position and the instantaneous velocity of vehicles every 0.8s. We are then able at each time step, to reconstruct an estimated density with the kernel method defined Section 1.3.2.We can recall that for the reconstruction, we set the range of the Gaussian d_0 equal to 85.1m value that we find to be optimal for this network that is homogeneous. In order to construct a FD, we need to reconstruct a velocity or a flux over the 2D plane using the data collected from Aimsun as well. In particular, we construct an interpolation of the velocity of all vehicles. Let $(v_k^n)_{(k,n)\in[1,\dots,K(n)]\times[1,\dots,N]}$ be the speeds of the vehicles of subscript k over the $K(n)$ vehicles present in the network at time t^n. The corresponding positions of these vehicles are $(x_k^n, y_k^n)_{(k,n)\in[1,\dots,K(n)]\times[1,\dots,N]}$. Using these data, we can — consistent with (3.10) — estimate the density $(\tilde{\rho}_{i,j}^n)_{(i,j)\times n\in[1,\dots,I]\times[1,\dots,J]\times[1,\dots,N]}$ by the Kernel Density Estimation method:

$$\tilde{\rho}_{i,j}^n = \sum_{k=1}^{K(n)} G_{2d}\Big(\begin{pmatrix} x_{C_{i,j}} \\ y_{C_{i,j}} \end{pmatrix} - \begin{pmatrix} x_k^n \\ y_k^n \end{pmatrix} \Big) \tag{2.10}$$

We can also estimate the velocity field $(\tilde{v}_{i,j}^n)_{(i,j)\times n\in[1,\dots,I]\times[1,\dots,J]\times[1,\dots,N]}$, by interpolation of each individual vehicle speed and then deduce the flow rate field $(\tilde{\Phi}_{i,j}^n)_{(i,j)\times n\in[1,\dots,I]\times[1,\dots,J]\times[1,\dots,N]}$ respectively, as follows:

$$\tilde{v}_{i,j}^n = \frac{\sum_{k=1}^{K(n)} G_{2d}\left(\begin{pmatrix} x_{C_{i,j}} \\ y_{C_{i,j}} \end{pmatrix} - \begin{pmatrix} x_k^n \\ y_k^n \end{pmatrix} \right) v_k^n}{\left| \sum_{k=1}^{K(n)} G_{2d}\left(\begin{pmatrix} x_{C_{i,j}} \\ y_{C_{i,j}} \end{pmatrix} - \begin{pmatrix} x_k^n \\ y_k^n \end{pmatrix} \right) \right|} \qquad \text{and} \qquad \tilde{\Phi}_{i,j}^n = \tilde{v}_{i,j}^n \, \tilde{\rho}_{i,j}^n \tag{2.11}$$

The number of data observation we obtain with the method presented just above can be really huge: for each discrete point and each time step we have a measure. This leads to redundant data, difficulty to read data and inconsistency of the estimation. For these reason, we apply a sampling over time and an aggregation over space. Let s_{t} the ratio between the time step of the sampling and the time step of the simulation. Let H and L be the number of cells aggregated over space. We denote by $(\bar{\rho}^n_{i,j})_{(i,j)\times n\in[1,\dots,\bar{I}]\times[1,\dots,\bar{J}]\times[1,\dots,\bar{N}]}$ and $(\bar{\Phi}^n_{i,j})_{(i,j)\times n\in[1,\dots,\bar{I}]\times[1,\dots,\bar{J}]\times[1,\dots,\bar{N}]}$ respectively the density and the flow after the sampling and aggregation and constructed as follows:

$$\bar{\rho}^n_{i,j} = \frac{1}{H.L}\sum_{h=H.(i-1)+1}^{H.i}\ \sum_{l=L.(j-1)+1}^{L.j}\tilde{\rho}^{s_{\mathrm{t}}.n}_{h,l} \qquad \text{and} \qquad \bar{\Phi}^n_{i,j} = \frac{1}{H.L}\sum_{h=H.(i-1)+1}^{H.i}\ \sum_{l=L.(j-1)+1}^{L.j}\tilde{\Phi}^{s_{\mathrm{t}}.n}_{h,l} \tag{2.12}$$

where $s_{\mathrm{t}} = 20$, $H = 10$ and $L = 10$.
Applying these reconstructions for all data, a fundamental diagram density–flow relation can be obtained. The result is shown as the points in Figure 2.11. We then fit a function $\tilde{\Phi}$ to these data points that satisfies the following constraints:

1. The flux is zero for a vanishing density: $\tilde{\Phi}(0) = 0$.
2. The flux returns to zero when the density reaches its maximum: $\tilde{\Phi}(\rho_{\max}) = 0$
3. The function $\tilde{\Phi}$ must be a concave down function.
4. The function $\tilde{\Phi}$ must be smooth.

The two first constraints ensure that the density remains between 0 and $\rho_{\max}$. We recall that we have chosen the following fundamental diagram that satisfies the above properties and that seems the most appropriate to the shape of the data we have:

$$\Phi(\rho) = v_{\max}\rho\Big(1 - \exp\Big(\frac{c}{v_{\max}}(1 - \frac{\rho_{\max}}{\rho})\Big)\Big) \tag{2.13}$$

For the simulations, we consider that the maximum density $\rho_{\max}$ is fixed and corresponds to the maximum density reconstructed (before doing sampling and aggregation) of the data collected from the simulation.

$$\rho_{\max} = \max_{(i,j)\times n}\tilde{\rho}^n_{i,j}, \qquad (i,j)\times n \in [1,\dots,I]\times[1,\dots,J]\times[1,\dots,N] \tag{2.14}$$

The estimation of the parameters $v_{\max}$ and c is done using the aggregated and sampled data. The optimization problem is solve with a toolbox of Matlab considering the following minimization problem:

$$\underset{v_{\max},c}{\operatorname{argmin}}\Big(\sum_{i=1}^{\bar{I}}\sum_{j=1}^{\bar{J}}\sum_{n=1}^{\bar{N}}\|\Phi(\bar{\rho}^n_{i,j}) - \bar{\Phi}^n_{i,j}\|_2^2\Big) \tag{2.15}$$

The scenario of simulation considered for the collection of data is the following. We consider the network described in Figure 2.6 initially congested. Then we open the network exits and

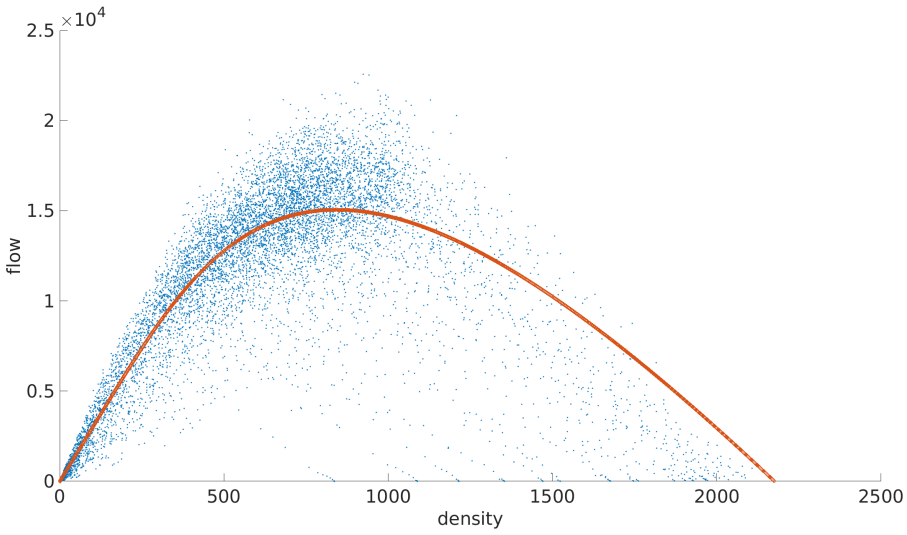

Figure 2.11: Estimation of the fundamental diagram with the function of Newell and Franklin.

stop the inflows. We collect data during the dissipation of the congestion which lasts 15 minutes. Every 0.8s, measures are collected from vehicle position and speed over the whole space. The aggregated and sampled data can be seen in Figure 2.11. We can emphasize that these data are only used for the estimation of $v_{\max}$ and c whereas $\rho_{\max}$ is given as the maximum of the untreated data. The curve is obtained for the value $\rho_{\max} = 2175$ vehicles/km^2, $v_{\max} = 29.9110$km/h and $c = 17.2089 km/h$.

Remark 2. *The two-dimensional maximum density (equal to* $2175 vhs/km^2$*) estimated by microsimulation is lower than the theoretical maximum density we could briefly compute (if there is a car every 6m on each of the 144 roads that have an average length of 100m) then the maximal density should be a little higher (around* $2400 vhs/km^2$*). However, in practice, the network always become totally congested/blocked before reaching this theoretical maximum. A illustration of this situation is provided in Figure 2.12.*

2.2.3.1 Scenario for comparison with microsimulation

In Section 1.3.2, we established a way to reconstruct a two-dimensional density from data of the microsimulator Aimsun. We are now able to compare a simulation of the 2D model with the microsimulator. With this aim, we build two scenarios. Recall that we assume that we have only a flow oriented towards the North-East direction for all simulation. The network is the same deformed 10×10 Manhattan grid as before. The minimum spacing between vehicles along the road is 6m. For the two scenarios, the parameters of the 2D model are the same as the ones estimated in the previous sections: $d_0 = 85.1$m, $\rho_{\max} = 2175$veh/km^2, $v_{\max} = 29.911$km/h, and $c = 17.2089 km/h$. The time step of Aimsun microsimulator is equal 0.8s and it could not be changed because the reaction time of drivers rely on this value. For this reason, the time step Δt of the 2D model has to be a multiple of this value. The

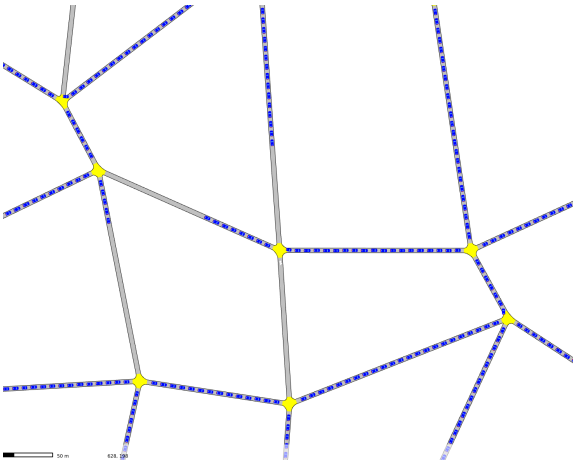

Figure 2.12: Illustration of a traffic network totally blocked but not fulfill

discretization Δx is chosen in order to respect the CLF condition.
In the Aimsun simulator, there is an important role of randomness (for instance at each intersection, the direction taken by a vehicle is a random variable with a probability dependent of the turning ratios). This implies that different runs of the same scenario could yields noticeably different results on a micro-scale. Thus, some congestion at a local level may appear at different place and time in two different run of microsimulation. Thus, to improve the robustness of our model comparison, we compute 100 different runs of the Aimsun simulation for each scenario. For each of these runs, we reconstruct a 2D density and then we use the average of these reconstructed densities as a means of comparison for our 2D model.

Scenario 1: Creation of a congestion. We set up Aimsun that there is an accident in the North-East corner of the domain, which causes a congestion to propagate over the network that is initially in free flow. It is not possible to define directly boundary condition in a comparable way for the two-dimensional model and the Aimsun simulator. For this reason, the comparison between the 2D model and Aimsum microsimulation is done on a subdomain, a square of 800m which starts in the left bottom corner, of the real network defined in the microsimulator. Outside this subdomain, a two-dimensional density is reconstructed from the microsimulation by the method described in Section 1.3.2. Finally, this density is used to feed the Ghost Cell of the 2D model as defined in Section 1.2.2. The split ratio at every intersection is set equal to 50%. This choice is consistent with the way of estimating the direction field in Section 2.1.2. The inflows in both the 2D model and the Aimsum simulator are identical: 800 vehicles per hour at each of the 16 entrances (see Figure 2.6 for an example of an Aimsun simulation which correspond to 6400 vehicles per hour and per km over the 2 km of entrance boundary of the 2D model. The simulation starts 3 mn after the beginning of the congestion and lasts 5mn00s. In Figure 2.13 the initial and final states of the microsimulation for scenario 1 are displayed. A video that shows the reconstruction of density and the distribution of vehicle for one instance of this scenario is available at `https://youtu.be/Nb-m2-fDxHY`. The 2D-model for this scenario are simulated

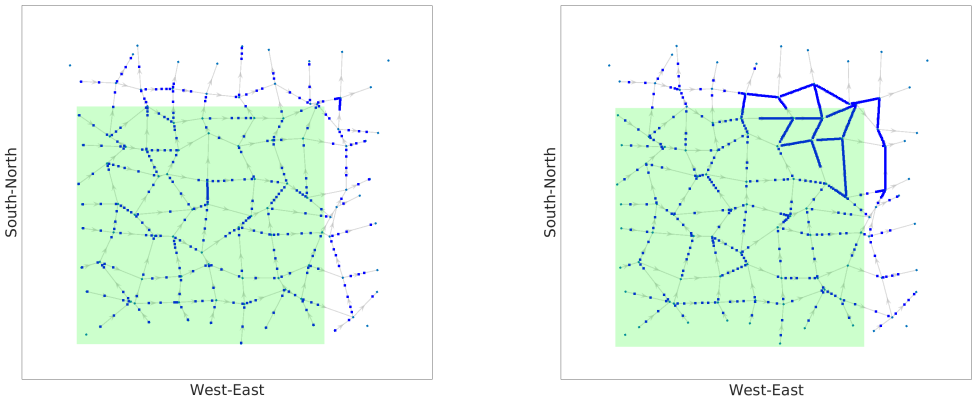

Figure 2.13: Distribution of vehicles during the Aimsun simulation for an individual run of the scenario 1 at the initial and final time of the simulation.

and compared only in the green subdomain. The parts of the network that are not considered in the 2D model are used to provide the boundary condition such that the condition of the 2D-model and the microsimulation are similar.

Scenario 2: Congestion dissipation. The second scenario consists of the dissipation of a congested area. We create a congestion in the microsimulation that fill the network during 15mn and then we start to dissipate it by opening all the outputs and stopping the inflow at the entrances of the model. One minute after the dissipation start, we reconstruct the 2D density from the Aimsun simulator and feed this density as initial state to the 2D model. Then we compare the evolution of the micro and the macro models over the next 5mn00s. The flow of vehicles can cross the boundary without any constraint. For this reason, it is not necessary to consider a specific subdomain as it is the case in scenario 1. The split ratio in the entire network are set equal to 50%. In Figure 2.14 the initial and final states of the microsimulation for one sample of scenario 2 are displayed. A video that shows the reconstruction of density and the distribution of vehicle for one instance of this scenario is available at `https://youtu.be/L8Q9MgYyBK4`.

As the two models are very different, it might be difficult to have a good precision in the results. However, the aim of this study is more to be able to capture the large scale features of traffic than to focus on detail at a local level.

Results of simulation scenario 1.

In this scenario, we are considering a creation of congestion. The results of the simulation can be seen in Figure 2.15. The figure represents a comparison of simulation results between the 2D model and the average of the reconstructed density from 100 runs in Aimsun.

First, we can notice that the main traffic features, which is the propagation of a wave moving backward is captured by the 2D model. During the first 2mn, for the considered selected square of 800m, the network is in free flow conditions because the congestion needs a

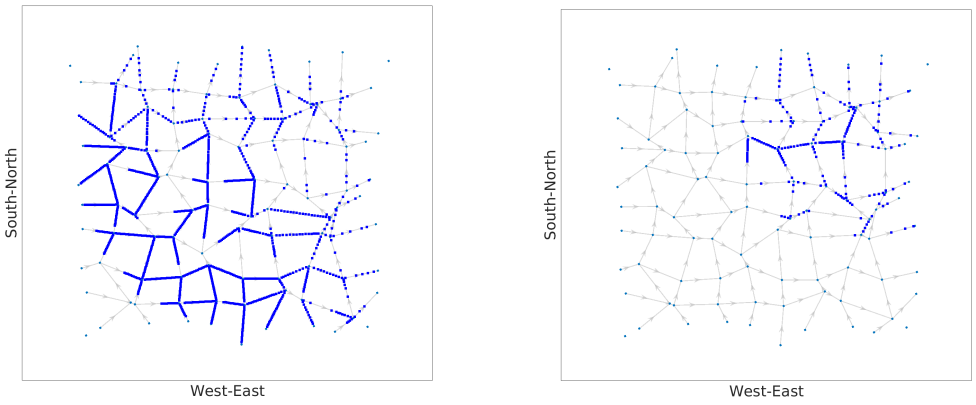

Figure 2.14: Distribution of vehicles during the Aimsun simulation for an individual run the scenario 2 at the initial and an interdiate time of the simulation.

sufficient time to appear. From $t = 120s$, a delay can be seen in the creation of the congestion in the 2D model. This might be explained by the choice of boundary condition. Indeed, the boundary conditions in the 2D model are defined using Ghost Cells. The values of these cells are computed by reconstruction of a two-dimensional density from the microsimulator. However, one feature of the two-dimensional reconstruction is its smoothness due to the Gaussian kernel, whereas the 2D model propagates sharp discontinuities. This difference is causing a delay at the time at which appears the congestion. This delay propagates during the duration of the simulation.
Furthermore, we can observe some difference regarding the shape of the shock wave. Indeed, the shock in the 2D model is really discontinuous whereas for the reconstruction from the microsimulation it is smooth. But, as the kernel use for the reconstruction is a Gaussian with a quite large range we could have expected this phenomenon. The simulation time is short in comparison with usual study case but this scale directly with the size of the network smaller than usual.

Scenario dissipation of congestion:
In the second scenario, we are considering a dissipation of a congestion. As in the previous simulation, the results represent a comparison of the density evolution between the 2D model and the average of 100 Aimsun simulation runs. The results can be seen in Figure 2.16.

The simulation of the dissipation of congestion seems to fit well the reconstruction of the Aimsun simulation. The speed of the dissipation looks also similar. Nevertheless, there is some fundamental difference. First starting from time $t = 30s$, one may notice that the 2D model includes a shock in the South-West of the congested area. This phenomena could not be captured by the reconstructed density which is smooth due to the Gaussian Kernel. On the other side of the congested area, a rarefaction wave that reduced can be observed. If the simulation time is short in comparison with usual study case, this could be directly link with the scaling of the size of the network.

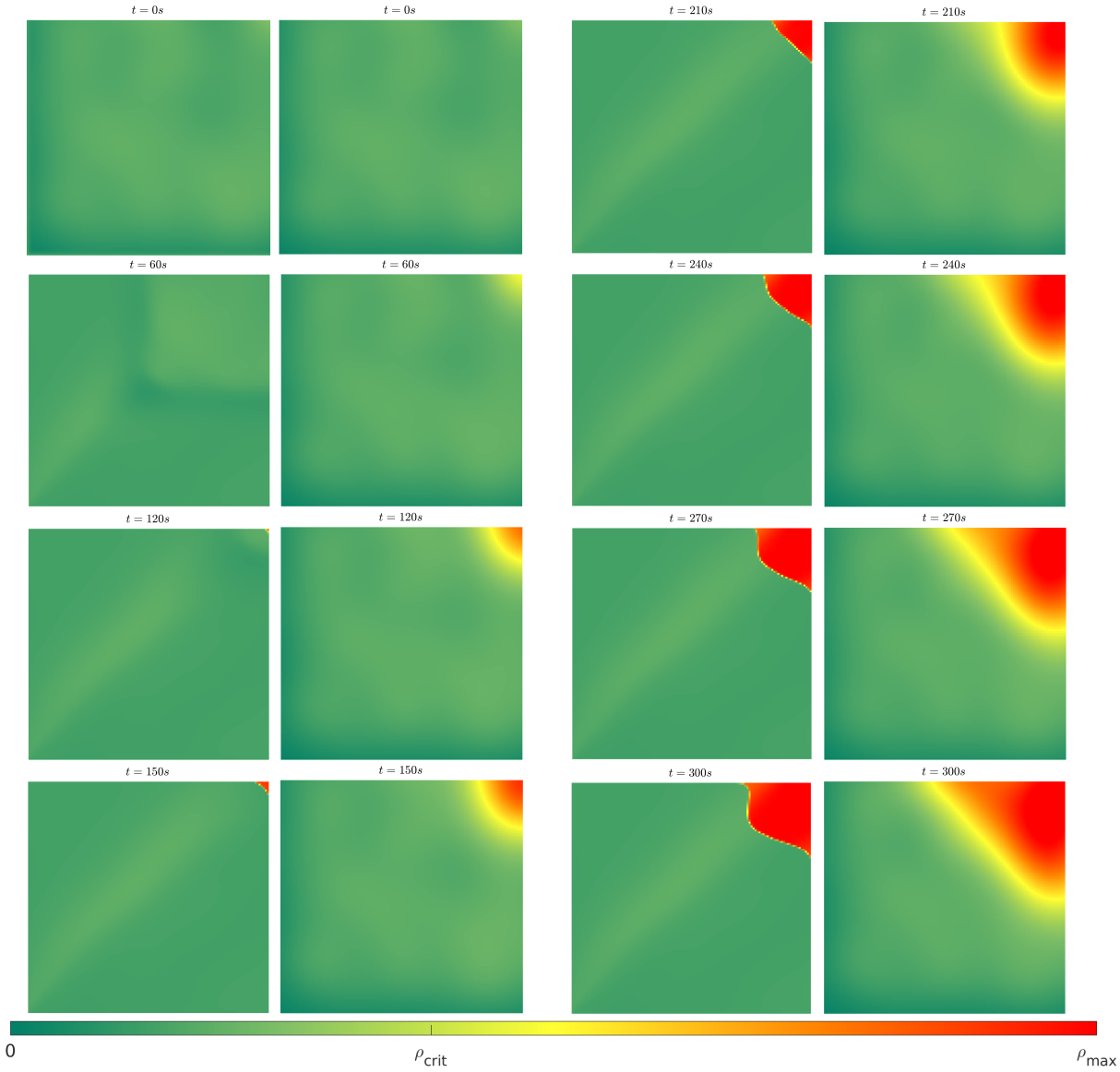

Figure 2.15: Comparison of two-dimensional (left) and the average microsimulator behavior (right) during the creation of a congestion. Video of the full simulation available at `https://youtu.be/Y9RGLFTIGSs`

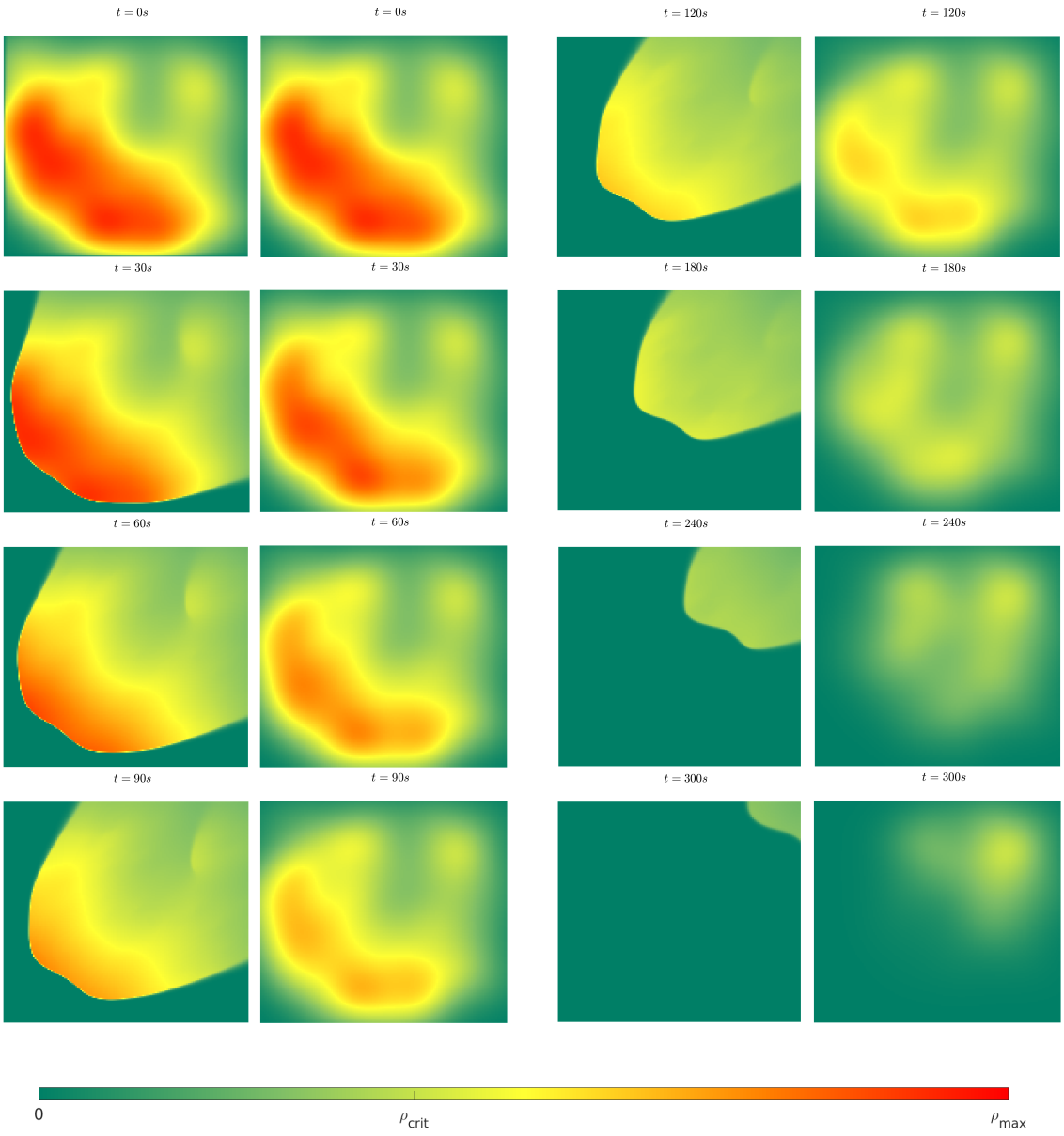

Figure 2.16: Comparison of two-dimensional (left) and the average microsimulator behavior (right) during the dissipation of a congestion. Video of the full simulation available at `https://youtu.be/OLGGyWU2jz4`

Chapter conclusion: Summary, limitations and possible extensions

In this chapter, we introduce a traffic model based on a simple two-dimensional conservation law. In comparison with the modeling in one dimension, the traffic density describes vehicles over areas. The flux of vehicles becomes a vector and it describes propagation of vehicles by both its magnitude and direction.
The direction is defined by a velocity field such that for each space position, only one direction is given. One can notice that this definition of the velocity field implies that the model can not represent crossing flow or vehicles passing each other. For this reason, we consider a network with a preferred direction of propagation which is a sufficient condition but not necessary to avoid crossing of flow.
A method for the estimation of the velocity field using only the network geometry has been presented. This estimation has the advantage to be easy to use but may not represent accurately the real situation. Other estimation methods will be developed later.
The choice of discretization is an interesting question. Usually, the model improves its accuracy when the discretization gets thinner. However, in traffic modeling, it can be questionable to push the discretization further than the scale of the vehicles even of the roads in 2D. In the end, we are more interested in the solution of a discrete model rather in the solution of the PDE itself.
Finally, we present a comparison of the model both with CTM and model of junctions and with microsimulations. The comparison arises the question of the metrics to compare different models. The difficulty is that these models describe traffic with their own variables. So, we consider a method to reconstruct a two-dimensional density from the trajectories of vehicles in Aimsun. But, even in this method reconstructing a two-dimensional density, the classical metrics as the L^2 norm are not ideal because they neglect the spatial component. To conclude, none of these approaches can be seen as the real truth so we just aim to see that the results of the different methods are comparable.

Chapter 3

Heterogeneous network with one direction of flow

Contents

3.1 Model construction

3.1.1 Intuition from 1D

In the classical LWR model in one dimension, the flux function Φ depends only on the density ρ with a relation given by the fundamental diagram (FD). In this section, we are interested in an extension of this model considers a flux function that depends also on space:

$$\begin{cases} \dfrac{\partial \rho(t,x)}{\partial t} + \dfrac{\partial \Phi(x,\rho(t,x))}{\partial x} = 0, & (t,x) \in \mathbf{R}^+ \times \mathbf{R} \\ \rho(0,x) = \rho_0(x). & x \in \mathbf{R} \end{cases} \tag{3.1}$$

A space dependent flux might represent the variation of the speed limit along the road or a change of the number of lanes which involve a change of the maximum density as it is shown in Figure 3.1. Let a_1, a_2 and a_3 be different maximum density and let b_1, b_2 and b_3 be different speed limits such that:

$$a_1 \leq a_2 \leq a_3 \quad \text{and} \quad b_1 \leq b_2 \leq b_3 \tag{3.2}$$

This results to a fundamental diagram that may change along the road modeled. An example of parameter variations for the fundamental diagram is shown in Figure 3.2. This space dependency in the flux function Φ involves a new formulation of the solutions. To study the

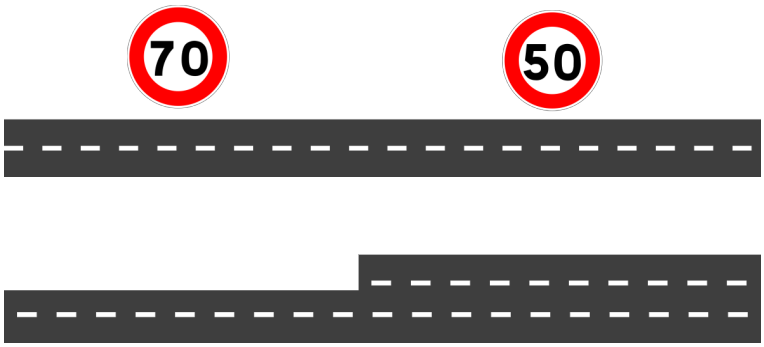

Figure 3.1: Variations of the speed limits or number of lanes in a road

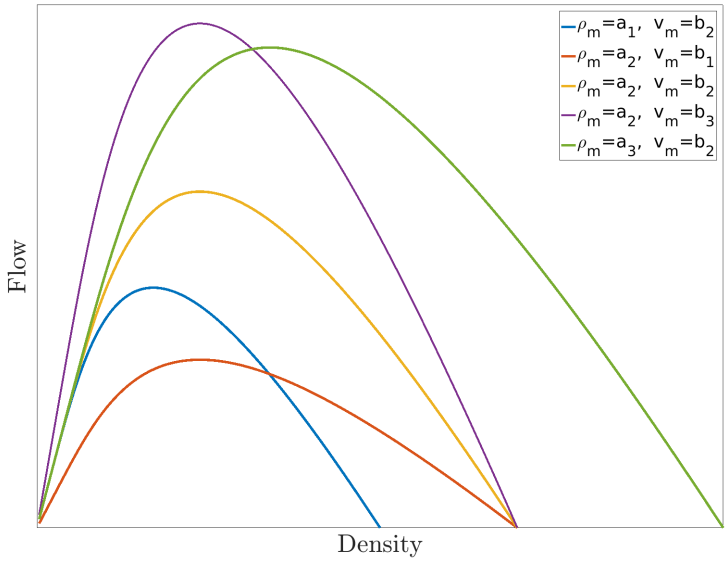

Figure 3.2: Variations of the parameters of the FD

solution of the system (3.1), we are interested of the case where the flux parameters changes in the space $x = 0$:

$$\begin{cases} \dfrac{\partial \rho}{\partial t} + \dfrac{\partial \Phi_l(x,\rho)}{\partial x} = 0, \quad \rho(0,x) = \rho_l, \quad x < 0 \\ \dfrac{\partial \rho}{\partial t} + \dfrac{\partial \Phi_r(x,\rho)}{\partial x} = 0, \quad \rho(0,x) = \rho_r, \quad x > 0 \end{cases} \tag{3.3}$$

where Φ_l and Φ_r are two expressions for the flux function, respectively in the left and in right part of the domain, and ρ_l and ρ_r are the given initial conditions for the density. Then, the problem can be split in two Riemann problems on each side of the discontinuity.

$$\rho(0,x) = \begin{cases} \rho_l & \text{if } x \leq 0 \\ \tilde{\rho}_l & \text{if } x = 0 \end{cases} \tag{3.4}$$

$$\rho(0,x) = \begin{cases} \rho_r & \text{if } x \geq 0 \\ \tilde{\rho}_r & \text{if } x = 0 \end{cases} \tag{3.5}$$

At the position $x = 0$ where the discontinuity occurs, we denote by $\tilde{\rho}_l$ and $\tilde{\rho}_r$ the value of the density. We notice that we do not required equality of these density in this point but we need the flux to be uniquely defined such that we keep the conservation of the mass.

- The waves in the left of the discontinuity are non increasing
- The waves in the right of the discontinuity are non decreasing
- The flux in the discontinuity is uniquely defined i.e. $\Phi_l(\tilde{\rho}_l) = \Phi_r(\tilde{\rho}_r)$

These conditions enable to define a method to find the solution as it is fully studied in [28]. The solution of this problem has several new features such as the creation of stationary waves. A stationary waves is a discontinuities in space of the density that is not propagating. Thus, the equilibrium point, for which the traffic density do not evolve, can appear for non constant density. An example of these solutions with this kind of waves is given in Figure 3.3. At

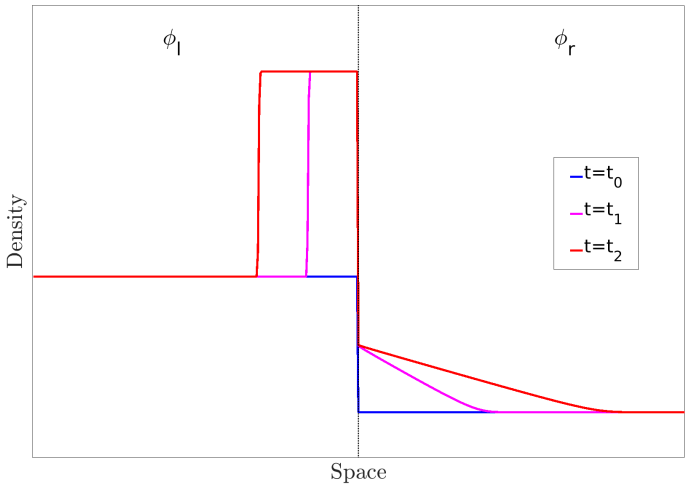

Figure 3.3: Solution of the Riemann problem described in (3.3) at different times

the position of the flux discontinuity, we can see a stationary wave. On the left side, there is a shock wave moving backward whereas on the right side, we see a rarefaction wave. The numerical simulation in Figure 3.3 is done with the same demand-supply formulation that the one given in Section 3.2.1 and give the theoretical result expected in [28].

3.1.2 Description of the model

In this section, we suggest an extension of the model introduced Section 2.1.1 including a space dependent flux function. This extension is even more relevant than in the one dimensional case for at least two reason:

- As a large scale network is considered, the hypothesis that the traffic parameters (maximum density and speed limit) for all these roads are identical does not hold.
- In a two-dimensional representation of traffic, the maximum density not only depends on the number of lanes but can also depend on the concentration of roads in a specific area.

The following model is considered:

$$\begin{cases} \dfrac{\partial \rho}{\partial t}(t,x,y) + \nabla \cdot \vec{\Phi}(x,y,\rho) = 0, & \forall t \in \mathbb{R}^+, \\ \rho(0,x,y) = \rho_0(x,y). & \forall (x,y) \in \mathbb{R}^2 \end{cases} \tag{3.6}$$

where the flux function can be expressed as the product between velocity and density:

$$\vec{\Phi}(x,y,\rho) = \rho \ \cdot \ \vec{v}(x,y,\rho) \tag{3.7}$$

and the velocity field $\vec{v}(x,y,\rho)$ is given by

$$\vec{v}(x,y,\rho) = \underbrace{v(x,y,\rho)}_{\text{magnitude}} \quad \cdot \quad \underbrace{\vec{d_\theta}(x,y)}_{direction}, \tag{3.8}$$

with $v(x,y,\rho) : \mathbb{R}^2 \times [0, \rho_{\mathrm{m}}(x,y)] \to [0, v_{\mathrm{m}}(x,y)]$. ρ_{m} and v_{m} denote respectively the maximum density field and maximum speed field. The magnitude is given by a space dependent fundamental diagram:

$$v(x,y,\rho) = v_{\mathrm{m}}(x,y)\left(1 - \exp\left(\alpha\Big(1 - \frac{\rho_{\mathrm{m}}(x,y)}{\rho}\Big)\right)\right) \tag{3.9}$$

The parameter α is chosen constant equal to 0.4 such that the ratio between the critical density field ρ_{c} and the maximum density field ρ_{m} remains constant.

3.1.3 Parameters estimation

In this section, we are interested in the estimation of the space dependent parameters for the fundamental diagram ρ_{m} and v_{m} and of the velocity field $\vec{d_\theta}$. The estimation of the velocity field follows the same methodology that developed in the Section 2.1.2. The result of the estimation can be seen in Figure 3.4. The estimation of the fundamental diagram paramaters is based on the method to reconstruct a two-dimensional density from the observation of individual vehicles using the Kernel Density Estimation (KDE) method as we described it in the Section 1.3.2. A short recall of the method can be given as follow: each individual vehicle have a contribution to the global density estimation with a Gaussian kernel centered in the vehicle position. Let $(x_k^n, y_k^n)_{k \in [1 \cdot K(n)]}$ be the position of vehicles within the network at time t^n. Then we can reconstruct the density at this time over the network as follows:

$$\tilde{\rho}^n(x,y) = \sum_{k=1}^{K(n)} G_{2d}\left(\begin{pmatrix} x \\ y \end{pmatrix} - \begin{pmatrix} x_k^n \\ y_k^n \end{pmatrix}\right) \tag{3.10}$$

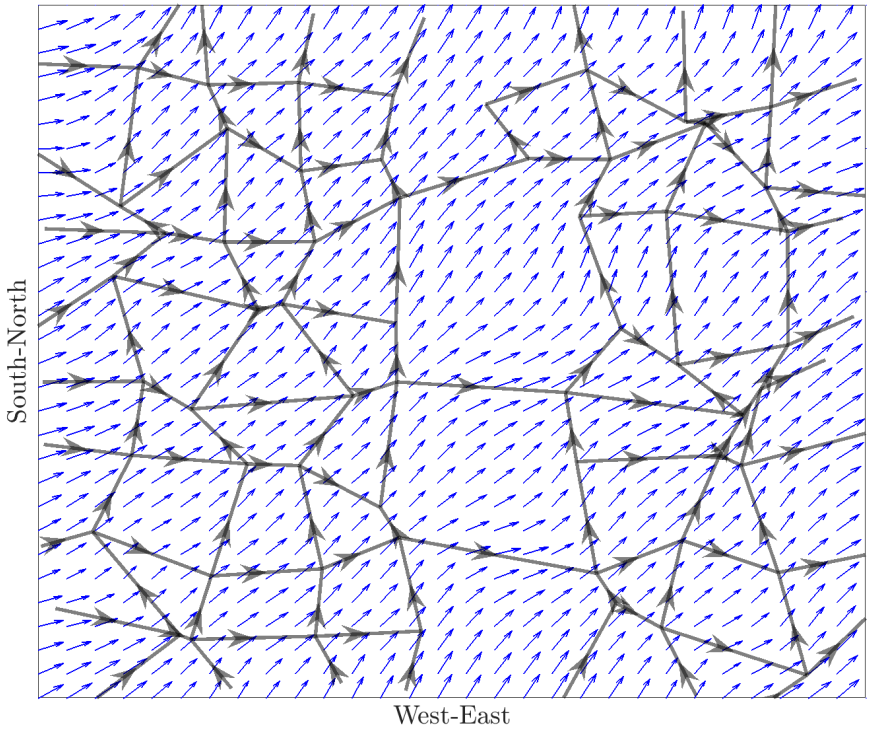

Figure 3.4: Estimation of the velocity field $\vec{d_\theta}$ for the considered network with a $\beta = 20$.

with

$$G_{2d}(x,y) = \frac{e^{-\frac{x^2+y^2}{2d_0^2}}}{2\pi d_0^2} \text{ s.t. } \iint_{\mathbb{R}^2} G_{2d}(x,y)\,dx\,dy = 1,$$

d_0 is a parameters that control the range of the Gaussian function. We set d_0 equal to 50m. This method allows to reconstruct a two-dimensional density either from real data (GPS probes) or from a microsimulator (for instance Aimsun).
With these notions, we are now able to describe the method to estimate the space dependent maximum density $\rho_{\mathrm{m}} : \Omega \to \mathbb{R}_+$. Let us now consider that we have a fully congested network. We set the headway between two consecutive vehicles equal to 6m which is a rough estimate of the value obtained from real traffic data in urban area [20]. Then, we assume that in every road and each 6m there is a vehicle. We denote by $(x_k, y_k)_{k\in\{1,\cdots,K_{\max}\}}$ the position of all these vehicles. Thus, we estimate the maximal density of the network as follows:

$$\rho_{\mathrm{m}}(x,y) = \sum_{k=1}^{K_{\max}} G_{2d}\left(\begin{pmatrix} x \\ y \end{pmatrix} - \begin{pmatrix} x_k \\ y_k \end{pmatrix}\right). \tag{3.11}$$

The estimated maximum density obtained with this method can be shown in Figure 3.5. For the color scale to represent the density, we define:

$$\rho_{\max} = \max_{(x,y)\in\mathbb{R}^2} \rho_{\mathrm{m}}(x,y). \tag{3.12}$$

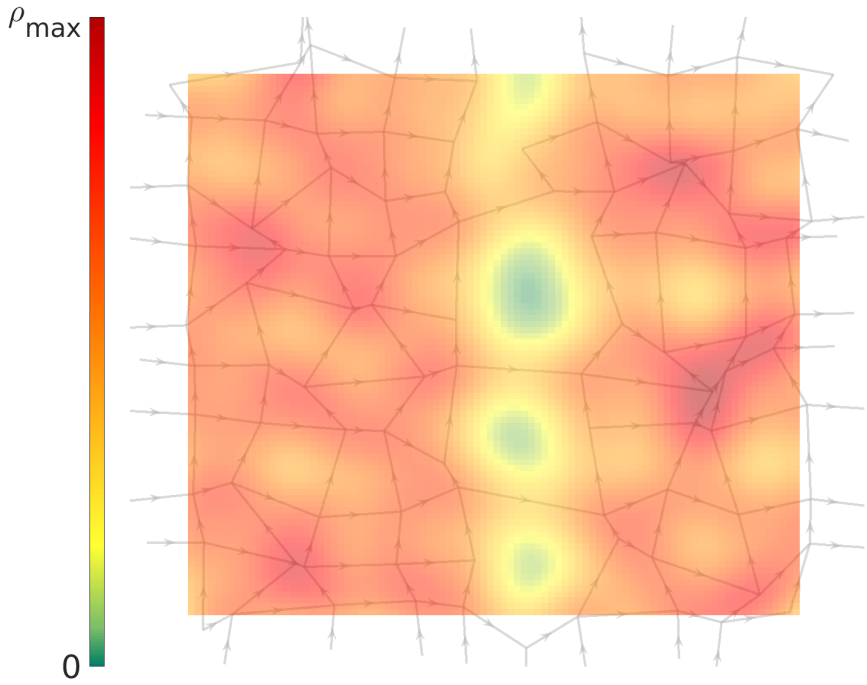

Figure 3.5: Estimation of the maximum density $\rho_{\mathrm{m}}(x, y)$ over the 2D-plane using the proposed method for a parameter d_0 set to 50m

We can notice that in the central area of the network, a lower concentration of roads involves a lower estimation of the maximum density. To avoid issue on the reconstruction near the boundary, we considered an extension of the network just for the estimation of the maximum density (see Figure 3.5 in comparison with Figure 3.6).
For the estimation of the maximum speed, we use an interpolation method as in Section 2.1.2. We keep the same notation with $q \in \{1, \cdots, Q\}$ the different roads and $\Psi^q : \ s \in [0, s_{\max}] \to (\Psi_1^q(s), \Psi_2^q(s)) \in \mathbb{R}^2$ the parametric curves that describes the paths of each road. Let $v^q(\Psi^q(s))$ be the speed limit of the road q at position $(\Psi_1^q(s), \Psi_2^q(s))$. The estimation of maximum velocity over the 2D-plane v_{m} is done by the spatial interpolation method:

$$v_{\mathrm{m}}(x, y) = \frac{\sum_{q=1}^{Q} \int_{s\in[0,s_{\max}]} w(l(x, y, s))v^q(\Psi^q(s))ds}{\left|\left| \sum_{q=1}^{Q} \int_{s\in[0,s_{\max}]} w(l(x, y, s))ds \right|\right|} \tag{3.13}$$

where $l : (x, y, s) \to \|(x, y) - (\Psi^q(s))\|$ is the distance from the point (x,y) to the road and where

$$w : X \to e^{-\beta X} \qquad \text{with} \qquad \beta > 0.$$

The estimated maximum velocity field can be seen in Figure 3.6. A path with a higher maximum speed is described along the arterial road as expected. For the interpolation of the maximum speed v_{m}, an important remark is that the estimation does not depend on the road concentration but only on the the value of the speed limit of the neighbouring roads.

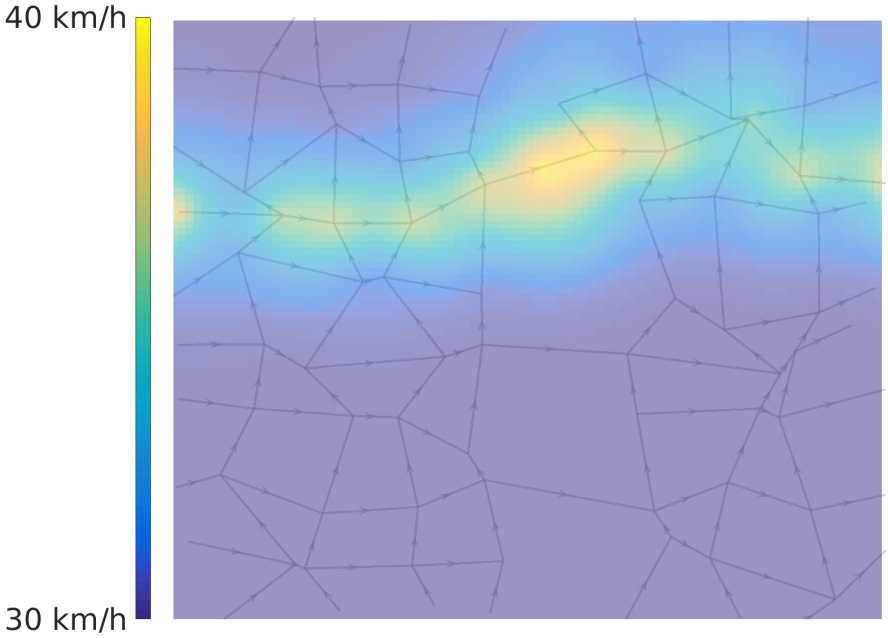

Figure 3.6: Interpolation of the maximum speed $v_{\mathrm{m}}(x, y)$ from the speed limit of the roads

3.2 Results of simulation

3.2.1 Adaptation of the numerical method

In this section, a extension of the numerical method presented in 1.2.1 with an adaptation to include the space dependencies. The dimensional splitting is still considered to solve the two-dimensional aspect but instead of considering the Godunov scheme to compute the flux in each dimension, we propose an extrapolation of the well know Cell Transmission Model [11] with a demand-supply formulation which includes the space dependencies.
Let $(C_{i,j})_{(i,j)\in[1..I]\times[1..J]}$ be the cell of the uniform rectangular space discretization and (x_i, y_j) be the coordinates of each cell center. Applying the method given in section 2.1.2, we can define a flux direction for each cell

$$\vec{d_\theta}(x_i, y_j) = \begin{cases} \cos(\theta_{i,j}) \\ \sin(\theta_{i,j}) \end{cases} \tag{3.14}$$

Let us define the density in the cells with $(\rho_{i,j})_{(i,j)\in[1..I]\times[1..J]}$, then the numerical flux is defined at cell interfaces with the notation $F_{i+\frac{1}{2},j} = F(\rho_{i,j}, \rho_{i+1,j})$ and the function F is defined as follows:

$$F_{i+\frac{1}{2},j} = \begin{cases} \min(D_{i,j}, S_{i+1,j}) \text{ if } \cos(\theta_{i+\frac{1}{2},j}) \geq 0 \\ \min(S_{i,j}, D_{i+1,j}) \text{ if } \cos(\theta_{i+\frac{1}{2},j}) < 0 \end{cases} \tag{3.15}$$

Here $\theta_{\mathrm{i,j}}$ is the angle (see (3.14)) of the unit vector direction of the flux $\vec{d_\theta}(x_{\mathrm{i}}, y_{\mathrm{j}})$ defined in Section 2.1.2 at cell $C_{i,j}$, and $\cos(\theta_{\mathrm{i}+\frac{1}{2},\mathrm{j}})$ is defined equal to $\frac{\cos(\theta_{\mathrm{i}+1,\mathrm{j}})+\cos(\theta_{\mathrm{i,j}})}{2}$. $D_{i,j}$ and $S_{i,j}$ are

respectively the demand and supply function of the cell $C_{i,j}$ which could be defined as follows:

$$D_{i,j} = \begin{cases} \Phi(x_i, y_j, \rho_{i,j}), & \text{if } \rho_{i,j} \leq \rho_{\mathrm{c}}(x_i, y_j) \\ \Phi_{\mathrm{m}}(x_i, y_j), & \text{if } \rho_{i,j} > \rho_{\mathrm{c}}(x_i, y_j) \end{cases} \tag{3.16}$$

$$S_{i,j} = \begin{cases} \Phi_{\mathrm{m}}(x_i, y_j), & \text{if } \rho_{i,j} \leq \rho_{\mathrm{c}}(x_i, y_j) \\ \Phi(x_i, y_j, \rho_{i,j}), & \text{if } \rho_{i,j} > \rho_{\mathrm{c}}(x_i, y_j) \end{cases} \tag{3.17}$$

with the flux $\Phi(x_i, y_j, \rho_{i,j}) = \rho_{i,j} \cdot v(x_i, y_j, \rho_{i,j})$ and his maximum $\Phi_{\mathrm{m}}(x_i, y_j) = \rho_{\mathrm{c}}(x_i, y_j) \cdot v(x_i, y_j, \rho_{\mathrm{crit}}(x_i, y_j))$. The velocity function v is the one defined in Section 3.1.2 with the parameters ρ_{m} and v_{m} estimated respectively in Section 3.1.3 and 3.1.3. $\rho_{\mathrm{c}}(x_i, y_j)$ is the corresponding critical density for a maximum density $\rho_{\mathrm{m}}(x_i, y_j)$. The vertical flux $F_{i,j+\frac{1}{2}}$ is defined analogously.
Let Δt be the time step, and Δx and Δy the space discretization with respect to the x-axis and the y-axis. Then the global scheme for the computation of the model can be defined with the dimensional splitting as follows:

$$\rho^*_{\mathrm{i,j}} = \rho^{\mathrm{n}}_{\mathrm{i,j}} - \frac{\Delta t}{\Delta x}\Big(\cos(\theta_{\mathrm{i}+\frac{1}{2},\mathrm{j}}) F^n_{\mathrm{i}+\frac{1}{2},\mathrm{j}} - \cos(\theta_{\mathrm{i}-\frac{1}{2},\mathrm{j}}) F^n_{\mathrm{i}-\frac{1}{2},\mathrm{j}} \Big), \tag{3.18}$$

$$\rho^{n+1}_{\mathrm{i,j}} = \rho^*_{\mathrm{i,j}} - \frac{\Delta t}{\Delta y}\Big(\sin(\theta_{\mathrm{i,j}+\frac{1}{2}}) F^*_{\mathrm{i,j}+\frac{1}{2}} - \sin(\theta_{\mathrm{i,j}-\frac{1}{2}}) F^*_{\mathrm{i,j}-\frac{1}{2}} \Big), \tag{3.19}$$

where the variables are:

- $\rho^{\mathrm{n}}_{\mathrm{i,j}}$, $\rho^{\mathrm{n+1}}_{\mathrm{i,j}}$ are the discrete density at time t^n and t^{n+1}
- $\rho^*_{\mathrm{i,j}}$ is an intermediate value used only for computation
- Δx, Δy, Δt are space and time step discretization
- $F^n_{\mathrm{i}+\frac{1}{2},\mathrm{j}}$ is the flux at the cell interface
- $\cos(\theta_{\mathrm{i}+\frac{1}{2},\mathrm{j}})$ and $\sin(\theta_{\mathrm{i,j}+\frac{1}{2}})$ are the contribution of the flow direction.

3.2.2 Results of simulation for a non homogeneous network

The validation of the model is done by comparing the model prediction and the one given by the microsimulator Aimsun. To this aim, a simulation for the same network and scenario is run for the two. In order to be able to compare these results, a two-dimensional density is reconstructed from the vehicles' trajectories of the Aimsun simulation using the method described in Section 1.3.2.

3.2.2.1 Scenario description

The scenario considered represents a dissipation of a congestion. In the microsimulator, an important concentration of vehicles is artificially generated in the East of the network and set as an initial condition for the simulation. The split ratio at each intersection is equal to 50% except for the roads across the network bottleneck where 70% of vehicles goes into the bottleneck. With the method described in Section 1.3.2, a two-dimensional density is reconstructed and given as initial condition of the 2D model. Then, the two models are run independently assuming that there is no inflows in both cases. The 2D model provides a propagation of density whereas the microsimulator describes the evolution of each vehicle's trajectory. At each time step (which has been synchronized), the results of the models can be compared by reconstructing a 2D density from the vehicles' position of the Aimsun Simulation. The network characteristics defined for the microsimulator are identical to those considered for the estimation of the model parameters. Thus, the minimum headway between vehicles is set to 6m and the road speed limits are set equal to 30 or 50km/h.

3.2.2.2 Results of the comparison with the microsimulator

We simulate the scenario described above. The comparison between the results of the two models can be seen in Figure 3.7. A first remark is that in the microsimulator the congestion does not propagate across the bottleneck and remain in the left side of the network. This phenomena is also captured by the two-dimensional model where a discontinuity in the density appears next to the network bottleneck. It is a stationary wave, a classical feature that can be seen when considering space dependent flux function. Globally, the predictions of the 2D-model and Aimsun are consistent even if the one given by the 2D-model seems more sharp. This can be explained by the shock in the macroscopic model that can not be captured by the density reconstruction due to the smoothing of the Gaussian kernels. Another remark is that we choose to show the comparison with absolute value of the density where the scale is given by the maximum over the space of the maximum density. This choice could give an impression that the network is only slightly congested.

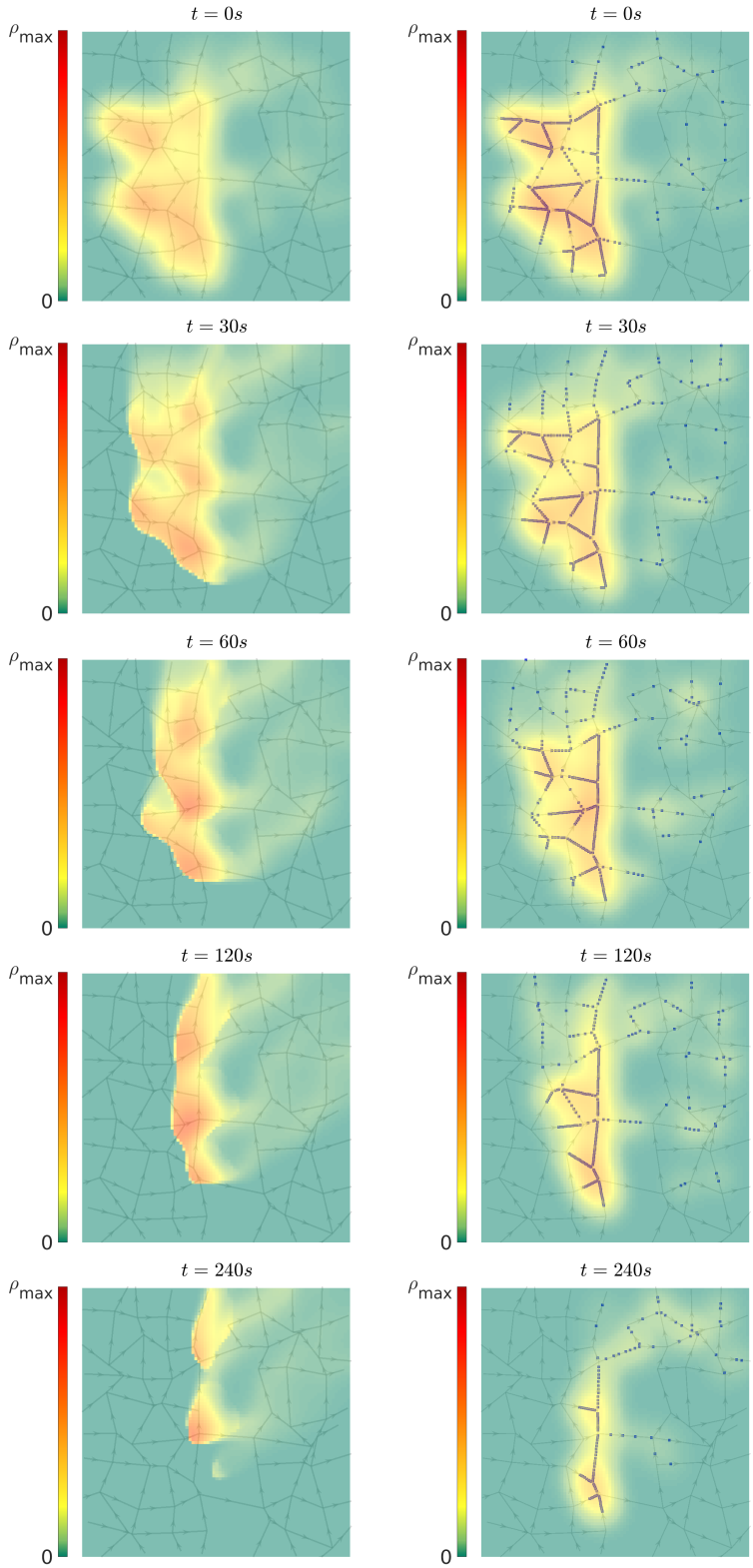

Figure 3.7: Comparison between the 2D model with space dependent flux function (left) and the 2D density reconstructed from the microsimulator (right) for a scenario of congestion dissipation. The blue squares represent vehicles of the microsimulation. A video of the simulation is available on `https://youtu.be/qWNnnpFJZeQ`.

Chapter conclusion: Summary, limitations and possible extensions

In one dimension, the hypothesis that the parameters of the Fundamental Diagram are constant variables is acceptable, because in many situations, the speed limit of the road and the number of lanes do not change. However, in a two-dimensional setting, especially when a large-scale is involved, it is very unlikely that these parameters remain constant. Indeed, the larger the network is, the higher is the probability that it contains roads with different speed limits. Furthermore, the maximum density does not only depend on the number of lanes but also the concentration of roads in this area.
In this chapter, we present an extension of the two-dimensional model with space-dependent parameters. The estimation of these parameters is based only on the network topology. These space-dependent parameters can represent bottlenecks of the network and enable the model to create traffic congestion.
One possible extension is to investigate the presence of capacity drop in 2D. In 1D, this corresponds to a reduction of capacity, due to the reduction of the number of lanes, higher than expected because of the interaction between vehicles trying to change their lane. It could be interesting to study if there exists this kind of phenomena at the network level when vehicles merge in a area with a lower concentration of roads.

Chapter 4

Networks with multiple directions of flow

Contents

4.1 Construction of a multilayer model

4.1.1 Intuition from 1D: Multiclass traffic flow modeling

Multiclass models, also called multipopulation models, aim to extend the LWR model to describe the different behavior of heterogeneous drivers. These models were proposed independently by Wong and Wong in [66] in 2002 and Benzoni in [5] in 2003. In Section 3, we

introduced the notion of heterogeneous networks which is different from the heterogeneous drivers' behavior that we can observe here. The n-population can be defined as follows:

$$\begin{cases} \dfrac{\partial \rho^{\ell_i}}{\partial t} + \dfrac{\partial \rho^{\ell_i} v^{\ell_i}(\sum_{k=1}^{n} \rho^{\ell_k})}{\partial x} = 0 \\ \rho^{\ell_i}(t=0,x) = \rho_0^{\ell_i}(x) \end{cases} \tag{4.1}$$

where $(\rho^{\ell_i})_{i\in[1,\cdots,n]}$ is the density of cars belonging to the class ℓ of drivers or categories of vehicles. For each class of drivers, the velocity function v^{ℓ_i} can have different parameters such as the maximum speed.

Example: We want to model mixed traffic on a highway with both cars and trucks. The speed limits are 90 km/h for the trucks and 130 km/h for the cars. With the classical model, the maximum speed of vehicles has to be set at an intermediate level that can fit both the cars and trucks. With a multipopulation model, it is not needed to look for a compromise as the two categories of vehicles can have different parameters. However, we can emphasise that in a multipopulation model, the different classes of vehicles are not independent and there are still interactions: the speed is computed using the total density and not only the density of one vehicle class.

Remark 3. *It is possible to represent the previous case with only one layer with multiples layers. Indeed, if all the classes have the same parameters, the propagation of the total density (the sum of the density of layers) in the multilayer model corresponds to the model with only one layer and the same parameters.*

4.1.2 Motivation and model description

In this chapter, we aim to extend the multiclass model for two-dimensional traffic models. In 1D, multiclass models are used mostly to describe vehicles with different speed limits. In 2D, we aim to consider multiclass model to describe categories of vehicles evolving in different directions. This change allows overcoming the limitation of the previous chapter of a "preferred" direction of propagation. The idea of representing multiple directions of traffic with multiclass model is studied in [48], [49]. To be able to describe multiple flows of vehicles evolving in different directions, several layers $\ell \in [1,\dots,L]$ of density ρ^{ℓ} are considered such that each layer represents a different direction of flow. The global density ρ is composed by the density of all the layers $\rho(t,x,y) = (\rho^1(t,x,y),\dots,\rho^L(t,x,y))$. Here, we consider a simple case where only two layers are considered, but the number of layers can be arbitrarily large. The only limitation is that we want the concentration of vehicles in each layer to be sufficient to justify the use of a macroscopic model. The model is based on a system of conservation

laws and can be described as follows:

$$\begin{cases} \dfrac{\partial \rho^{\ell_1}(t,x,y)}{\partial t} + \nabla \cdot \vec{\Phi^{\ell_1}}(\rho(t,x,y)) = 0, \\ \dfrac{\partial \rho^{\ell_2}(t,x,y)}{\partial t} + \nabla \cdot \vec{\Phi^{\ell_2}}(\rho(t,x,y)) = 0, \quad \forall t \in \mathbb{R}^+, \forall (x,y) \in \Omega \\ \rho^{\ell_1}(0,x,y) = \rho_0^{\ell_1}(x,y), \\ \rho^{\ell_2}(0,x,y) = \rho_0^{\ell_2}(x,y), \end{cases} \tag{4.2}$$

where

- ρ^{ℓ_1}, ρ^{ℓ_2} are the two dimensional densities of the vehicles for two different layers ℓ_1, ℓ_2
- $\rho_0^{\ell_1}$, $\rho_0^{\ell_2}$ are the initial densities of the layers
- $\vec{\Phi^{\ell_1}}$, $\vec{\Phi^{\ell_2}}$ are the flows of vehicles with respect to each layer which are described as:

$$\vec{\Phi^{\ell}}(\rho(t,x,y)) = \rho^{\ell}(t,x,y) \cdot v^{\ell}(\Psi^{\ell}(\rho(t,x,y))) \cdot \vec{d_\theta^{\ell}}(x,y) \tag{4.3}$$

with

- $v^{\ell} : [0, \rho_{\max}] \to [0, v_{\max}]$ the velocity magnitude of vehicles of the layer ℓ corresponding to the Fundamental Diagram (FD).
- $\vec{d_\theta^{\ell}}$ the unit vector direction field of the layer ℓ that represents the direction of propagation of the vehicles of this layer.
- Ψ^{ℓ} the effective density function, or the interaction term. This is a function of the global density $\rho = (\rho_{\ell_1}, \rho_{\ell_2})$ and measures how the velocity is affected by the density of the different layers.

In practice, we consider the simplest case where the effective density is equal to the sum of the density of the different layers:

$$\begin{aligned} &\Psi^{\ell_1}, \Psi^{\ell_2} : [0, \rho_{\max}]^2 \to [0, \rho_{\max}] \\ &\Psi^{\ell_1}(\rho) = \Psi^{\ell_2}(\rho) = \rho^{\ell_1} + \rho^{\ell_2} \end{aligned} \tag{4.4}$$

Overall, the model has three parameters: the direction field of the two layers $\vec{d_\theta^{\ell_1}}$ and $\vec{d_\theta^{\ell_2}}$, the maximum density $\rho_{\max}$ and the maximum velocity $v_{\max}$ that all rely on the considered network.

4.1.3 Model structure (Hyperbolicity)

Hyperbolic partial differential equations (PDE) correspond to a class of PDE that describes phenomena propagating with finite speed. The wave equation, the transport equation and

many conservation laws are hyperbolic. Models developed in traffic flow, such as the LWR model, are also hyperbolic and many numerical methods have been developed for this kind of equation. Thus, it can be interesting to study the hyperbolicity of the presented model. In practice, the investigation of hyperbolicity is done by the analysis of the Jacobian matrix of the flux see [8], [63]. For simplicity, we investigate only the case of 2 layers.

Case L=2: We consider the case where we have only 2 layers with the densities ρ^{ℓ_1} and ρ^{ℓ_2}. We have the following model:

$$\begin{cases} \dfrac{\partial \rho^{\ell_1}(t,x,y)}{\partial t} + \dfrac{\partial \Phi_{\mathrm{x}}^{\ell_1}(\rho(t,x,y),x,y)}{\partial x} + \dfrac{\partial \Phi_{\mathrm{y}}^{\ell_1}(\rho(t,x,y),x,y)}{\partial y} = 0 \\ \dfrac{\partial \rho^{\ell_2}(t,x,y)}{\partial t} + \dfrac{\partial \Phi_{\mathrm{x}}^{\ell_2}(\rho(t,x,y),x,y)}{\partial x} + \dfrac{\partial \Phi_{\mathrm{y}}^{\ell_2}(\rho(t,x,y),x,y)}{\partial y} = 0 \\ \rho^{\ell_1}(0,x,y) = \rho_0^{\ell_1}(x,y) \\ \rho^{\ell_2}(0,x,y) = \rho_0^{\ell_2}(x,y) \end{cases}, \qquad \forall t \in \mathbb{R}^+, \forall (x,y) \in \Omega \tag{4.5}$$

Definition: We denote by Φ_x and Φ_y the flux function for the x and y dimension. Then, the system is hyperbolic if $\forall \alpha \in [0, \ldots, 2\pi)$, the matrix:

$$A = \cos(\alpha)\mathrm{Jac}_{\Phi_x} + \sin(\alpha)\mathrm{Jac}_{\Phi_y} \tag{4.6}$$

has real eigenvalues.

Thus, we have to compute the eigenvalues of the matrix A. Lets start with the flow vector for the x-space dimension:

$$\Phi_x = \begin{cases} \Phi_x^{\ell_1} \\ \Phi_x^{\ell_2} \end{cases} = \begin{cases} \rho^{\ell_1} v^{\ell_1}(\Psi^{\ell_1}(\rho,\theta))\cos(\theta^{\ell_1}) \\ \rho^{\ell_2} v^{\ell_2}(\Psi^{\ell_2}(\rho,\theta))\cos(\theta^{\ell_2}) \end{cases} \tag{4.7}$$

The Jacobian matrix of this flux function is computed by taking the derivatives with respect to ρ^{ℓ_1} and ρ^{ℓ_1}:

$$\mathrm{Jac}_{\Phi_x} = \begin{pmatrix} \cos(\theta^{\ell_1})\left(v^{\ell_1}(\Psi^{\ell_1}(\rho,\theta)) + \rho^{\ell_1}\dfrac{\partial \Psi^{\ell_1}}{\partial \rho^{\ell_1}}\dfrac{\partial v^{\ell_1}}{\partial \Psi^{\ell_1}}\right) & \cos(\theta^{\ell_1})\rho^{\ell_1}\dfrac{\partial \Psi^{\ell_1}}{\partial \rho^{\ell_2}}\dfrac{\partial v^{\ell_1}}{\partial \Psi^{\ell_1}} \\ \cos(\theta^{\ell_2})\rho^{\ell_2}\dfrac{\partial \Psi^{\ell_2}}{\partial \rho^{\ell_1}}\dfrac{\partial v^{\ell_2}}{\partial \Psi^{\ell_2}} & \cos(\theta^{\ell_2})\left(v^{\ell_2}(\Psi^{\ell_2}(\rho,\theta)) + \rho^{\ell_2}\dfrac{\partial \Psi^{\ell_2}}{\partial \rho^{\ell_2}}\dfrac{\partial v^{\ell_2}}{\partial \Psi^{\ell_2}}\right) \end{pmatrix} \tag{4.8}$$

Similarly, the flow vector for the y-space dimension is:

$$\Phi_y = \begin{cases} \Phi_y^{\ell_1} \\ \Phi_y^{\ell_2} \end{cases} = \begin{cases} \rho^{\ell_1} v^{\ell_1}(\Psi^{\ell_1}(\rho,\theta))\sin(\theta^{\ell_1}) \\ \rho^{\ell_2} v^{\ell_2}(\Psi^{\ell_2}(\rho,\theta))\sin(\theta^{\ell_2}) \end{cases} \tag{4.9}$$

And we can write the Jacobian matrix of this flux as:

$$\mathrm{Jac}_{\Phi_y} = \begin{pmatrix} \sin(\theta^{\ell_1})\left(v^{\ell_1}(\Psi^{\ell_1}(\rho,\theta)) + \rho^{\ell_1}\dfrac{\partial \Psi^{\ell_1}}{\partial \rho^{\ell_1}}\dfrac{\partial v^{\ell_1}}{\partial \Psi^{\ell_1}}\right) & \sin(\theta^{\ell_1})\rho^{\ell_1}\dfrac{\partial \Psi^{\ell_1}}{\partial \rho^{\ell_2}}\dfrac{\partial v^{\ell_1}}{\partial \Psi^{\ell_1}} \\ \sin(\theta^{\ell_2})\rho^{\ell_2}\dfrac{\partial \Psi^{\ell_2}}{\partial \rho^{\ell_1}}\dfrac{\partial v^{\ell_2}}{\partial \Psi^{\ell_2}} & \sin(\theta^{\ell_2})\left(v^{\ell_2}(\Psi^{\ell_2}(\rho,\theta)) + \rho^{\ell_2}\dfrac{\partial \Psi^{\ell_2}}{\partial \rho^{\ell_2}}\dfrac{\partial v^{\ell_2}}{\partial \Psi^{\ell_2}}\right) \end{pmatrix} \tag{4.10}$$

Then, we compute the characteristic polynomial $P(\lambda)$ of the matrix A:

$$P(\lambda) = \left(\lambda - (\cos(\alpha)\cos(\theta^{\ell_1}) + \sin(\alpha)\sin(\theta^{\ell_1}))\left(v^{\ell_1}(\Psi^{\ell_1}(\rho,\theta)) + \rho^{\ell_1}\frac{\partial\Psi^{\ell_1}}{\partial\rho^{\ell_1}}\frac{\partial v^{\ell_1}}{\partial\Psi^{\ell_1}}\right)\right)$$

$$\left(\lambda - (\cos(\alpha)\cos(\theta^{\ell_2}) + \sin(\alpha)\sin(\theta^{\ell_2}))\left(v^{\ell_2}(\Psi^{\ell_2}(\rho,\theta)) + \rho^{\ell_2}\frac{\partial\Psi^{\ell_2}}{\partial\rho^{\ell_2}}\frac{\partial v^{\ell_2}}{\partial\Psi^{\ell_2}}\right)\right)$$

$$-\rho^{\ell_1}\rho^{\ell_2}\left(\cos(\alpha)\cos(\theta^{\ell_1}) + \sin(\alpha)\sin(\theta^{\ell_1})\right)$$

$$\left((\cos(\alpha)\cos(\theta^{\ell_2}) + \sin(\alpha)\sin(\theta^{\ell_2})\right)\left(\frac{\partial\Psi^{\ell_1}}{\partial\rho^{\ell_2}}\frac{\partial v^{\ell_1}}{\partial\Psi^{\ell_1}}\right)\left(\frac{\partial\Psi^{\ell_2}}{\partial\rho^{\ell_1}}\frac{\partial v^{\ell_2}}{\partial\Psi^{\ell_2}}\right)$$

Finally, the discriminant Δ of the characteristic polynomial can be written as:

$$\Delta = \left(\cos(\alpha-\theta^{\ell_1})\left(v^{\ell_1}(\Psi^{\ell_1}(\rho,\theta)) + \rho^{\ell_1}\frac{\partial\Psi^{\ell_1}}{\partial\rho^{\ell_1}}\frac{\partial v^{\ell_1}}{\partial\Psi^{\ell_1}}\right) - \cos(\alpha-\theta^{\ell_2})\left(v^{\ell_2}(\Psi^{\ell_2}(\rho,\theta)) + \rho^{\ell_2}\frac{\partial\Psi^{\ell_2}}{\partial\rho^{\ell_2}}\frac{\partial v^{\ell_2}}{\partial\Psi^{\ell_2}}\right)\right)^2$$

$$+4\rho^{\ell_1}\rho^{\ell_2}\cos(\alpha-\theta^{\ell_1})\cos(\alpha-\theta^{\ell_2})\left(\frac{\partial\Psi^{\ell_1}}{\partial\rho^{\ell_2}}\frac{\partial v^{\ell_1}}{\partial\Psi^{\ell_1}}\right)\left(\frac{\partial\Psi^{\ell_2}}{\partial\rho^{\ell_1}}\frac{\partial v^{\ell_2}}{\partial\Psi^{\ell_2}}\right)$$

We aim at determining the condition for which this quantity is positive. As the first term in square is always positive, the determinant can be negative only if the second term is negative. We notice that $\forall\theta, \exists\alpha$ such that $\cos(\alpha-\theta^{\ell_1})\cos(\alpha-\theta^{\ell_2}) < 0$. Furthermore, we have $\dfrac{\partial\Psi}{\partial\rho}$ and $\dfrac{\partial v}{\partial\Psi}$ that should be respectively positive and negative as the interaction term Ψ should increase with the density whereas the velocity should decrease with the density. Thus, the second term of the determinant could be negative in most of the case.
However, there are two exceptions. First, if there are no interactions between layers i.e. $\dfrac{\partial\Psi^{\ell_2}}{\partial\rho^{\ell_1}}$ or $\dfrac{\partial\Psi^{\ell_1}}{\partial\rho^{\ell_2}}$ are null then the system is hyperbolic. Second, it is also the case if the direction fields of the two layers in the entire space are identical i.e. $\cos(\alpha-\theta^{\ell_1})\cos(\alpha-\theta^{\ell_2}) = \cos(\alpha-\theta)^2$.
If the second term is negative, the sign of the determinant needs to be studied as follow. The interaction term is defined by $\Psi^{\ell_1} = \Psi^{\ell_2} = \rho^{\ell_1} + \rho^{\ell_2}$ and the flux function is described by the Greenshield's Fundamental Diagram.
Let $\Delta\theta = |\theta^{\ell_1} - \theta^{\ell_2}|[2\pi]$ be the angle between the direction vector $d_\theta^{\ell_1}$ and $d_\theta^{\ell_2}$.
In this case, we test numerically for all α and for all $\Delta\theta$ what is the admissible domain of densities such that the system remains hyperbolic. The result of the test can be seen in Figure 4.1. The domain of densities for which the system remains hyperbolic is represented in green and the density for which the system becomes elliptic is in red.

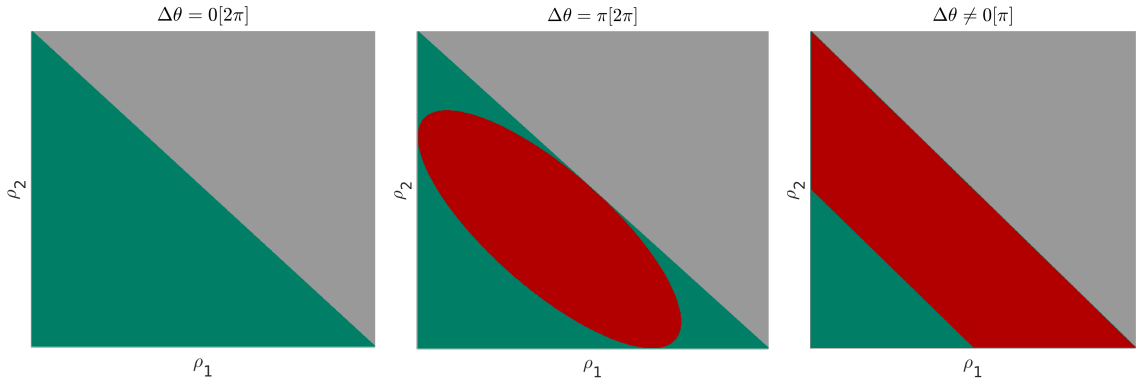

Figure 4.1: Domain of density where the model is hyperbolic (green) or elliptic (red) for angles in the same directions (left), in opposite directions (middle) or in different directions (right)

We observe three different situations. When the two layers are exactly in the same direction, then the system is hyperbolic for all admissible densities and for all $\alpha \in [0, 2\pi)$. Another particular case is when the two layers are exactly in opposite directions. Then, there are some values of α, for which if the value of density is inside an ellipse, the system becomes non hyperbolic. This is consistent with the results of [21]. Indeed, the authors studied a one-dimensional pedestrian model, where pedestrians evolve in opposite directions and found the same condition for hyperbolicity (ellipse). Finally, in the most common case, the directions of the flow of the two layers are just different. In this case, after testing for all $\alpha \in [0, 2\pi)$, we can observe that the system is not hyperbolic if the total density (the sum of the densities of the two layers) is in the congested phase. There is an exception if the density of one of the two layers is null. In this case, even if the total density is congested, the system remains hyperbolic because the second term cancels.

4.1.4 Non symmetric interaction term and limitation

The interaction terms defined in (4.4) could be seen as a strong simplification of reality. Indeed, it assumes that vehicles impact the speed of all the surrounding vehicles independently of their respective travel direction. Physically, it means that vehicles going in this same direction, vehicles crossing at an intersection or vehicles evolving in opposite direction have the same impact on traffic propagation. For this reason, it could be interesting to find a new definition of interaction. Instead of considering that the interaction is the sum of the densities, one could suggest investigating an interaction term based on any linear combination of the two densities:

$$\begin{aligned} &\Psi^{\ell_1} : [0, \rho_{\max}]^2 \to [0, \rho_{\max}] \\ &\Psi^{\ell_1}(\rho) = \alpha_1 \rho^{\ell_1} + \alpha_2 \rho^{\ell_2} \end{aligned} \tag{4.11}$$

$$\begin{aligned} &\Psi^{\ell_2} : [0, \rho_{\max}]^2 \to [0, \rho_{\max}] \\ &\Psi^{\ell_2}(\rho) = \beta_1 \rho^{\ell_1} + \beta_2 \rho^{\ell_2} \end{aligned} \tag{4.12}$$

with $\alpha_1, \alpha_2, \beta_1, \beta_2 \in [0, 1]$
The idea behind this new formulation of the interaction is to give different weights to the densities of different layers. Two layers could have more or less interaction between them depending on the direction of their flows.
The hyperbolicity of the model can be analyzed as it was done in Section 4.1.3 and lead to similar results. However, this formulation of the interaction can lead to difficulty to define properly the maximum density.
This can be understood with the help of an example. Assume that we consider the simple system where $\alpha_1 = \beta_2 = 1$ and $\alpha_2 = \beta_1 = 0.5$. Let the density of the first layer be totally congested $\rho^{\ell_1}(x, y) = \rho_{\max}$ and the second layer be empty $\rho^{\ell_2}(x, y) = 0$. Then, the interaction term of the first layer $\Psi^{\ell_1}(x, y) = \rho_{\max}$ and there is no propagation in the layer 1 in this point. However, the interaction term of the second layer $\Psi^{\ell_1}(x, y)$ equal to $\frac{\rho_{\max}}{2}$ such that the vehicles of layer 2 can still propagate and then increase the interaction of the first layers which was already at the maximum.

4.2 Simulation of the hyperbolic-elliptic model

Numerical methods generally used in traffic flow modeling are usually designed for hyperbolic equations. The simulation of a non-hyperbolic model can lead to oscillation as it has been observed in [21]. Thus, we present in this section a high order and stable numerical method. Furthermore, numerical simulation will be presented to demonstrate the model features.

4.2.1 Adaptation of the simulation method

In this section, we consider a numerical method that combines the WENO scheme, the Total Variation Diminishing (TVD) Runge-Kutta time discretization and the dimensional splitting. It is a high order method in space and time: fifth-order in space, third order in time. At the cell interfaces, the numerical flux considered is Lax-Friedrichs. We introduce first the notion of the different methods and then we present the final numerical method that combines these different parts.
Let space be discretized with a rectangular regular grid with a step Δx. The time is discretized uniformly with a step Δt. We denote by $C_{i,j}$ the cells of the grid and by $\rho_{i,j}$ the discrete density.
The Weighted Essentially Non-Oscillatory (WENO) is a high order numerical method that can achieve both accuracy in smooth regions and maintain sharp discontinuity and non-oscillatory transition of the solution. Contrary to first order method, with the WENO method, the values of the density at the interface $\rho^-_{i+1,j}$ and $\rho^+_{i,j}$ are not set equal to the density of the closest cell but estimated by spatial polynomial interpolation of the five neighboring densities. We refer to [59] for a detailed description of the method.

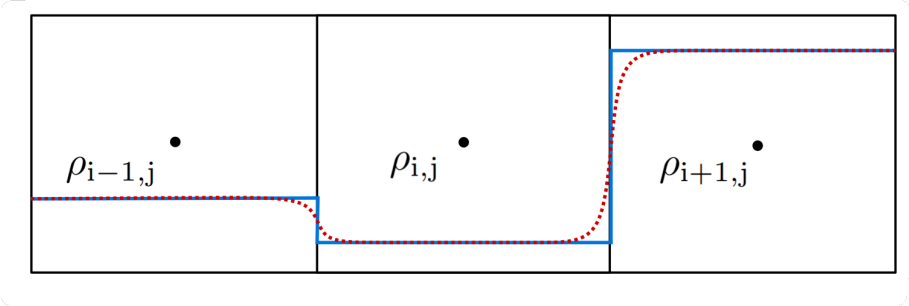

Figure 4.2: Illustration of the WENO method: WENO interpolation (in red) of the discrete density (in blue)

An illustration of the method is shown in Figure 4.2. To avoid drawbacks in the interpolation close to strong discontinuities, we consider the adaptation for the interpolation as described in [59].
Regarding the flux at the interfaces, we decide to use the Lax-Friedrichs Flux that can be defined as follows:

$$F_{i+\frac{1}{2},j} = \frac{1}{2}(\Phi(\rho^-_{i+1,j}) + \Phi(\rho^+_{i,j}) - v_{\max}(\rho^+_{i,j} - \rho^-_{i+1,j})). \tag{4.13}$$

The dimensional splitting is a method that computes a numerical flux in several dimensions by splitting of the different dimension components. The flux is computed first in one dimension, then all the densities are updated and the flux is computed in the second dimension. More details on this method can be found in [40].
The scheme can be described as follows $\forall i, j$:

$$\begin{aligned} \rho^{int}_{i,j} &= \rho^{prev}_{i,j} + \tfrac{\Delta t}{\Delta x}(\cos(\theta_{\mathrm{i}-\frac{1}{2},\mathrm{j}})F^{prev}_{i-\frac{1}{2},j} - \cos(\theta_{\mathrm{i}+\frac{1}{2},\mathrm{j}})F^{prev}_{i+\frac{1}{2},j}) \\ \rho^{next}_{i,j} &= \rho^{int}_{i,j} + \tfrac{\Delta t}{\Delta y}(\sin(\theta_{\mathrm{i},\mathrm{j}-\frac{1}{2}})F^{int}_{i,j-\frac{1}{2}} - \sin(\theta_{\mathrm{i},\mathrm{j}+\frac{1}{2}})F^{int}_{i,j+\frac{1}{2}}) \end{aligned} \tag{4.14}$$

where $F_{i+\frac{1}{2},j}$ is the numerical flux at the interface between two cells $C_{i+1,j}$ and $C_{i,j}$. The numerical flux considered is the one of Lax-Friedrich as described in Equation (4.13). The subscript (prev, int, next) represent the different steps of the scheme and the density considered to evalued each flux. We denote by L the operator that represents the evolution of the dimensional splitting such that

$$L : \rho^{prev}_{i,j} \to \rho^{next}_{i,j} \tag{4.15}$$

as described in Equation (4.14). Figure 4.3 gives a visual representation of the two steps of the dimensional splitting.

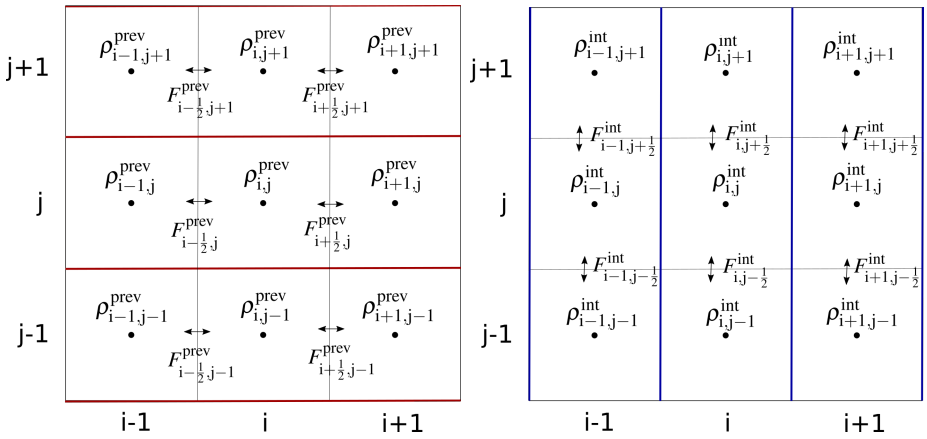

Figure 4.3: Description dimensional splitting: on the left, the propagation is done for every line along the x-dimension and on the right, the propagation is done for every column along the y-dimension.

The discretization in time of the scheme is done by the popular Total Variation Diminishing (TVD) Runge-Kutta time discretization method, which is a third order method. The idea is to divide the evolution of each time step in three steps that can be described as follows:

$$\begin{aligned}
\rho^{\mathrm{TVD}_1} &= \rho^n + \Delta t L(\rho^n) \\
\rho^{\mathrm{TVD}_2} &= \tfrac{3}{4}\rho^n + \tfrac{1}{4}\rho^{\mathrm{TVD}_1} + \tfrac{1}{4}\Delta t L(\rho^{\mathrm{TVD}_1}) \\
\rho^{n+1} &= \tfrac{1}{3}\rho^n + \tfrac{2}{3}\rho^{\mathrm{TVD}_2} + \tfrac{2}{3}\Delta t L(\rho^{\mathrm{TVD}_2})
\end{aligned} \tag{4.16}$$

where L denotes the numerical method developed in Equation (4.15) (dimensional splitting coupled with WENO method).
Finally, for each layer of density, each time step of the numerical scheme proposed is divided into six steps: three steps correspond to the TVD limiter introduced in Equation (4.16) themselves divided into two steps by the dimensional splitting (propagation in x and y direction). For each of the substeps, the evolution of the densities is computed using Lax-Friedrich Numerical Flux and WENO interpolation. A visual representation is given in Figure 4.4.

4.2.2 Network topology and parameters estimation

The network is an artificial network of 25x25 roads on a grid of 5km^2. The roads are spaced on average of approximately 200m. This network is close to a Manhattan grid but the nodes (junctions) have been perturbed with a Gaussian noise to reduce the regularity of the network. The network can be seen in Figure 4.5.

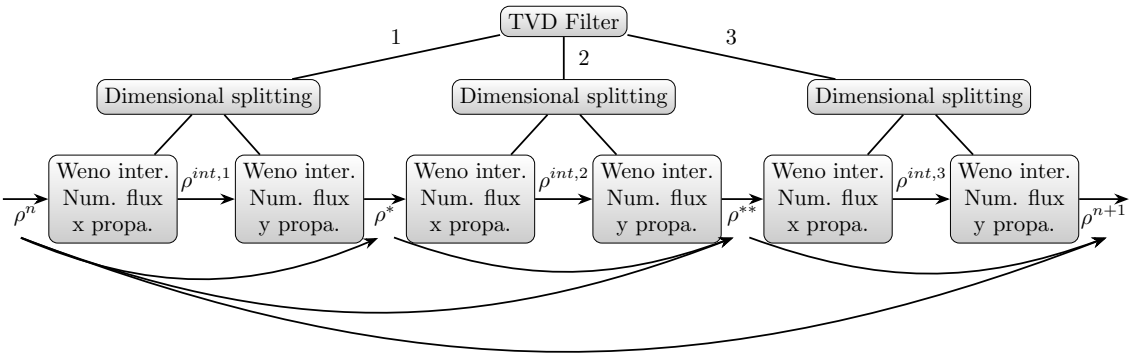

Figure 4.4: Dependence scheme for the numerical method combining WENO method, dimensional splitting and TVD filtering

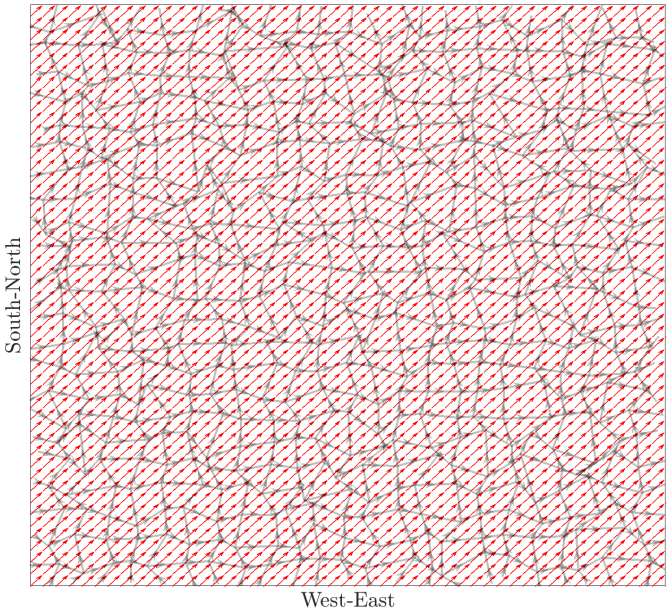

Figure 4.5: Direction field reconstructed for layer 1. The network topology is presented by grey arterials

This network contains 1104 links and at this level it starts to be computationally costly to describe it with network models with modeling of junction or with a microscopic approach. As it has been shown in [46], it is possible to consider space dependent parameters. For simplicity, the parameters of the FD have been chosen constant. Also, we choose as FD the function defined by Greenshields as:

$$v(\rho) = (1 - \frac{\rho}{\rho_{\max}})v_{\max} \tag{4.17}$$

The direction field of the different layers is defined using the network geometry with the method based on inverse distance weighting described in Section 2.1.2. However, in the situation we

want to model, there are two main streams of flows. Layer 1 is globally oriented toward the North-East direction and is displayed in Figure 4.5 and Layer 2 is globally oriented toward the North-West direction. Thus, we extract two sub-networks from the original network such that each partition contains only the roads used for the direction of the layer it represents. These sub-networks can overlap as some roads can serve for both layers.

4.2.3 Results of simulation

Study case 1: Delay in the traffic demand
In this study case, we aim to test how a delay in the traffic demand can improve traffic status. We assume that there are two main streams in the network. One is directed from the South-East to the North-West and the other from the South-West to the North-East. If the main part of traffic demand starts at the same time, then it leads to congestion in the center. For this reason, we investigate a scenario in which we delay the demand of one stream and compare the result with the simulation without intervention. The time horizon of the simulation, T_{horizon} is 30 minutes.
Let us denote by L_{x} and L_{y} the length of the network side. The initial condition is defined as follows:

$$\begin{cases} \rho_0^1(x,y) = \frac{e^{-\frac{C_a}{10}}}{4} + \frac{e^{-\frac{C_b}{10}}}{4} + \frac{e^{-\frac{C_c}{10}}}{4} \\ \rho_0^2(x,y) = \frac{e^{-\frac{C_d}{10}}}{4} \end{cases}, \tag{4.18}$$

where

$$C_a = \sqrt{(x-0.2L_{\text{x}})^2 + (y-0.4L_{\text{y}})^2}$$

$$C_b = \sqrt{(x-0.4L_{\text{x}})^2 + (y-0.2L_{\text{y}})^2}$$

$$C_c = \sqrt{(x-0.25L_{\text{x}})^2 + (y-0.25L_{\text{y}})^2}$$

$$C_d = \sqrt{(x-0.75L_{\text{x}})^2 + (y-0.25L_{\text{y}})^2}$$

We assume that the operators of the network give advice to the users of the layer 1 to start their trip 6 min later to avoid congestion. The aim of this study case is to compare a scenario, where 90% of the layer 1 users follow the advice given by the operator, with a normal scenario, where no advice is given. The results of the simulation and comparison with the control experiment are presented in Figure 4.6.
The applied strategy allows desynchronizing the high density of vehicles crossing from different origins and then avoiding the creation of congestion in the middle of the network. There is less congestion in the scenarios with delayed departure. We can notice that the vehicles waiting for departure are displayed in the density of Figure 4.6 but it is only visual: the drivers are not waiting in their car but stay at home or work later. Thus, the time of the delay is included in travel time statistics and the delay is not a time loss for drivers.
For both the scenarios with and without control, the total number of drivers that carry out a trip is equal to 24 470. A trip corresponds to the trajectories of drivers from their initial position to the outside of the network. The average number of vehicles within the network

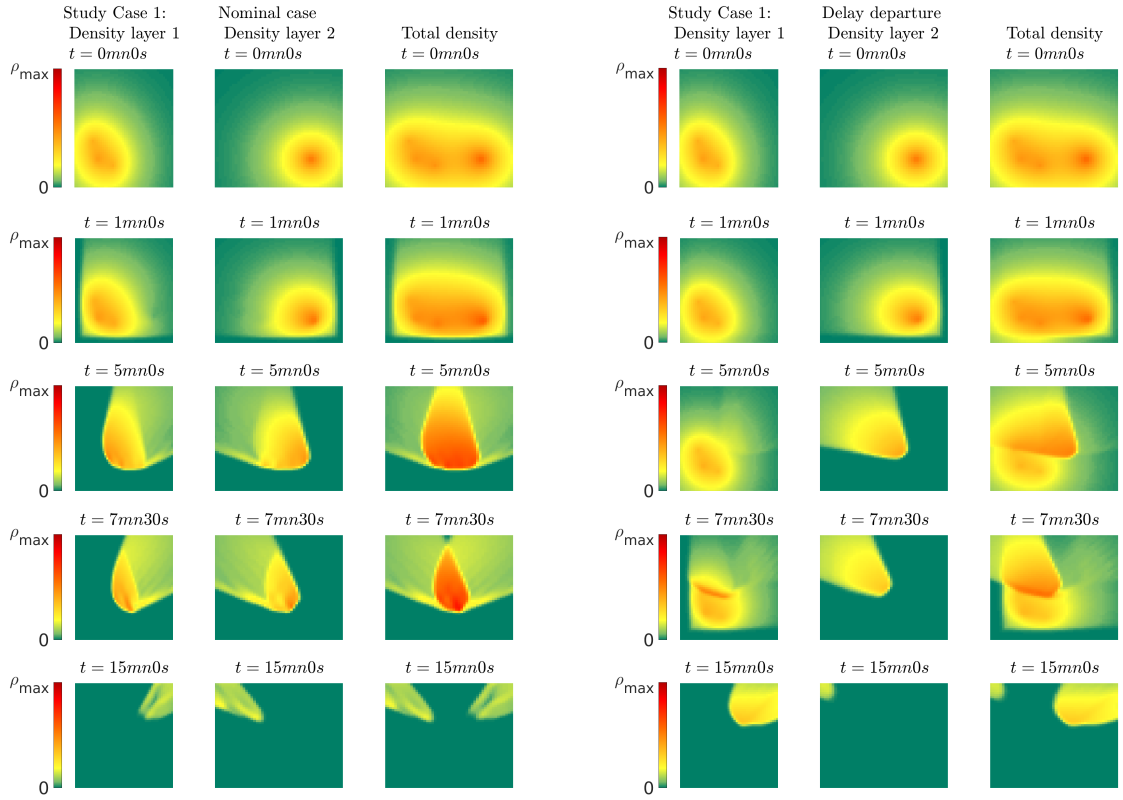

Figure 4.6: Simulation results of the study case 1, on the left for the nominal case and on the right for the scenario with control by driver advice (delay in departure). The left column corresponds to the layer of density 1, the middle column to the layer 2 and the right column to the total density. A video of the complete simulation is available online at `https://youtu.be/Jvt0eGI4D7c`.

over the time horizon is equal to 7 374 for the scenario without intervention from the operator and 6 340 for the scenario where the operator advises the users to leave later. From these numbers, the average travel time of drivers can be deduced as follow:

$$\text{Average trip time} = \frac{\text{Average number of user}}{\text{Total number of user}} \times T_{\text{horizon}} \tag{4.19}$$

The results of the simulation are summed up in Table 4.1. In this table, TTT represents the Total Traveling Time of drivers. The average travel time of users without advice of the

	Nominal case: No delay	Delay in departure
Number trip	24 470 vehicles	24 470 vehicles
Average trip time	9mn02s	7mn46s
TTT	3687 hours	3170 hours

Table 4.1: Comparison of the results of simulation for the study-case: delay in demand

operator (late departure) is equal to 9mn02s. With the advice of the operator, the average travel time decreases to 7mn46s. In total for all the users, this difference corresponds to have 517 hours of congestion less and a reduction of the TTT of 14%.

Study case 2: Congestion due to a protest march

In this study case, we aim to predict how a protest march can impact traffic conditions. A zone corresponding to this protest march is defined in the North-Center of the network and we assume that no vehicle can enter this area.

Let us denote by L_{x} and L_{y} the length of the network side. The initial condition is:

$$\begin{cases} \rho_0^1(x,y) = \begin{cases} \frac{6}{16}\rho_{\max} & \text{if}(x,y) \in D_a \\ 0 & \text{otherwise} \end{cases} \\ \rho_0^2(x,y) = \begin{cases} \frac{3}{16}\rho_{\max} & \text{if}(x,y) \in D_b \\ 0 & \text{otherwise} \end{cases} \end{cases}, \tag{4.20}$$

where

$$D_a = \{(x,y) \in \Omega,\ \frac{2}{16}L_{\text{x}} \leq x \leq \frac{7}{16}L_{\text{x}}\ \&\ \frac{2}{16}L_{\text{y}} \leq y \leq \frac{7}{16}L_{\text{y}}\}$$
$$D_a = \{(x,y) \in \Omega,\ \frac{9}{16}L_{\text{x}} \leq x \leq \frac{14}{16}L_{\text{x}}\ \&\ \frac{2}{16}L_{\text{y}} \leq y \leq \frac{7}{16}L_{\text{y}}\}$$

and with a constant inflow equal to $\frac{4}{25}v_{\max}\rho_{\max}$ on the network boundary $\partial\Omega$. The time horizon of the simulation is 30 minutes.

The aim of this study case is to analyze the impact of the protest march by considering different scenarios: one with no protest march, the second one with a small protest march and the last one with a large protest march. The results of the simulation and comparison between the case with and without protest march are shown in Figure 4.7. We can notice that congestion is created in all the three scenarios. Moreover, the level of congestion reached varies significantly. If the scenario without protest march is considered as the reference, we

can notice that the average density of the scenario with a small protest march is 11 % higher and the one with a large protest march is 21% higher.

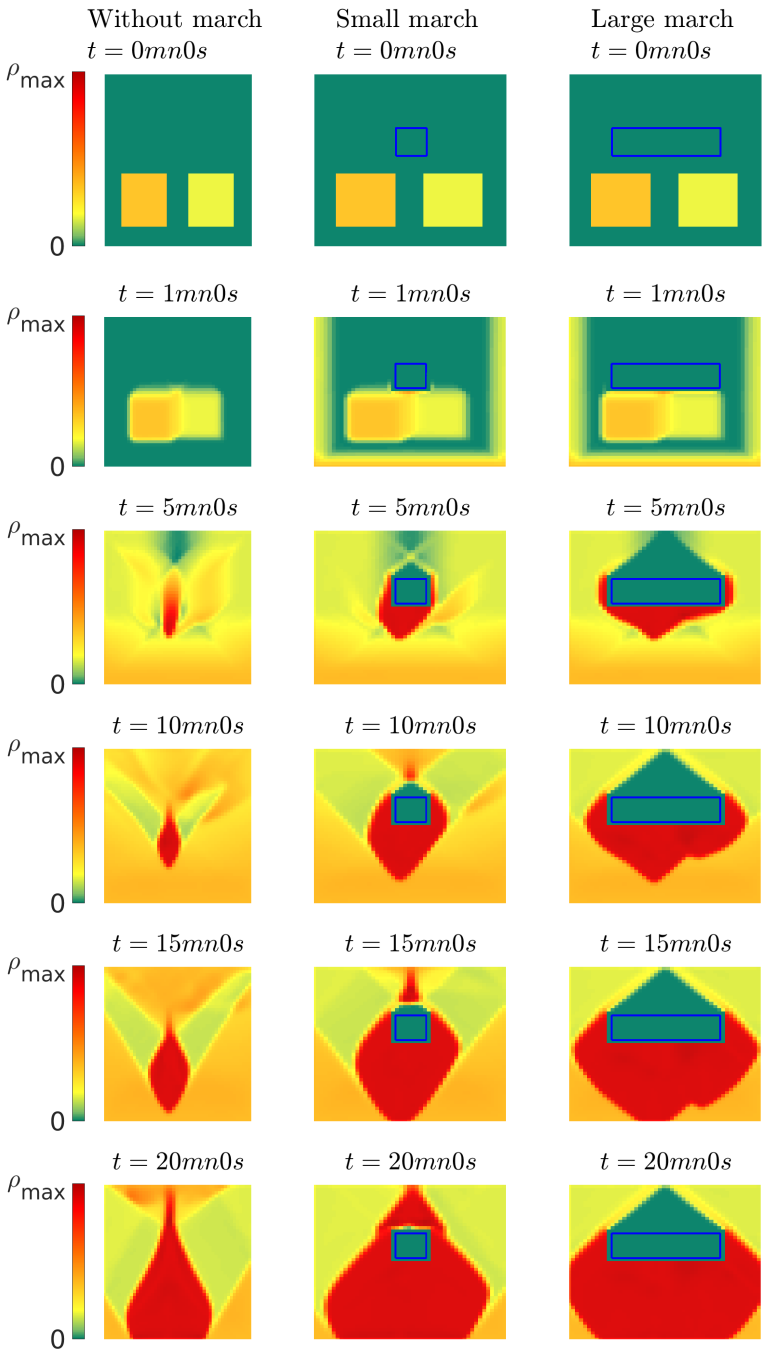

Figure 4.7: Results of a simulation comparing the total density of three scenarios for the study case 2 of a protest march: on the left the scenario with no protest march, on the middle with a small protest march and on the right with a large protest march. A video of the complete simulation is available online at `https://youtu.be/nkieROrzBiI`.

Remark 4. *The advantage of physical dynamical models compared to purely data based models is the ability to test scenarios that occurred only a few times in the past and take a decision according to the result.*

4.3 Estimation of multilayer direction field based on data

The estimation of the direction field from the network geometry works with a preferred direction of propagation. For multi-directional traffic flow, with two ways roads, the method can not be used. In Section 4.2.2, the road network has been split into two sub-networks according to the direction of density layers. However, this method is not generic and could not be extended to any network and layers. Thus, we suggest in this section a method to estimate a direction field for each layer based on data of density and using optimal transport.

4.3.1 Optimal transport and approximation of the Wasserstein distance

To compare several density distributions, it is relevant to have an appropriate metric. The classical L^p norm can work, but it is not always the best choice. For instance, if we look at the three densities displayed in Figure 4.8, a comparison based on L^p would conclude that they are two by two at the same distance. However, one could instinctively think that the two densities on the right are closer and may look for a metric able to identify that. In this

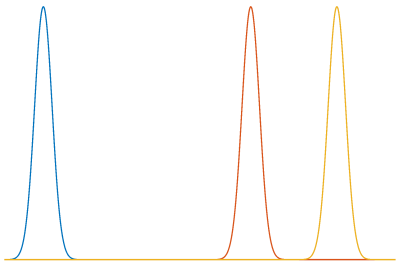

Figure 4.8: Comparison of three densities with similar mass located at different space positions.

subsection, we introduce a new methodology based on an approximation of the Wasserstein distance. We will show how this metric can be used both to compare two density distributions and also to estimate the direction field from vehicles' densities.
The idea of considering optimal transport to estimate parameters of traffic flow comes from the assumption that drivers tend to minimize the effort when they are going from one destination to another. Then, by applying optimal transport on successive density data, we should be able to extract the information of vehicle trajectories.
The Wasserstein distance comes from the optimal transport theory and can be described as follows. Assume that you have two density distributions ρ^0 and ρ^1 with equal masses $\int_{\mathbb{R}^n} \rho^0(x)\partial x = \int_{\mathbb{R}^n} \rho^1(x)\partial x$. Then, the Wasserstein distance measures the cost to rearrange the

density ρ^0 to the density ρ^1. It can be formulated as:

$$W_p(\rho^0, \rho^1) = \left(\min_{T \in \mathbb{T}(\rho^0, \rho^1)} \int_{\mathbb{R}^n \times \mathbb{R}^n} ||x - y||^p_{\mathbb{R}^n} \, T(x, y) \, \partial x \partial y \right)^{\frac{1}{p}} \tag{4.21}$$

where $\mathbb{T}(\rho^0, \rho^1)$ is the set of all the transport maps from the density ρ^0 to ρ^1.
In practice, we are not interested in computing the real Wasserstein distance between two density distributions, but we want to estimate a discrete approximation of this distance. This discrete approximation was proposed in [3].
Let us consider a discretization of the space in cells $(C_k)_{k \in [1, \cdots, N]}$. The approximation of the Wasserstein distance can be formulated as follows:

$$\tilde{W}_p(\rho^0, \rho^1) = \min_{(\mu_{j,k})_{j,k \in [1, \cdots, N]}} \left(\sum_{j,k=1}^{N} c_{j,k} \mu_{j,k} \right) \tag{4.22}$$

$$\text{under constraints} \quad \sum_{i=1}^{N} \mu_{j,i} = m_j^0 \quad \text{and} \quad \sum_{i=1}^{N} \mu_{i,k} = m_k^1, \quad \forall j, k \in [1, \cdots, N] \tag{4.23}$$

where

- $\mu_{j,k}$ is the transferred mass from the density ρ^0 in cell j to the density ρ^1 the cell k.
- m_j^0 and m_j^1 are the masses in cell j of, respectively, the density distribution ρ^0 and ρ^1.
- $c_{j,k}$ is the cost of transfer from cell j to cell k. Here, $c_{j,k} = d_{j,k}^{1+\varepsilon}$ with $d_{j,k}$ the Euclidean distance between Cell j and k and $\varepsilon << 1$.

Remark 5. *In traffic flow modeling, the most relevant cost to minimize would be the traveling time. However, in a homogeneous network, with similar speed limits on the roads, the Euclidean distance should be proportional to the traveling time.*

Remark 6. *The Euclidean distance contains power $1 + \varepsilon$. This allows to reduce the number of solutions for the optimization problem by favouring the transfer on short distance. More specifically in the case of traffic flow, this assumption means that among the possible solutions of density transfer, we will choose the one for which the drivers do not overtake. An illustrative example is given in Figure 4.9.*

In this example, the two vehicles move from the position shown on the top of the figure to the position on the bottom. However, there are two possible ways to obtain this change of position: both vehicles move (red arrow) or only the backward vehicle moves (blue arrow). These two solutions would minimize the cost in terms of Euclidean distance. However, by adding a small power $1+\varepsilon$ the solution with no overtaking (red arrow) is the only one that minimizes the cost.

Example 1:
Let us consider two discrete density distributions of equal mass (21 units) that are represented

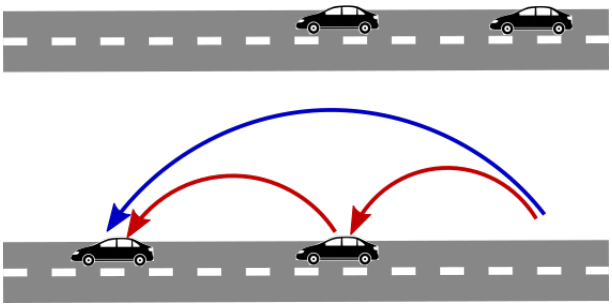

Figure 4.9: Example of a situation with several admissible solutions for optimal transfer. The top picture corresponds to the first situation and the bottom picture corresponds to the second situation. We aim to reconstruct the optimal transfer to go from situation 1 to situation 2.

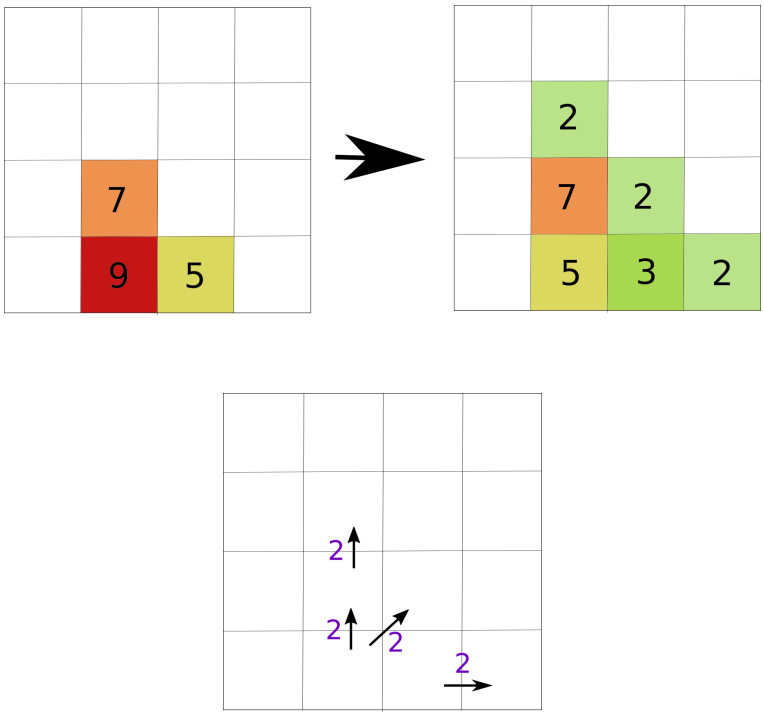

Figure 4.10: Example of optimal transport. The two images on the top represent two discrete density distributions of the same mass. The figure on the bottom represents the mass transfer needed to rearrange the density on the left to obtain the density on the right with a minimal cost.

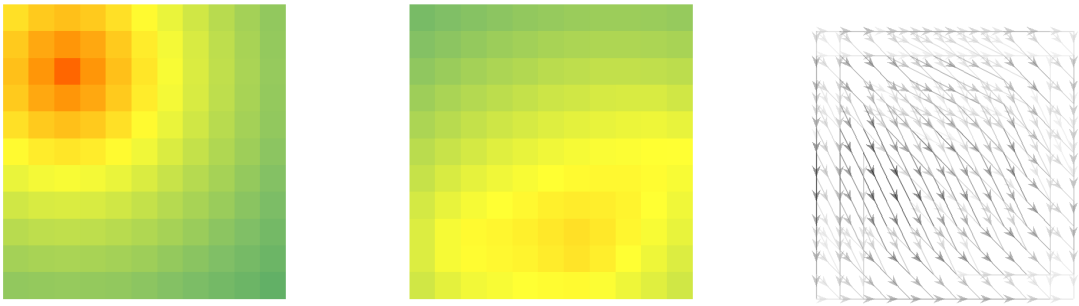

Figure 4.11: Mass transfer represented by the collored arrows (right) with a minimal cost between two density distributions (left and center)

both in Figure 4.10. The algorithm aims to find how we can transfer the density from the left distribution to the right distribution minimizing the cost. The obtained results are shown in the last picture, where the quantity of the mass that was moved is indicated with the arrows. If we set the distance between two cells of the discretization to 1, we can then compute the Wasserstein distance between the two densities: $2 \times 1 + 2 \times 1 + 2 \times 1 + 2 \times \sqrt{(2)} = 6 + 2\sqrt{2}$.

Example 2:
If we focus on a more complex example, the Wasserstein distance can be computed numerically using the Optimization Toolbox of Matlab with the function *linprog*. In Figure 4.11, we study the results of the Wasserstein distance applied on two density distributions with a 10×10 discretization (100 cells).

The arrows on the right picture represents the path of mass transfer needed to rearrange the density distribution on the left to obtain the density distribution on the middle. The transfer of mass that solves the optimization problem can occur from and to any cells of the discretization even if the cost function tend to favor the shortest transfer i.e. without overtaking. The mass transfer can have high or low value and is represented by arrow of different intensities.

A major constraint to apply this method relies on the fact that it can only compare density of equal mass. In modeling, the Wasserstein distance could be considered as a metric to compare the results obtained for the different models with the result obtained by the two-dimensional model. This metric may be able to capture details that the simple L^2 norm can not. However, the requirement that the density have the same mass is not always fulfilied and, thus, the normalization can be a source of error. In the following, we focus on the application of the Wasserstein distance to density data of successive time steps in order to reconstruct directions of flow.

4.3.2 Estimation of the velocity from data using optimal transport

We aim to design a method to reconstruct the direction field from density data. To test this method, we build an experiment using microsimulation in which the different directions are

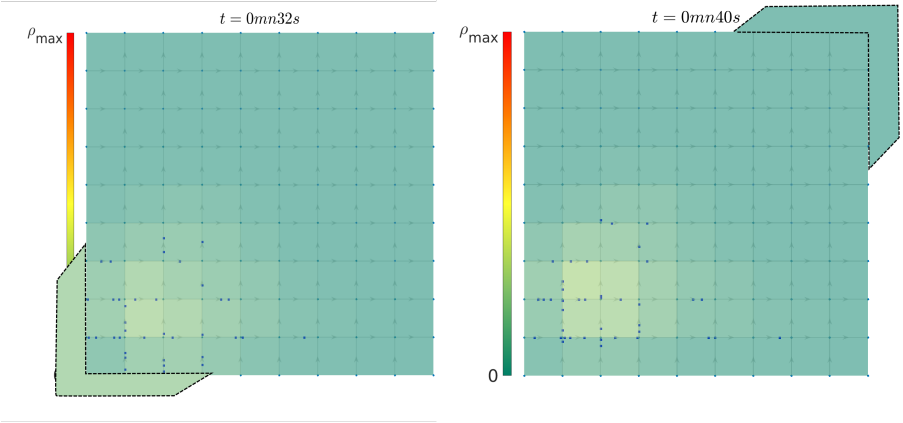

Figure 4.12: Artificial extension of the network to compensate non constant mass

distributed in different layers according to their OD matrices. The vehicles trajectories are collected and used to reconstruct a two-dimensional density. Finally, we apply the computation of the Wasserstein distance on successive time steps.
But, the total mass of two successive time steps is constant only if the inflows of the network equal its outflows. We consider an extension of our domain next to the boundary to artificially add vehicles entering or exiting between the two time steps. An illustration is given in Figure 4.12. From these successive data, we can obtain the set of all the mass transfer from a time step to the following. The direction field we aim to estimate is defined uniquely for each space position whereas the mass transfer we have just compute can go in multiple directions and is changing with respect to time. Thus, we average the direction of transfer in time and space to obtain a velocity field.

4.3.3 Simulation results

For the simulation, we consider an Manhattan-like, $2km$ square network in an urban area. The speed limits are set equal to 50 km/h on all the roads. The maximum density is defined as constant $\rho_{\max} = 2000\text{veh/km}^2$. The vehicle trip demand is fluctuating during the days but we assume that, for a given period of the days, we can extract some main trend by analysing the vehicles' direction. In this scenario, we consider that there are two majors axis for trajectories of vehicles: one from the South-East to the North-West and the other from the South-West to the North-East. The microsimulator Aimsun will be use both to calibrate the model and to do a first validation. We collect the data with the method that was presented in Section 1.3.4. However, we can highlight here that we are able to associate the vehicles trajectories by OD matrices and then by layers. This means that each layer of the model can to be compared to the microsimulation of the same layer. This could be important for future processes of validation especially to study non symmetric interaction terms.
The estimation of the direction field is done using the method based on optimal transport. The results of the simulation are shown in Figure 4.13. The direction field reconstructed with this method tends to represent more the motion parallel to the boundary. Furthermore, in

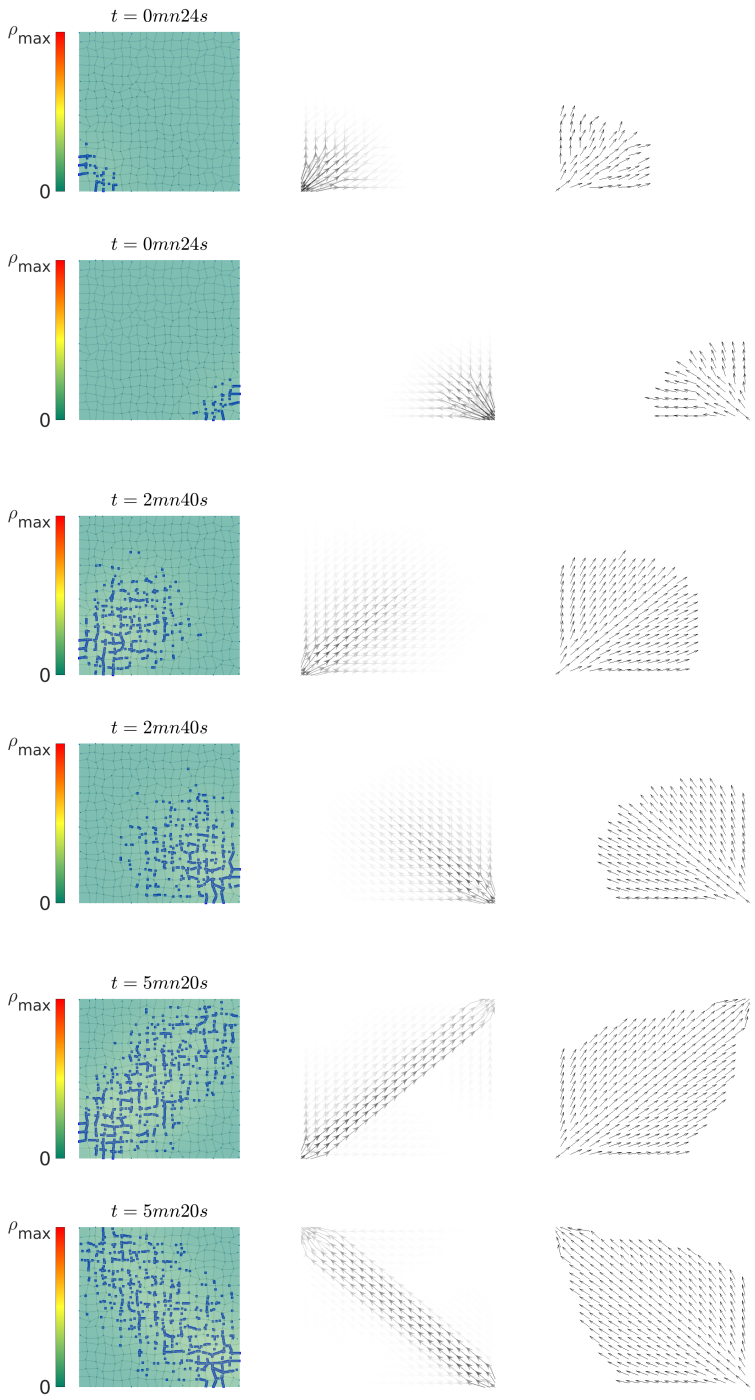

Figure 4.13: Estimation of the direction field using the Wasserstein distance. On the left, column we can see the 2D density reconstruction from Aimsun simulation. The middle column shows the transfer of density (solution) at the current time. The right column is the average velocity field estimated by the method at the corresponding stage.

the final direction field, we need a value for each space coordinate. An empty area can lead to difficulty to evaluate the direction field in this position.

Remark 7. *Solving the optimal transport problem is costly. Thus, the computation time increases fast with an increase of the model discretization. However, the direction field is a parameter of the model and can be computed offline.*

Scenario construction: The objectives of these results are to study the advantages and the limits of the multilayer model defined in (4.2). The demand is assumed to be constant and is defined by Origin-Destination matrices for the first 12mn. Then, the inflow stops and there is no more demand for vehicles to enter. The maximum density is assumed to be constant as it was the case in Chapter 2. The results of these simulations are displayed in Figure 4.14.

We can see that the propagation of vehicles in the free flow is consistent between the microsimulation and the two-dimensional model. The interaction of flow from different layer appear in the 2D model but is significantly different from what can be observed in the microsimulation. In the microsimulation, the congestion starts from the center and grows up around it. In the two-dimensional model, the interaction terms affect only the border of the merging area between the two layers. As a consequence, the congested vanishes faster in the two-dimensional model after the inflow has been stopped.

4.4 Towards a hyperbolic multilayer model

4.4.1 Formulation of a specific hyperbolic model

The formulation of the multilayer model considered previously always leads to a mixed model (hyperbolic-elliptic). We want to investigate if a different formulation of the interaction term could lead to a hyperbolic model. To simplify the calculation, we consider a model with two layers of density ρ^{ℓ_1} and ρ^{ℓ_2}. In addition, we assume that they have perpendicular direction such that: $\vec{d}_\theta^{\ell_1}$ is parallel to the x-axis and $\vec{d}_\theta^{\ell_2}$ is parallel to the y-axis.
The formulation of the interaction term we suggest to study is the following:

$$\begin{cases} \dfrac{\partial \rho^{\ell_1}}{\partial t} + \dfrac{\partial \Phi(\rho^{\ell_1})\Psi(\rho^{\ell_2})}{\partial x} = 0 \\ \dfrac{\partial \rho^{\ell_2}}{\partial t} + \dfrac{\partial \Phi(\rho^{\ell_2})\Psi(\rho^{\ell_1})}{\partial y} = 0 \end{cases}, \qquad \forall t \in \mathbb{R}^+, \forall (x,y) \in \Omega \tag{4.24}$$

This new formulation changes the conception of what is physically related to the interaction. In (4.2), we assumed the interaction term to represent a density. Now in (4.24), the interaction term will impact directly the speeds of vehicles.

Definition: We denote by Φ_x and Φ_y the flux function for the x and y dimension. Then, the system is hyperbolic if $\forall \alpha_1, \alpha_2 \in \mathbb{R}$, the matrix:

$$A = \alpha_1 \mathrm{J}_{\Phi_x} + \alpha_2 \mathrm{J}_{\Phi_y} \tag{4.25}$$

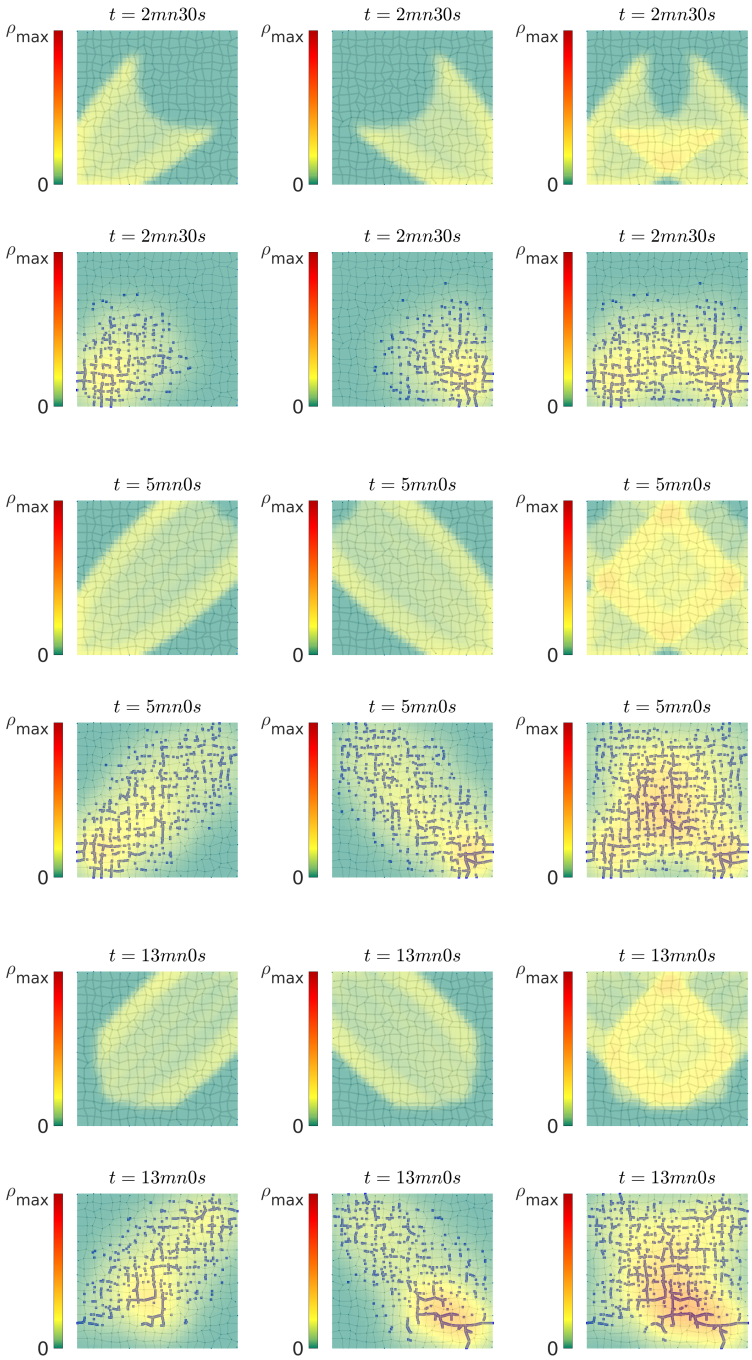

Figure 4.14: Comparison of Aimsun with the non-hyperbolic multilayer model. At the top of each block, we have the results of the two-dimensional model and at the bottom, we can see the microsimulation with 2D reconstruction. The first layer and second layer are respectively in the left and the middle column and the total density is in the right column.

has real eigenvalues.
Then, we compute the Jacobian matrix of the flux for the x dimension:

$$\mathrm{J}_{\Phi_x} = \begin{pmatrix} \dfrac{\partial \Phi(\rho^{\ell_1})\Psi(\rho^{\ell_2})}{\partial \rho^{\ell_1}} & \dfrac{\partial \Phi(\rho^{\ell_1})\Psi(\rho^{\ell_2})}{\partial \rho^{\ell_2}} \\ 0 & 0 \end{pmatrix} = \begin{pmatrix} \Phi'(\rho^{\ell_1})\Psi(\rho^{\ell_2}) & \Phi(\rho^{\ell_1})\Psi'(\rho^{\ell_2}) \\ 0 & 0 \end{pmatrix} \tag{4.26}$$

We can do the same for the y dimension:

$$\mathrm{J}_{\Phi_y} = \begin{pmatrix} 0 & 0 \\ \Phi(\rho^{\ell_2})\Psi'(\rho^{\ell_1}) & \Phi'(\rho^{\ell_2})\Psi(\rho^{\ell_1}) \end{pmatrix} \tag{4.27}$$

Then, we can compute the caracteric polynomial of the matrix A:

$$P(\lambda) = (\lambda - \alpha_1\Phi'(\rho^{\ell_1})\Psi(\rho^{\ell_2}))(\lambda - \alpha_2\Phi'(\rho^{\ell_2})\Psi(\rho^{\ell_1}))$$

$$+4\alpha_1\alpha_2\Phi(\rho^{\ell_1})\Phi(\rho^{\ell_2})\Psi'(\rho^{\ell_1}))\Psi'(\rho^{\ell_2}))$$

In order to have a hyperbolic system, we need to show that the following determinant is positive:

$$\Delta = (\alpha_1\Phi'(\rho^{\ell_1})\Psi(\rho^{\ell_2}) - \alpha_2\Phi'(\rho^{\ell_2})\Psi(\rho^{\ell_1}))^2 + 4\alpha_1\alpha_2\Phi(\rho^{\ell_1})\Phi(\rho^{\ell_2})\Psi'(\rho^{\ell_1})\Psi'(\rho^{\ell_2}) \tag{4.28}$$

We are looking for the condition for the function Ψ that could lead to a hyperbolic system.
Let us consider the condition of hyperbolicity again.

$$\Delta = \underbrace{(\alpha_1\Phi'(\rho^{\ell_1})\Psi(\rho^{\ell_2}) - \alpha_2\Phi'(\rho^{\ell_2})\Psi(\rho^{\ell_1}))^2}_{A} \underbrace{+4\alpha_1\alpha_2\Phi(\rho^{\ell_1})\Phi(\rho^{\ell_2})\Psi'(\rho^{\ell_1})\Psi'(\rho^{\ell_2})}_{B} \tag{4.29}$$

First, we can notice that:

$$\Delta < 0 \Longrightarrow B < 0 \tag{4.30}$$

This means that the system can be non hyperbolic only if the second term B is negative.
We can notice that $\Phi \geq 0$ as the flux function is positive by definition and does not change its direction over time. In addition, it should be reasonable to have the condition $\Psi' \leq 0$ i.e. the interactions increase when the density increases.
Then, it means that:

$$\Delta < 0 \Longrightarrow \alpha_1\alpha_2 < 0 \tag{4.31}$$

In other words, we can conclude that if $\alpha_1\alpha_2 \geq 0$ then the determinant is non negative. As the system is hyperbolic if the determinant is positive for all α_1, α_2, we focus on α that can make the determinant negative.
Let us assume that we have $\alpha_1\alpha_2 < 0$.
We can notice that:

$$(A = 0 \quad \text{and} \quad \alpha_1\alpha_2 < 0) \Longrightarrow \Delta \leq 0 \tag{4.32}$$

It is not necessary to have $A = 0$ in order to not have a hyperbolic system. However, if the term A is cancelled, the determinant would be non positive and so it can be an interesting

case to study.
We know that:

$$\Psi(\rho) \geq 0 \tag{4.33}$$

and

$$\begin{cases} \Phi'(\rho) > 0 & \text{if} \quad \rho < \rho_{\text{crit}} \\ \Phi'(\rho) < 0 & \text{if} \quad \rho > \rho_{\text{crit}} \end{cases} \tag{4.34}$$

Thus, if $\rho^{\ell_2} > \rho_{\text{crit}}$ and $\rho^{\ell_1} < \rho_{\text{crit}}$, i.e one layer is in free flow and the other is congested. Then we can set:

$$\alpha 1 = \Phi'(\rho^{\ell_2})\Psi(\rho^{\ell_1}) \tag{4.35}$$

$$\alpha 2 = \Phi'(\rho^{\ell_1})\Psi(\rho^{\ell_2}) \tag{4.36}$$

Such that we still have $\alpha_1\alpha_2 < 0$ and such that $A = 0$. The only chance to keep the system hyperbolic in this condition would be to have the second term B null also.
Thus, we suggest a specific function for which the system is hyperbolic:

$$\Phi(\rho) = \begin{cases} v_{\max}\rho & \text{if} \quad \rho \leq \rho_{\text{crit}} \\ (\rho_{\text{crit}} v_{\max})\frac{\rho_{\max}-\rho}{\rho_{\max}-\rho_{\text{crit}}} & \text{otherwise} \end{cases} \tag{4.37}$$

$$\Phi'(\rho) = \begin{cases} v_{\max} & \text{if} \quad \rho \leq \rho_{\text{crit}} \\ -\frac{\rho_{\text{crit}} v_{\max}}{\rho_{\max}-\rho_{\text{crit}}} & \text{otherwise} \end{cases} \tag{4.38}$$

$$\Psi(\rho) = \begin{cases} 1 & \text{if} \quad \rho \leq \rho_s \\ \frac{\rho_{\max}-\rho}{\rho_{\max}-\rho_s} & \text{otherwise} \end{cases} \tag{4.39}$$

$$\Psi'(\rho) = \begin{cases} 0 & \text{if} \quad \rho \leq \rho_s \\ \frac{-1}{\rho_{\max}-\rho_s} & \text{otherwise} \end{cases} \tag{4.40}$$

We set $\rho_{\text{crit}} < \rho_s$. This condition combined with the choice of a constant interaction term for densities bellow ρ_s enables to maintain the hyperbolicity when one layer is congested and the one other is in the free flow. This situation could usually be problematic, as we discussed it previously.
Case 1: $\rho^{\ell_1} \leq \rho_s$, then $\Psi'(\rho^{\ell_1}) = 0$ and so:

$$\Delta = (\alpha_1\Phi'(\rho^{\ell_1})\Psi(\rho^{\ell_2}) - \alpha_2\Phi'(\rho^{\ell_2})\Psi(\rho^{\ell_1}))^2 \geq 0 \tag{4.41}$$

Thus, the system is hyperbolic.

Case 2: $\rho^{\ell_2} \leq \rho_s$, then $\Psi'(\rho^{\ell_2}) = 0$ and we get:

$$\Delta = (\alpha_1\Phi'(\rho^{\ell_1})\Psi(\rho^{\ell_2}) - \alpha_2\Phi'(\rho^{\ell_2})\Psi(\rho^{\ell_1}))^2 \geq 0 \tag{4.42}$$

So the system is hyperbolic.
Case 3: $\rho^{\ell_1}, \rho^{\ell_2} \geq \rho_s$, then:

$$\Delta = \left(\alpha_1(-\frac{\rho_{\text{crit}} v_{\max}}{\rho_{\max} - \rho_{\text{crit}}})(\frac{\rho_{\max} - \rho^{\ell_2}}{\rho_{\max} - \rho_s}) - \alpha_2(-\frac{\rho_{\text{crit}} v_{\max}}{\rho_{\max} - \rho_{\text{crit}}})(\frac{\rho_{\max} - \rho^{\ell_1}}{\rho_{\max} - \rho_s})\right)^2$$
$$-4\alpha_1\alpha_2(\frac{\rho_{\text{crit}} v_{\max}}{\rho_{\max} - \rho_{\text{crit}}})^2(\frac{1}{\rho_{\max} - \rho_s})^2(\rho_{\max} - \rho^{\ell_1})(\rho_{\max} - \rho^{\ell_2})$$

Then, we can rewrite this determinant as follows:

$$\Delta = \left(\alpha_1(\frac{\rho_{\text{crit}} v_{\max}}{\rho_{\max} - \rho_{\text{crit}}})(\frac{\rho_{\max} - \rho^{\ell_2}}{\rho_{\max} - \rho_s}) + \alpha_2(\frac{\rho_{\text{crit}} v_{\max}}{\rho_{\max} - \rho_{\text{crit}}})(\frac{\rho_{\max} - \rho^{\ell_1}}{\rho_{\max} - \rho_s})\right)^2$$

And we have $\Delta \geq 0$ so the system is hyperbolic.
To conclude, we derived conditions for the model (4.24) to be hyperbolic (but not a strictly hyperbolic model).

Remark 8. *However, we can notice that in Case 1, 2 and 3 the determinant Δ can still be zero. In this situation, the eigenvalues can be equal. The system is thus hyperbolic but the stability or the well posedness of the model is not guaranteed.*

Remark 9. *This example can be extended to the case where the direction of the two layers is not perpendicular. The conclusion remains the same and it is still possible to have a hyperbolic model under the same condition.*

4.4.2 Simulation and discussion about the hyperbolic formulation

We consider the same scenario as in Section 4.3.3 but with the interaction formulation that leads to a hyperbolic model. We can notice that with the hyperbolic model, we do not require the WENO methods to make stable simulation. We simply use finite volume method with dimensional splitting as it was presented in Section 1.2.1 except that we should consider separately the two layers. The results of the simulation that we can obtain are similar to what we can see in Figure 4.14 except the interaction seems to have less effect.
Indeed, we remark that this interaction term does not create new congestion in the network. The interaction term has an impact only if one of the two layers is already congested. Thus, it can to emphasize existing congestion but it can not trigger the creation of a new one. There are only few ways to model the creation of congestion in traffic. Network bottleneck is one of those and the convergence of many flows in one area should be another.
More generally, the definition of the maximum density is specific for each layer. The global maximum for the two layers can be defined as the sum of the maximum density of each layer. If the global maximum density could be reasonably defined given a road network, the maximum density of each layer can be more complex to evaluate.

Chapter conclusion: Summary, limitations and possible extensions

In this chapter, we studied the extension of the single-layer two-dimensional model that required a preferred direction of traffic, towards a multilayer two-dimensional model which is able to describe multiple directions of flow simultaneously. This approach offers new opportunities and challenges for the model design.
One of them is the formulation of the interaction terms, i.e., how the vehicles of one layer affect the vehicles of other layers. We proposed an interaction formulation for which the speed function is evaluated based on the total density (and not just the density of the corresponding layers). Due to the interaction between the layers, the model becomes a mixed hyperbolic-elliptic PDE which can have an impact on its stability or its well-posedness. Even if the stability of the model is uncertain, we present a numerical method that is able to generate solutions to this simulation-based model. One could claim that the interaction described as the sum of the density is already a (too) strong simplification of the traffic reality. So, we studied the extension of interaction based on the linear combination of density of the layers instead of the sum, and we discover that it should be manipulated carefully to retain the physical meaning of the model.
Another challenge is the choice of the number of layer and the method to decouple them. Indeed, some parameters of the model have to be estimated for each layer as it is the case for the direction field. The direction field was previously estimated from the network geometry but it can be difficult to split the network in any number of subnetworks. Thus, we develop a new estimation method of the direction field based on the Origin-Destination matrices and synthetic data extracted from microsimulation. The aim is to split the vehicles into different layers according to their OD matrices and then to evaluate, for each layer, the direction field from successive density estimation using the Wasserstein distance. More generally, this idea opens the door of calibrating parameters of the model or even the model itself using the data directly and can be a promising direction for future study.
Finally, we investigated a formulation of the interaction terms such that the model remains hyperbolic. This shows that the hyperbolicity of the model is not necessarily lost due to the construction of a multilayer 2D model with interaction terms and it can be a starting point for further analysis. However, the constraints to keep the model hyperbolic in terms of model design are strong. For instance, the interaction in this approach can not be the origin of a congestion creation. Also, it can be complex to represent many layers within this formulation. We can highlight one property of the interaction defined as the sum of density: it is consistent for any number of layers. Thus, the quality of the representation of the vehicles trajectories can be increased by adding layers such that each layer can focus on describing very precisely the trajectories of the vehicles they represent. To study the limit toward very high number of layers, the future research could be interested in a kinematic representation of the model.

Chapter 5

Application to a real scenario: Grenoble network

Contents

In this chapter, we aim to test and study the 2D approach in a real case scenario. However, we do not have the data yet to conduct a rigorous analysis, the investigation will focus on a half realistic scenario, where some assumptions are realistic and the others are hypothetic.

To sump up, the realistic parts are:

- The topology of the network: An area in the center of Grenoble. The roads are described by an oriented graph as they are in the reality.
- Some inflows (4 roads), read from the existing sensors of the city.

The parts that are assumed/non-realistic:

- The origin-destination matrices (which impact the choice of the layers' number and representation) are assumed.
- The inflows in the unmeasured roads are assumed.
- The signalization is not included (e.g. traffic lights ...).
- The inflow/outflow generation of vehicles from Parking is not included.

Thus, this chapter should be seen as an assessment of the opportunity and the limitation of the current model rather than as a real-case validation, which could be done in the future of the project thanks to the access to the real data.

5.1 Area of application: Grenoble Network

Grenoble is a French city that is also the 11th largest urban area in France with about 700 000 inhabitants including agglomeration. In Grenoble traffic system, there are approximately 326 000 cars in circulation every day that lead regularly to traffic congestions.

5.1.1 ERC Scale-FreeBack project: GTL Ville

The research of this thesis takes part in the ERC Scale-FreeBack Project `http://scale-freeback.eu/`. This project aims to develop new methods for modeling and control complex physical networks of an arbitrary size.
One of the objectives of this project is to set up a field experiment called "GTL-Ville". The GTL-Ville `http://gtlville.inrialpes.fr/` is an extension at the city level of the previous project developed by the team called GTL (Grenoble Traffic Lab) that focused only on one main arterial in the South of Grenoble `https://gtl.inrialpes.fr`. This field experiment aims to validate the theoretical finding of the project with real-data. Several sources of data are collected at different scopes. First, real time average speed on most of the roads of the entire Grenoble network are collected through TomTom GPS. An example of data that can be collected this way is represented in Figure 5.1.

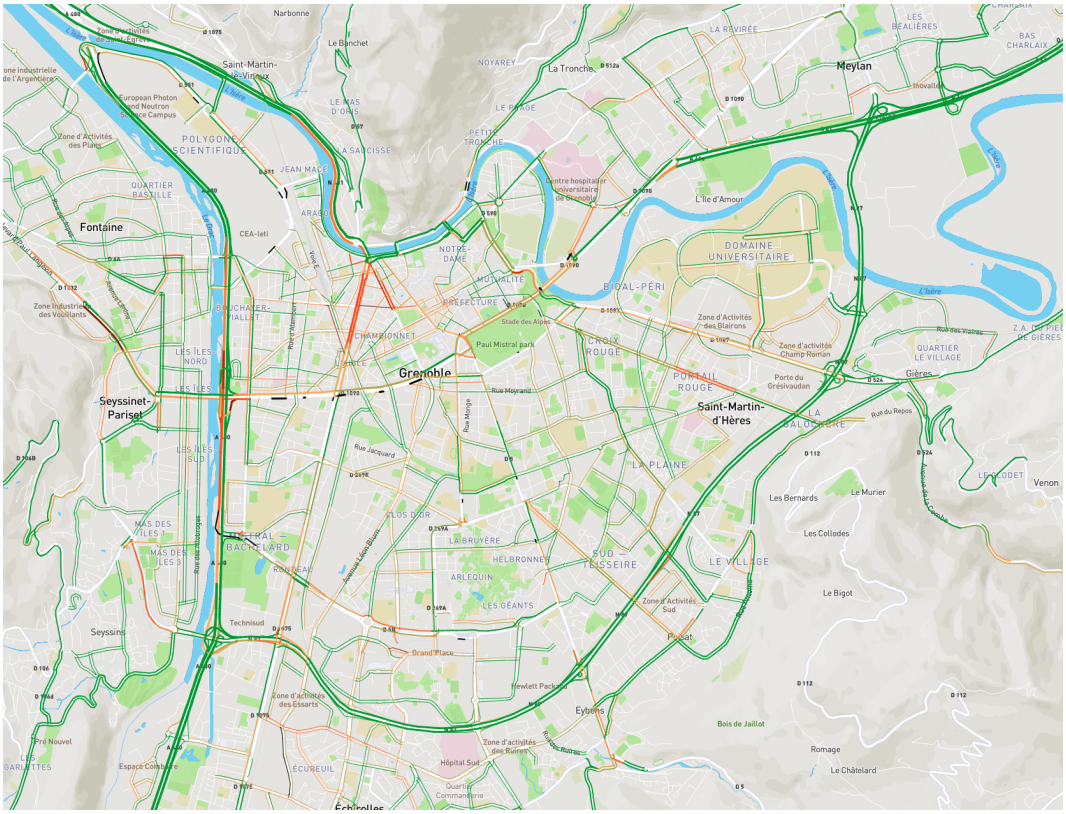

Figure 5.1: GT-Ville project: Network of Grenoble and TomTom data

These data are estimated from aggregation of GPS traces. As the penetration rate is not maximal, the speed data can be estimated from historical data. We can notice that the data cover most of the road network even if some small road are not included. Another source of the data is the loop sensors owned by the MetroMobility (Grenoble public services).
Information on vehicles' speed is a good start but is not sufficient to reconstruct the traffic states. For the future of the project, a portion of Grenoble center is going to be equipped by different kinds of sensors to be able to reconstruct the full density and the Origin-Destination matrices in this part of the city. The data collected and the tools developed in the "GTL-Ville" aim to give a representation of the evolution of the traffic conditions, contrary to the existing tools (Waze, Google Maps, ...) that give only few information on the travel time condition. The knowledge of traffic dynamics such as the density of vehicles, is relevant for both the estimation of pollutant emission and control of the road network. These two applications are especially relevant for the city of Grenoble as the area is regularly subject to traffic restrictions to limit air pollution. More detailed knowledge of the traffic emission would enable to improve the efficiency of restriction. In terms of control, the city of Grenoble is regularly congested and can have really complex management (tramways priority, bus dedicated lanes, public work, ...). Control of a traffic network can be implemented by traffic light synchronization, that is usually developed to optimize traffic locally, or Speed Limits Control. Furthermore, the recent development of new technology recently offers the potential for a new kind of control. For instance, the GPS can be used to give the drivers a path that do not only minimizes his own travel time, but also the average travel time of drivers.

5.1.2 Choice of the area selected for analysis

As it is mentioned in the previous section, we aim to select a sub-network in Grenoble to test different models of the project including the kind of two-dimensional approach that we consider in this thesis. The network selected must satisfy many criteria (modeling, budget ...) but we focus here on the criteria important for the two-dimensional approach:

- **The network has to be dense**, with many possible paths to reach each destination. This criterion is necessary to extract benefit from the two-dimensional representation. Indeed, if only one major arterial contains most of the flux, the classical one-dimensional LWR would be more relevant. For instance, in the network of Grenoble, there is a major beltway in the south of the city (studied in the GTL). A small area containing this road will be mainly represented by it and then will be difficult to include in an aggregated model.

- **The network has to present varying traffic condition**, from free-flow to congestion. This condition is required to validate the model for any type of traffic conditions such as congestion creation, congestion propagation, resolution of congestion.

- **The network has to take advantage of the existing sensors**. Some of the sensors already existing in Grenoble should be within this area of interest. This condition is important for our model, since it enables to consider a larger network for a given budget.

The two-dimensional models are suited for large networks. The area selected should be as large as possible.

According to these criteria and many others that were not listed here, the area of the application selected is rectangular and is located inside the city center of a size of 1.4×1.1 km. In theory, this size of the network corresponds to the lower bound for which the kind of 2D-plane approximation we investigated could represent an interest in term of modeling cost. On the other hand, this is already a large network (600 roads) to collect the data and recover all the traffic states in the future.
Also, this area of study has been chosen to have a traffic condition varying regularly from the free flow to the congestion and vice versa. As we do not have any information on the density, we evaluate the presence of congestion using vehicles' speeds from the TomTom data. The absolute speed of vehicles is not directly representative of the traffic state in a city. The speed of vehicles can be low both if the roads is crowded or if the speed limit of the roads is low. For this reason, we consider a new variable, the traffic fluidity. The traffic fluidity represents the ratio between the current absolute density and the density observed in the free-flow (e.g. at night). This comparison enables to detect congestion from vehicles speed. An example of these observations is displayed in Figure 5.2. The roads in red are the congested roads

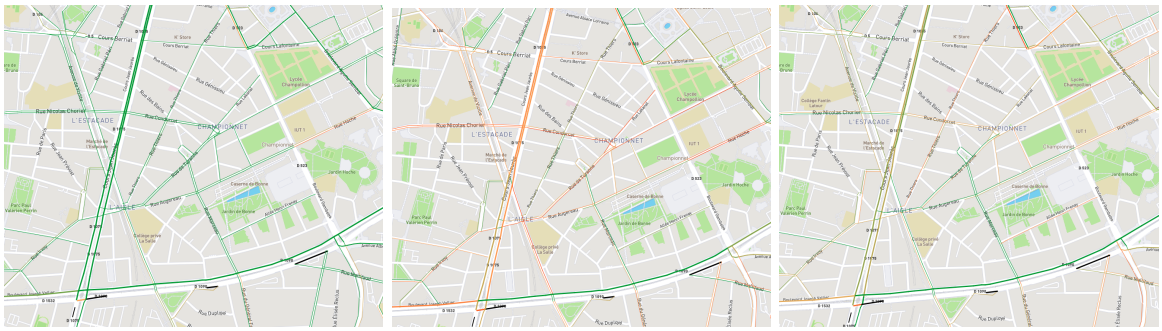

Figure 5.2: GTL ville project : TomTom real time traffic fluidity extracted from vehicles average speed. From the left to the right, the three pictures represent different three times: 7:00 am, 8:12 am and 9:45 am

and the green roads are the ones in the free-flow. We can see that at 7:00 am, traffic flow has not really started yet and all the roads are in the free-flow. Then at 8:22am, the rush hour occurs, since all the people are on the way to the work and the network becomes very crowded. Finally, at 9:45 am, there are still car on the roads but the congestion has already decreased. The traffic condition in this part of the Grenoble network is changing over the whole day.
In the area considered, there are several sensor loops that belong to the public administration including four that could be used to measure the inflow. Their location in the selected area can be seen in Figure 5.3. We can notice that only the sensors indicated in green are currently functional.
Furthermore, Figure 5.4 shows the variation of the flow from the four sensors located in the entrance during one workday. As we notice it from the TomTom traffic fluidity, there are vehicles inside the domain all the day but with peaks in the morning and in the evening.

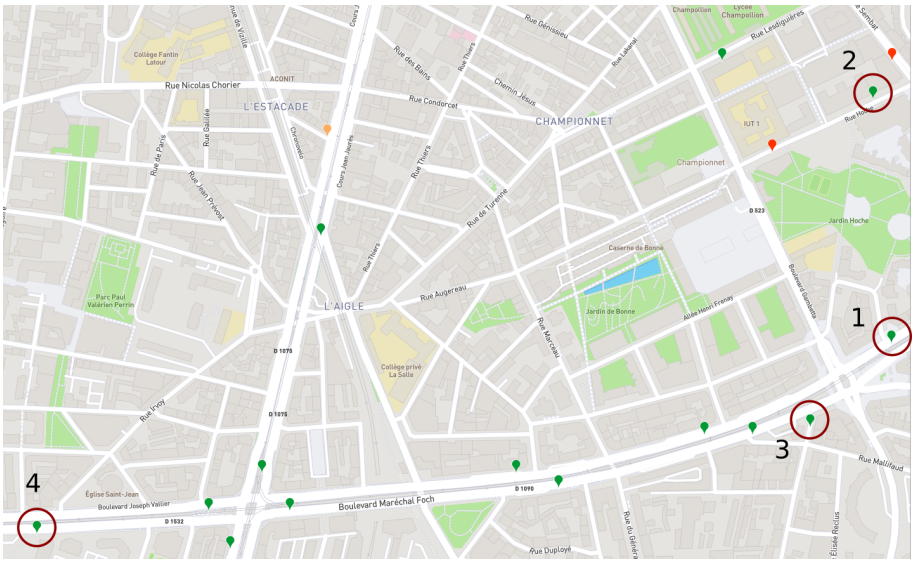

Figure 5.3: Position of the working sensors (green) and existing but not working sensors (red) in the area considered. The numbered sensors (between the red circles) are used for analysis.

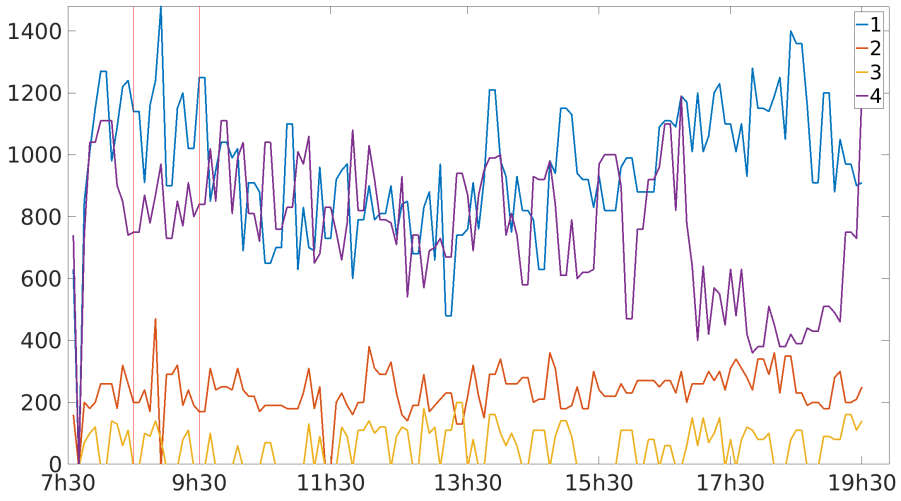

Figure 5.4: Analysis during a typical work day of the data collected by four existing loop sensors located in the entrance of the area studied

However, the values collected have a lot of fluctuation. We can see for instance that there is a peak in the morning between 8:45 am and 9:30 am but it last only a couple of minutes. We can see that three categories of roads appear: some major roads, where the flow of vehicles vary from 600 veh/h to 1400 veh/h, some medium roads where the flow of vehicles oscillates from 150 veh/h to 400 veh/h and finally small roads where the flow of vehicles varies from 0 to 150 veh/h. These quantities will be used to construct a reasonable microsimulation.

Remark 10. *The road where is located the sensor "2" is not considered as an entering road in the following scenario but the value of the sensor is used to qualify inflow of the "medium sized" roads.*

5.2 Simulations in the considered area

5.2.1 Description of the scenario

In this section, we aim to define a study case that could be realistic. This scenario will be then simulated in Aimsun and compared with the 2D model presented in this manuscript.
The scenario includes two layers representing different traffic directions: South-East-> North-West and South-West -> North-East. In the microsimulator, these layers are represented by Origin-Destination matrices (OD matrices). These OD matrices may be representative of real traffic demand. Indeed, the residential area of Grenoble is mainly located in the south of the studied section. Towards the North-West direction, there is the Scientific Polygon, which contains many research labs. In the North-East direction, there is the center of Grenoble with all the stores.
The inflows are set equal to what can be estimated for the existing sensors and are roughly estimated for the non-equipped roads. Then, we can notice that inflow should be defined along a line for the two-dimensional model. We consider an interpolation of the discrete inflow (given for each road) and we display the results in Figure 5.5.
We want to define a scenario that could represent the rush hour during the morning. Thus,

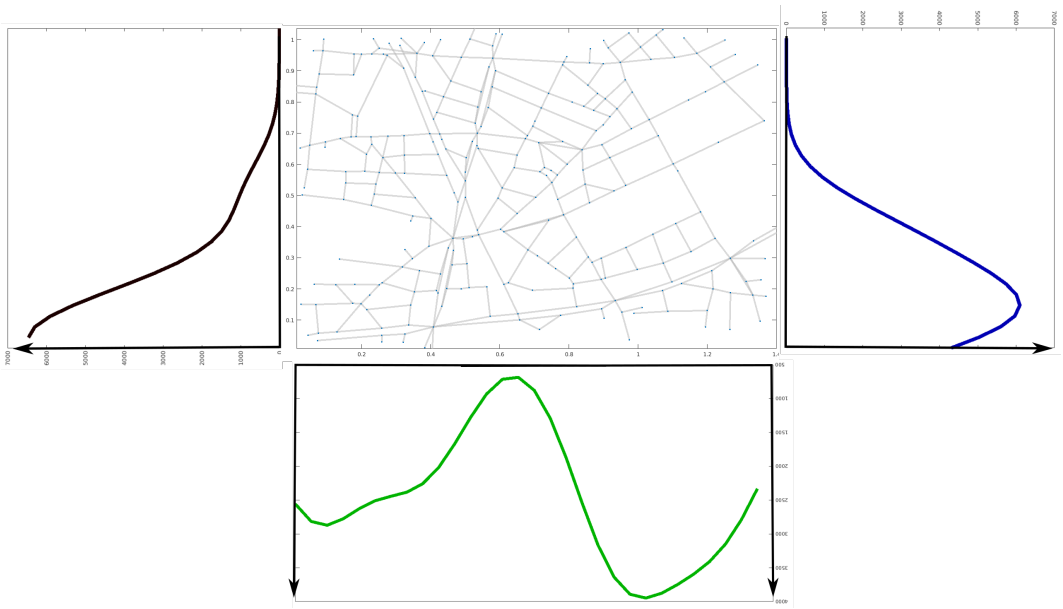

Figure 5.5: Interpolation along the border of the inflow for the macroscopic 2D model. Each curve against the network represents the inflow function (continuous in space) for the corresponding boundary.

we define three phases which last 15mn each. In the first phase, the network starts as empty and we apply an inflow equal to 50% of the maximum within Figure 5.5. Then, the second phase corresponds to the rush hour with the maximum demand. Finally, the inflows of the last phase go down to 50% of the maximum. The target of this scenario is to create congestion due to the high inflow and see how it dissipates when the demand goes back to a normal level. These three phases of transition can be observed through the number of vehicles inside the network displayed in Figure 5.6

One can notice that the number of vehicles inside the network does not exceed 600. However,

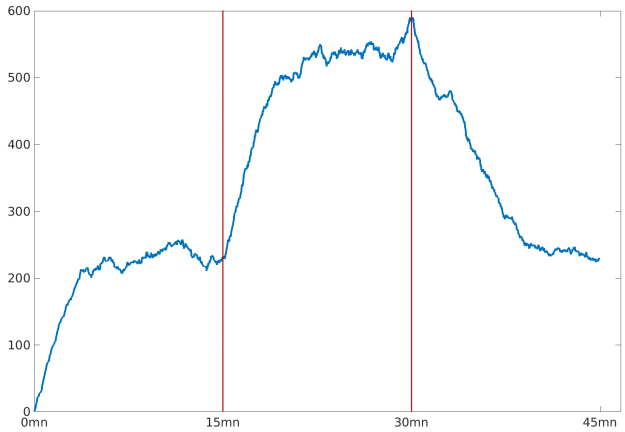

Figure 5.6: Number of vehicles over time in Aimsun simulation for the considered scenario

the total number of vehicles traveling inside the network during the simulation time is around 5000. Regarding the 2D model simulation, we consider the same model as the one defined in (4.2). The interaction between the layers is represented by the total density (sum of the different layers). The flux function is described by the fundamental diagram of Newell with a critical density, $\rho_c = \frac{1}{7}\rho_m$. We can notice that the critical density is lower that is usually seen in 1D modeling. This can be explained by the fact the theoretical maximum density in a road network is high compared to what is sufficient to create a congestion. The maximum velocity $v_{\max}$ is set equal to 30km/h. The maximum density is estimated with the method described in Chapter 2 and the results is displayed in Figure 5.7. We can notice that the network is quite regular even if there is some fluctuation in the concentration of roads. The maximum of maximum density field, $\tilde{\rho}_{\max} = \max_{x,y} \rho_m(x,y)$ is equal to $5.6 * 10^3 \text{veh/km}^2$. The direction field is estimated using the Wasserstein method developed in Section 4.3. The results of estimation are shown in Figure 5.8.

5.2.2 Results of simulations

We aim to test the model against microsimulation in Aimsun in order to understand the advantages and limitations of the model. The numerical simulation is done using the method developed in Section 4.2.1.

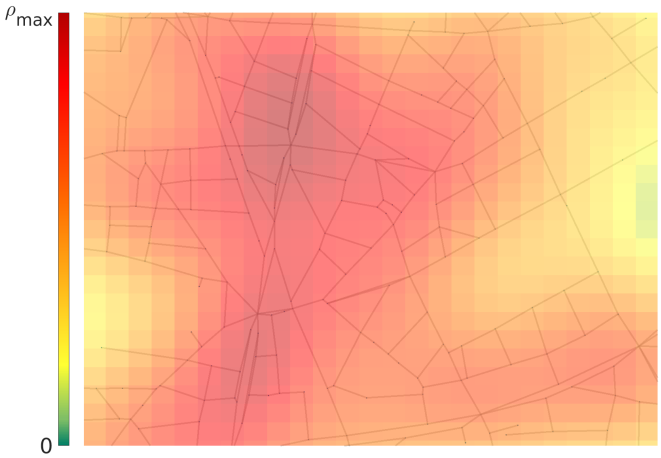

Figure 5.7: Maximum density field estimated on the Grenoble network

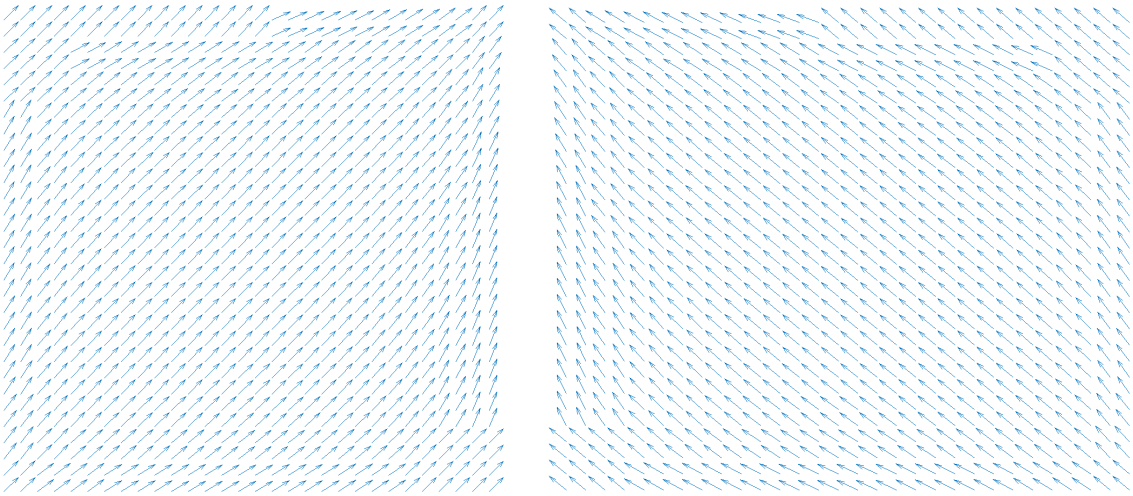

Figure 5.8: Direction field estimated for the two layers on the Grenoble network

The results of simulation are shown in Figure 5.9 and 5.10. The results of the 2D model are represented on the top, whereas the microsimulation is on the bottom. On the left, we display the layer representing OD matrices oriented towards the North-East, on the middle the OD matrices towards the North-West and on the right the total density. We can notice that the speed of propagation and the different transition on the inflow demand can be reproduced decently by the model. However, the model does not represent the fluctuation in demand existing in the microsimulator. The congestion observed in the 2D model is much smaller than the one in the microsimulator. The congestion can be achieved by lowering the critical density. However, the presence of multiple layers could lead to the creation of spillback responsible for a very strong traffic jam. In Figure 5.11, we show a simulation for the same scenario with a critical density $\rho_c = \frac{1}{12}\rho_m$. We can see that this time the congestion is

captured too strongly. We can also notice that the congestion in the 2D simulation with multiple layers have no guarantee to dissipate after the inflow was reduced. Indeed, densities of vehicles from different layers in opposite directions can block each other as we can start to see it in the simulation. The formulation of the interaction is not able to reproduce both the formation and the dissipation of the congestion. It would be interesting to consider new formulations in the future. A final remark is that the direction fields are not able to capture all the motions of the vehicles and do not describe precisely their trajectories. Thus, the positions of the congestions observed in 5.11 do not correspond exactly to the congestion of the microsimulation. A possible solution to solve this issue would be to increase the number of layers used to describe the flow.

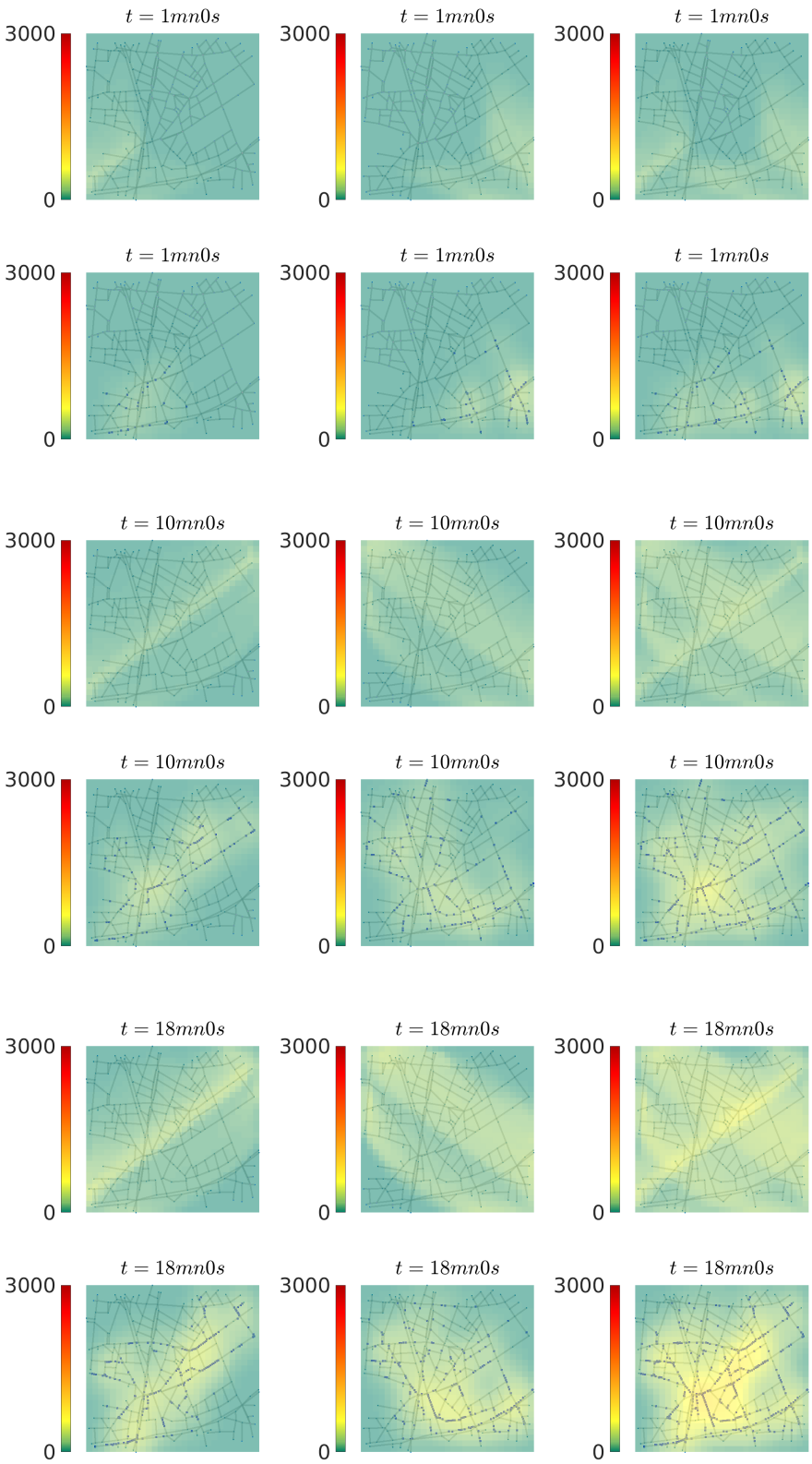

Figure 5.9: Simulation on the Grenoble network at different time steps with $\rho_c = \frac{1}{7}\rho_m$. On the top of each image, there is the Aimsun simulation and its reconstruction and on its bottom, we have the prediction by the 2D model. On the left and middle, we have the two individual layers and on the right the total density.

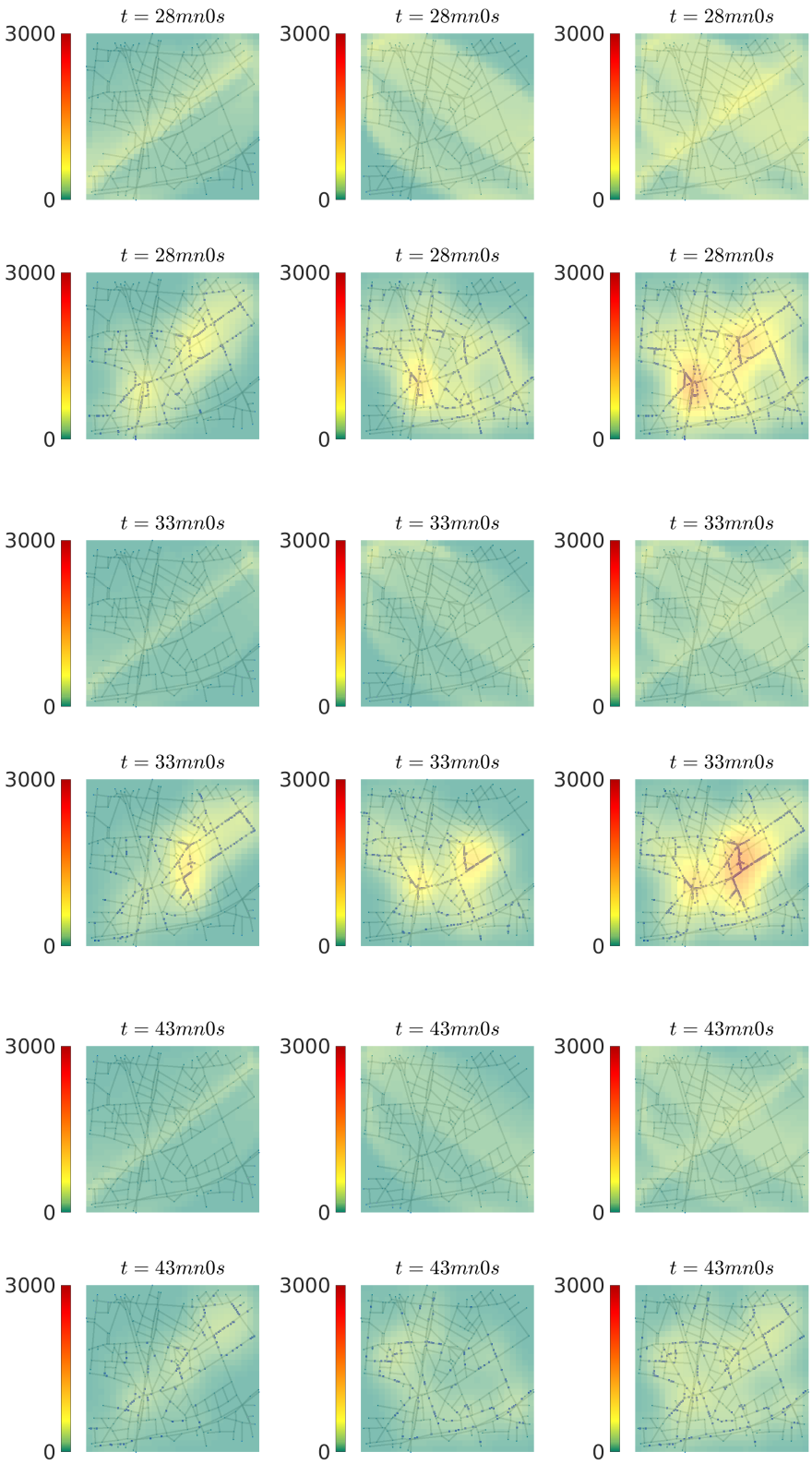

Figure 5.10: Simulation in the Grenoble network at different time step with $\rho_c = \frac{1}{7}\rho_m$. On the top of each image, there is the Aimsun simulation and reconstruction, on its bottom the prediction by the 2D model. On the left and middle, we have the two individual layers and on the right the total density.

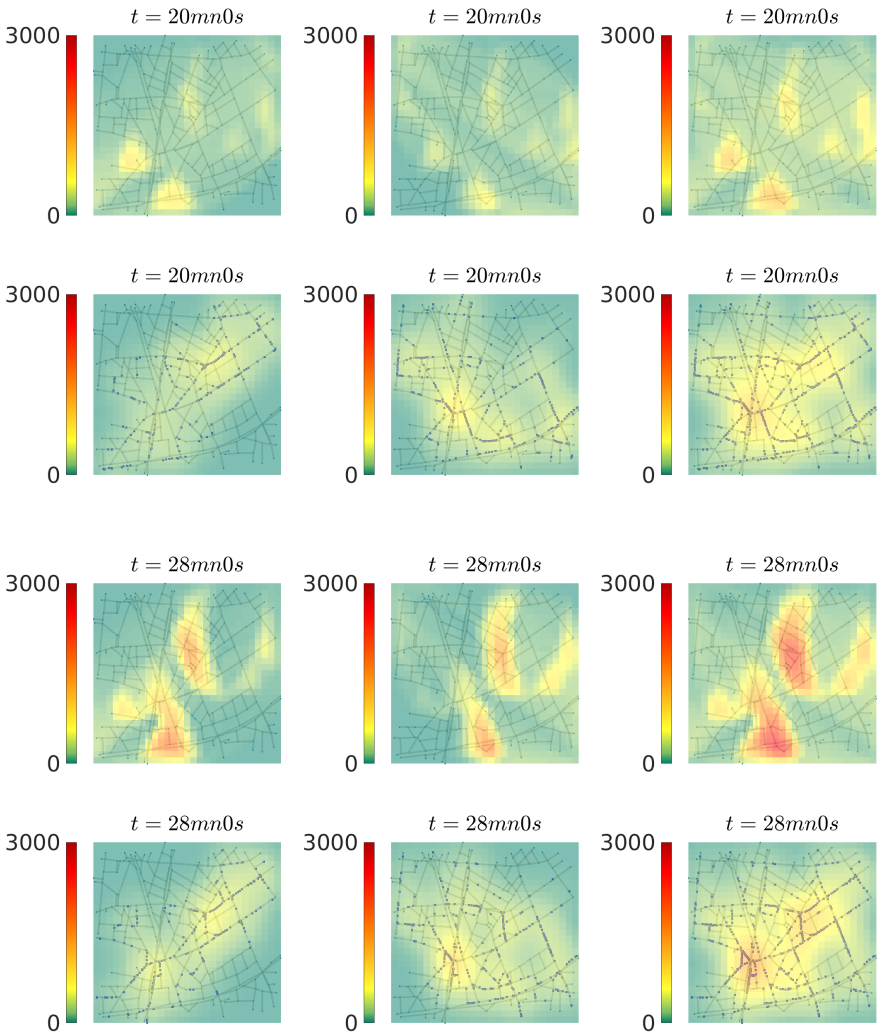

Figure 5.11: Simulation in the Grenoble network at different time steps with low critical density $\rho_c = \frac{1}{12}\rho_m$. On the top of each image, there is the Aimsun simulation and reconstruction, on its bottom the prediction by the 2D model. On the left and middle, we have the two individual layers and on the right the total density.

Conclusion

Traffic modeling, and particularly on a large-scale network, is a challenging problem. Currently, no model exists to accurately predict the traffic evolution. Nevertheless, the existing models have their own strengths and weaknesses. In this thesis, we study a new approach that represents traffic flow through a two-dimensional PDE. For such an abstraction to be accurate, we considered large and dense traffic networks, like urban areas. The model can be seen as an aggregated representation, that is useful in tracking the spatial traffic propagation.

Contribution

The contribution of this Ph.D. thesis can be divided into three parts: the model formulation and its characteristics, the methodology to estimate its parameters, and the comparison of the simulation results with others approaches.

- **Model development and properties:** We studied in this thesis successive extension of the model starting from a simple formulation towards a more complex one. First, we introduced a two-dimensional model with three parameters: the direction field, the maximum velocity and the maximum density. As the direction of propagation was uniquely defined at each space position, we had only considered traffic network with all the roads oriented toward a preferred direction. The parameters of the FD were constant and thus the model could only represent a homogeneous network, for which traffic conditions was similar everywhere. Then, we studied the extension to a heterogeneous network by considering space-dependent maximum velocity and maximum density. These networks could represent traffic bottlenecks and thus could model the creation of congestion. Finally, multiple directions of flow were considered through a multilayer model. A key point was the formulation of the interaction between the density of different layers i.e. how different directions of flow could impact each other. Due to these interactions, these models are not always hyperbolic which could impact the stability and the well-posedness of the model. Thus, we introduced a formulation of the interaction such that the model remained hyperbolic but this highly constrained the possibilities of adaptation towards the reality of traffic flow.
- **Methodology for estimation and calibration of parameters:** For each stage of the model development, we constructed a method of estimation for the parameters. Most of the estimations we investigated, were based on network geometry. If the model represented vehicles evolving in a 2D-plane, then the propagation of vehicles strongly relied on the underlying network. We included this aspect in the model. We suggested a first estimation method for the direction field using the orientation of the roads. Then, using again only the network geometry, we proposed an estimation of the space-dependent

maximum velocity and density in a heterogeneous network. Thus, it captured that, the areas where the concentration of road is less dense, could act as a bottleneck of the network. Finally, for models with multiple directions of traffic propagation, the estimation of the direction field using only the network can be not realistic. Then, we suggest an estimation method based on data and using optimal transport. The strength of the method is to be able to reconstruct the vehicles' propagation from the aggregated density.

- **Simulation results and method for the comparisons:** The development of each step of the model was supported by numerical simulations. These simulations were based on finite volume methods, mainly using the Godunov scheme coupled with dimensional splitting to include the two-dimensional aspect. To simulate non-hyperbolic model, we described a high order method based on WENO method and TVD limiter. Another contribution of this thesis was the comparison of the 2D modeling with other approaches: CTM coupled with a model of junctions, microsimulation in Aimsun defined by using split ratio or OD matrices. The difficulty of the comparison lied in the fact that the models did not have the same variables. Thus, we defined a method to reconstruct a two-dimensional density from vehicles trajectories in the microsimulation.

Perspective and extension

While a Ph.D. thesis offers a good opportunity to study deeply a research topic, I found plethora of new questions in the pursuit of the questions I asked in the beginning. Therefore, I would like to conclude this thesis by writing the most relevant questions that I have in mind. These research trails can be split according to their level of sophistication or difficulty.
First, there are ideas that are not presented in this thesis, which are straightforward to consider and do not require new material.

- Vehicles generation within the network can be added easily in the numerical implementation. Indeed, source terms in conservation laws are generally numerically implemented using a splitting method, which we are already using, and so, the implementation is direct. These extensions need to be considered in the future because a very large scale network contains necessarily a large number of vehicles parked almost everywhere. Also, drivers looking for a parking have a specific behavior, especially in terms of direction, and they may be represented by another layer.

Then, there are other possible extensions to investigate, or questions that need answers. These research trails have different levels of complexity with a range going from simple extensions to open questions:

- To include the signalization in the model, one may use specific interaction terms. One very exciting perspective would be to include the notion of priority through the interaction. For instance, in Europe, vehicles coming from the left in a roundabout have

priority. In an unsignalized intersection in Europe, vehicles coming from the right have the priority. In a junction equipped with traffic lights, the priority changes according to traffic cycles. It could be interesting to define an interaction varying over space to describe these situations.

- A general method to choose the number and the content of the layers could be developed. We can remind that within a layer, it is not possible to include a crossing flow. Then, one could develop a metric to evaluate the number of layers needed to represent the OD matrices of the vehicles (or, directly their trajectories) in a traffic situation. It can be interesting to notice that some models –where the interaction is defined by the sum– can consider any number of layers without losing consistency. At the limits, the multilayer model will become a mesoscopic model.

- Finally, new formulations of the model could be investigated to have a hyperbolic model which is well defined and has a better representation of real traffic. An idea to push towards this direction would be to rely directly on data to design the formulation of the model. The use of data to improve a model required generally a metric to compare different models. The Wasserstein distance that we described in the thesis may be a good candidate.

The possible extensions presented above are what we consider to be the main one. Several secondary trails to improve the model have been introduced in the chapters' conclusions.

Bibliography

[1] Rafegh Aghamohammadi and Jorge A. Laval. "A continuum model for cities based on the macroscopic fundamental diagram: A semi-Lagrangian solution method". In: Transportation Research Part B: Methodological (2019) (cit. on p. 17).

[2] Rafegh Aghamohammadi and Jorge A Laval. "Dynamic Traffic Assignment using the Macroscopic Fundamental Diagram: A Review of Vehicular and Pedestrian Flow Models". In: arXiv preprint arXiv:1801.02130 (2018) (cit. on p. 16).

[3] Caterina Balzotti et al. "Understanding Human Mobility Flows from Aggregated Mobile Phone Data". In: IFAC-PapersOnLine 51.9 (2018), pp. 25–30 (cit. on p. 84).

[4] Martin Beckmann. "A continuous model of transportation". In: Econometrica: Journal of the Econometric Society (1952), pp. 643–660 (cit. on p. 13).

[5] Sylvie Benzoni-Gavage and Rinaldo M Colombo. "An n-populations model for traffic flow". In: European Journal of Applied Mathematics 14.5 (2003), pp. 587–612 (cit. on p. 69).

[6] Malachy Carey and Michael Bowers. "A review of properties of flow–density functions". In: Transport Reviews 32.1 (2012), pp. 49–73 (cit. on p. 5).

[7] Gui-Qiang Chen, Dening Li, and Dechun Tan. "Structure of Riemann solutions for 2-dimensional scalar conservation laws". In: journal of differential equations 127.1 (1996), pp. 124–147 (cit. on p. 23).

[8] Gui-Qiang G Chen. "Multidimensional conservation laws: overview, problems, and perspective". In: Nonlinear conservation laws and applications. Springer, 2011, pp. 23–72 (cit. on p. 72).

[9] B.N. Chetverushkin, N.G. Churbanova, and M.A. Trapeznikova. "Traffic Flow Simulation by 2D Macro- and Microscopic Models". In: Latest Trends on Urban Planning Transportation. 2010 (cit. on p. 17).

[10] Giuseppe Maria Coclite, Mauro Garavello, and Benedetto Piccoli. "Traffic flow on a road network". In: SIAM journal on mathematical analysis 36.6 (2005), pp. 1862–1886 (cit. on pp. 10, 44).

[11] Carlos F Daganzo. "The cell transmission model: A dynamic representation of highway traffic consistent with the hydrodynamic theory". In: Transportation Research Part B: Methodological 28.4 (1994), pp. 269–287 (cit. on pp. 9, 44, 63).

[12] Carlos F Daganzo and Nikolas Geroliminis. "An analytical approximation for the macroscopic fundamental diagram of urban traffic". In: Transportation Research Part B: Methodological 42.9 (2008), pp. 771–781 (cit. on p. 13).

[13] Fabio Della Rossa, Carlo D'Angelo, and Alfio Quarteroni. "A distributed model of traffic flows on extended regions." In: NHM 5.3 (2010), pp. 525–544 (cit. on p. 16).

[14] Jie Du et al. "Revisiting Jiang's dynamic continuum model for urban cities". In: Transportation Research Part B: Methodological 56 (2013), pp. 96–119 (cit. on p. 16).

[15] Shimao Fan. Data-fitted generic second order macroscopic traffic flow models. Temple University, 2013 (cit. on p. 28).

[16] Shimao Fan, Michael Herty, and Benjamin Seibold. "Comparative model accuracy of a data-fitted generalized Aw-Rascle-Zhang model". In: arXiv preprint arXiv:1310.8219 (2013) (cit. on p. 28).

[17] Ronald P Fedkiw et al. "A non-oscillatory Eulerian approach to interfaces in multimaterial flows (the ghost fluid method)". In: Journal of computational physics 152.2 (1999), pp. 457–492 (cit. on p. 26).

[18] R. E. Franklin. "The structure of a traffic shock wave". In: (1961) (cit. on pp. 5, 46).

[19] Mauro Garavello and Benedetto Piccoli. Traffic flow on networks. Vol. 1. American institute of mathematical sciences Springfield, 2006 (cit. on p. 10).

[20] Nikolas Geroliminis and Carlos F Daganzo. "Existence of urban-scale macroscopic fundamental diagrams: Some experimental findings". In: Transportation Research Part B: Methodological 42.9 (2008), pp. 759–770 (cit. on pp. 13, 14, 61).

[21] Paola Goatin and Matthias Mimault. "A mixed system modeling two-directional pedestrian flows". In: Mathematical biosciences and engineering 12.2 (2015), pp. 375–392 (cit. on pp. 74, 75).

[22] Sergei Konstantinovich Godunov. "A difference method for numerical calculation of discontinuous solutions of the equations of hydrodynamics". In: Matematicheskii Sbornik 89.3 (1959), pp. 271–306 (cit. on pp. 9, 24).

[23] Laurent Gosse. "A two-dimensional version of the Godunov scheme for scalar balance laws". In: SIAM Journal on Numerical Analysis 52.2 (2014), pp. 626–652 (cit. on p. 24).

[24] Bruce Douglas Greenshields et al. "The photographic method of studying traffic behavior". In: Highway Research Board Proceedings. Vol. 13. 1934 (cit. on pp. 5, 6).

[25] Mohammad Hajiahmadi et al. "Optimal dynamic route guidance: A model predictive approach using the macroscopic fundamental diagram". In: Intelligent Transportation Systems-(ITSC), 2013 16th International IEEE Conference on. IEEE. 2013, pp. 1022–1028 (cit. on p. 15).

[26] Michael Herty, Adrian Fazekas, and Giuseppe Visconti. "A two-dimensional data-driven model for traffic flow on highways". In: Networks and Heterogeneous Media 13 (2018), pp. 217–240 (cit. on p. 17).

[27] HW Ho and SC Wong. "Two-dimensional continuum modeling approach to transportation problems". In: Journal of Transportation Systems Engineering and Information Technology 6.6 (2006), pp. 53–68 (cit. on p. 13).

[28] Helge Holden and Nils Henrik Risebro. Front tracking for hyperbolic conservation laws. Vol. 152. Springer, 2015 (cit. on p. 59).

[29] Serge P. Hoogendoorn et al. "Continuum modelling of pedestrian flows: From microscopic principles to self-organised macroscopic phenomena". In: Physica A: Statistical Mechanics and its Applications 416 (2014), pp. 684 –694 (cit. on p. 17).

[30] Roger L Hughes. "A continuum theory for the flow of pedestrians". In: Transportation Research Part B: Methodological 36.6 (2002), pp. 507–535 (cit. on p. 37).

[31] Yan-Qun Jiang, Pei-Jie Ma, and Shu-Guang Zhou. "Macroscopic modeling approach to estimate traffic-related emissions in urban areas". In: Transportation Research Part D: Transport and Environment (2015) (cit. on p. 16).

[32] Yanqun Jiang et al. "A dynamic traffic assignment model for a continuum transportation system". In: Transportation Research Part B: Methodological 45.2 (2011), pp. 343–363 (cit. on p. 16).

[33] Kenneth H Karlsen, Michel Rascle, Eitan Tadmor, et al. "On the existence and compactness of a two-dimensional resonant system of conservation laws". In: Communications in Mathematical Sciences 5.2 (2007), pp. 253–265 (cit. on p. 23).

[34] Franziska Klügl and Guido Rindsfüser. "Large-scale agent-based pedestrian simulation". In: German conference on multiagent system technologies. Springer. 2007, pp. 145–156 (cit. on p. 17).

[35] Stanislav Nikolaevich Kruzhkov. "First order quasilinear equations in several independent variables". In: Matematicheskii Sbornik 123.2 (1970), pp. 228–255 (cit. on p. 22).

[36] Raphaël Lamotte and Nikolas Geroliminis. "The morning commute in urban areas with heterogeneous trip lengths". In: Transportation Research Procedia 23 (2017). Papers Selected for the 22nd International Symposium on Transportation and Traffic Theory Chicago, Illinois, USA, 24-26 July, 2017., pp. 591 –611 (cit. on p. 15).

[37] JP Lebacque and MM Khoshyaran. "First order macroscopic traffic flow models for networks in the context of dynamic assignment". In: Transportation Planning (2004), pp. 119–140 (cit. on pp. 10, 17).

[38] Ludovic Leclercq, Alméria Sénécat, and Guilhem Mariotte. "Dynamic macroscopic simulation of on-street parking search: A trip-based approach". In: Transportation Research Part B: Methodological 101 (2017), pp. 268 –282 (cit. on p. 15).

[39] Ludovic Leclercq et al. "Macroscopic traffic dynamics with heterogeneous route patterns". In: Transportation Research Procedia 7 (2015), pp. 631–650 (cit. on p. 15).

[40] Knut-Andreas Lie. "A dimensional splitting method for quasilinear hyperbolic equations with variable coefficients". In: BIT Numerical Mathematics 39.4 (1999), pp. 683–700 (cit. on pp. 24, 76).

[41] Michael J Lighthill and Gerald Beresford Whitham. "On kinematic waves. II. A theory of traffic flow on long crowded roads". In: Proceedings of the Royal Society of London A: Mathematical, Physical and Engineering Sciences. Vol. 229. 1178. The Royal Society. 1955, pp. 317–345 (cit. on p. 7).

[42] ZY Lin et al. "A predictive continuum dynamic user-optimal model for a polycentric urban city". In: Transportmetrica B: Transport Dynamics 5.3 (2017), pp. 228–247 (cit. on p. 17).

[43] Guilhem MARIOTTE. "Dynamic Modeling of Large-Scale Urban Transportation Systems". Theses. Université de Lyon, Nov. 2018 (cit. on p. 16).

[44] Guilhem Mariotte and Ludovic Leclercq. "Flow exchanges in multi-reservoir systems with spillbacks". In: Transportation Research Part B: Methodological 122 (2019), pp. 327 –349 (cit. on p. 15).

[45] Guilhem Mariotte, Ludovic Leclercq, and Jorge A Laval. "Dual expression of macroscopic urban models: analytical and numerical investigations with piecewise linear functions". In: 96th Transportation Research Board Annual Meeting. Transportation Research Board-TRB. 2017, 20–p (cit. on p. 15).

[46] Stéphane Mollier, Maria Laura Delle Monache, and Carlos Canudas-de-Wit. "2D-LWR in large-scale network with space dependent fundamental diagram". In: 2018 21st International Conference on Intelligent Transportation Systems (ITSC). Maui, United States: IEEE, 2018, pp. 1640–1645 (cit. on p. 78).

[47] Stephane Mollier, Maria Laura Delle Monache, and Carlos Canudas-de-Wit. "A Simple Example of a Two-Dimensional Model for Traffic: Discussion about Assumptions and Numerical Methods". In: Transportation Research Record 2672.20 (2018), pp. 249–261 (cit. on p. 37).

[48] Stéphane Mollier, Maria Laura Delle Monache, and Carlos Canudas de Wit. "A decision support and planning mobility method for large scale traffic networks". In: ECC 2019 - European Control Conference. Naples, Italy, June 2019, pp. 1–6 (cit. on p. 70).

[49] Stéphane Mollier, Maria Laura Delle Monache, and Carlos Canudas de Wit. "A step towards a multidirectional 2D model for large scale traffic networks". In: TRB 2019 - 98th Annual Meeting Transportation Research Board. Washington D.C., United States, Jan. 2019, pp. 1–7 (cit. on p. 70).

[50] Stéphane Mollier et al. "Two-dimensional macroscopic model for large scale traffic networks". In: Transportation Research Part B: Methodological 122 (2019), pp. 309 –326 (cit. on p. 46).

[51] Gordon F Newell. "A theory of traffic flow in tunnels". In: Theory of Traffic Flow (1961), pp. 193–206 (cit. on pp. 5, 46).

[52] Gordon Frank Newell. "A simplified car-following theory: a lower order model". In: Transportation Research Part B: Methodological 36.3 (2002), pp. 195–205 (cit. on p. 7).

[53] Legesse L Obsu et al. "Traffic flow optimization on roundabouts". In: Mathematical Methods in the Applied Sciences 38.14 (2015), pp. 3075–3096 (cit. on p. 12).

[54] Paul I Richards. "Shock waves on the highway". In: Operations research 4.1 (1956), pp. 42–51 (cit. on p. 7).

[55] Luis Romero Perez and Francisco Garcia Benitez. "Outline of Diffusion Advection in Traffic Flow Modeling". In: Transportation Research Board 87th Annual Meeting. 08-1503. 2008 (cit. on p. 16).

[56] Elena Rossi. In: Hyperbolic Differential Equations (2017), to appear (cit. on p. 23).

[57] Mohammadreza Saeedmanesh and Nikolas Geroliminis. "Dynamic clustering and propagation of congestion in heterogeneously congested urban traffic networks". In: Transportation Research Procedia 23 (2017). Papers Selected for the 22nd International Symposium on Transportation and Traffic Theory Chicago, Illinois, USA, 24-26 July, 2017., pp. 962 –979 (cit. on p. 15).

[58] Tibye Saumtally. "Modèles bidimensionnels de trafic". PhD thesis. Université Paris-Est, 2012 (cit. on p. 17).

[59] Chi-Wang Shu. "High order weighted essentially nonoscillatory schemes for convection dominated problems". In: SIAM review 51.1 (2009), pp. 82–126 (cit. on pp. 75, 76).

[60] Kwami Seyram Sossoe and Jean-Patrick Lebacque. "Reactive Dynamic Assignment for a Bi-dimensional Traffic Flow Model". In: International Conference on Systems Science. Springer. 2016, pp. 179–188 (cit. on p. 17).

[61] Gilbert Strang. "On the construction and comparison of difference schemes". In: SIAM Journal on Numerical Analysis 5.3 (1968), pp. 506–517 (cit. on p. 24).

[62] Alina Borisovna Sukhinova et al. "Two-dimensional macroscopic model of traffic flows". In: Mathematical models and computer simulations 1.6 (2009), p. 669 (cit. on p. 17).

[63] Eleuterio F Toro. Riemann solvers and numerical methods for fluid dynamics: a practical introduction. Springer Science & Business Media, 2013 (cit. on pp. 24, 72).

[64] Femke van Wageningen-Kessels et al. "Genealogy of traffic flow models". In: EURO Journal on Transportation and Logistics 4.4 (2015), pp. 445–473 (cit. on p. 7).

[65] David H Wagner. "The Riemann Problem in Two Space Dimensions for a Single Conservation Law." In: 1983 (cit. on p. 23).

[66] SC Wong. "Multi-commodity traffic assignment by continuum approximation of network flow with variable demand". In: Transportation Research Part B: Methodological 32.8 (1998), pp. 567–581 (cit. on pp. 13, 69).

[67] Jun Zhang et al. "Ordering in bidirectional pedestrian flows and its influence on the fundamental diagram". In: Journal of Statistical Mechanics: Theory and Experiment 2012.02 (2012), P02002 (cit. on p. 18).

Résumé — Les fréquentes congestions que connaissent les réseaux routiers des grandes métropoles mondiales ont de lourdes conséquences économiques et environnementales. La compréhension et la modélisation dynamique des mécanismes à l'origine de ces congestions permettent d'en prédire l'évolution et donc d'améliorer l'efficacité des politiques de régulations utilisées par les opérateurs du réseau. La modélisation des réseaux routiers a commencé par le cas d'une route isolée puis a été étendue à des réseaux urbains. Ce changement d'échelle présente de nombreuses difficultés en matière de temps de calcul, de calibrage et de scénarisation, ce qui a incité la communauté scientifique à s'intéresser à des modèles agrégés, décrivant une représentation simplifiée de la réalité. Un de ces modèles vise à représenter de denses réseaux urbains par une équation aux dérivées partielles continue dans le plan. Ainsi, les véhicules sont représentés par une densité bi-dimensionnelle et leurs trajectoires sont décrites comme des directions de flux. L'objectif de la thèse est de développer cette approche et de proposer des méthodes pour son calibrage et sa validation. Les contributions correspondent à trois extensions successives du modèle. Tout d'abord, un simple modèle bi-dimensionnel est proposé pour le cas de réseaux homogènes –avec des limitations de vitesse et des concentrations de routes similaires en tout point– et dans lesquels une direction de propagation privilégiée existe. Une méthode de comparaison avec un microsimulateur est présentée. Ensuite, le modèle est étendu au cas de réseaux hétérogènes –avec des limitations de vitesse et des concentrations de routes variables– mais toujours avec une direction privilégiée. Ces dépendances spatiales permettent de décrire les phénomènes d'engorgement existant dans les réseaux routiers. Enfin, un modèle constitué de plusieurs couches, chacune représentant une direction de flux différente, est étudié. La complexité de la modélisation réside dans la formulation des interactions entre les différentes directions. Ce type de modèle n'est pas toujours hyperbolique ce qui impacte sa stabilité.
Mots clés : Modélisation du trafic routier, Simulation numérique, Equation aux dérivées partielles

Abstract — Congestion in traffic networks is a common issue in big cities and has considerable economic and environmental impacts. Traffic policies and real-time network management can reduce congestion using prediction of dynamical modeling. Initially, researchers studied traffic flow on a single road and then, they extended it to a network of roads. However, large-scale networks present challenges in terms of computation time and parameters' calibration. This led the researchers to focus on aggregated models and to look for a good balance between accuracy and practicality. One of the approaches describes traffic evolution with a continuous partial differential equation on a 2D-plane. Vehicles are represented by a two-dimensional density and their propagation is described by the flow direction. The thesis aims to develop these models and devises methods for their calibration and their validation. The contributions follow three extensions of the model. First, a simple model in two-dimensional space to describe a homogeneous network with a preferred direction of flow propagation is considered. A homogeneous network has the same speed limits and a similar concentration of roads everywhere. A method for validation using GPS probes from microsimulation is provided. Then, a space-dependent extension to describe a heterogeneous network with a preferred direction of flow propagation is presented. A heterogeneous network has different speed limits and a variable concentration of roads. Such networks are of interest because they can show how bottleneck affects traffic dynamics. Finally, the case of multiple directions of flow is considered using multiple layers of density, each layer representing a different flow direction. Due to the interaction between layers, these models are not always hyperbolic which can impact their stability.
Keywords: Traffic flow modeling, Numerical simulation, Partial differential equation

GIPSA-lab, 11 Rue des Mathématiques
Saint-Martin-d'Hères